

Disruption of bacterial spores using microwaves and nanoparticles

by

Dmitry Malyshev



A thesis submitted for the degree of
Philosophiae Doctor (Ph.D) in Cardiff University

August 2018

Cardiff School of Pharmacy and Pharmaceutical Science

Cardiff University

Summary

This thesis shows how microwaves and nanoparticles can be used to enhance the disruption of spores in the context of a novel microwave-based bacterial detector.

Infections linked to *Clostridium difficile* are a significant cause of suffering. In hospitals, the organism is primarily acquired through the faecal-oral route as spores excreted by infected patients contaminate the healthcare environment. Microwave-based spore disruption is the focus of this project offers a potential rapid diagnostic method to detect spores, including *C. difficile* spores by making them release DNA which is then detected. One of the limiting factors of this method was the power required and it was hypothesised that by using a new microwave cavity and adding nanoparticles, the DNA release from spores can be achieved with less power.

First, the spore surface properties of the different isolates of *C. difficile* were compared. A significant variation in both spore morphology and spore hydrophobicity of clinical isolates of *C. difficile* was observed. In particular, the “pineapple-like” shape of strains was associated with higher hydrophobicity in spores, while the loose outer exosporium layer was associated with lower hydrophobicity.

The isolates were then tested for DNA release in response to microwaving. Spores were shown to release single-stranded, but no double stranded DNA. The spores were also not visibly changed by microwave exposure, suggesting a non-destructive mechanism of disruption. To study this mechanism further, the microwave system was updated to remove overall sample heating and tested under electric fields, magnetic fields and a combination of the two. The electric field was shown to be causing the disruption of spores, field showed a positive correlation with increasing disruption.

Finally, the spores with tested with microwaves and nanoparticles, where nanoparticles showed a significant improvement in two of the four tested isolates. A computer model of the spore and nanoparticle interactions was made, which offered a plausible mechanism for the nature of microwave mediated disruption and the improvement in disruption caused by nanoparticles.

Acknowledgements

I would first like to thank my supervisors: Prof. Les Baillie and Prof. Adrian Porch, who brought together their expertise in microbiology and electrical engineering and made this multidisciplinary project possible.

I would also like to thank Dr. Jonathan Lees and the team who originally built the microwave system used in this project.

Many thanks to others in the School of Engineering and School of Pharmacy, especially James Blaxland, Heungae Choi and Jerome Cuenca and Catrin Williams. Thank you to Dr. Emmanuel Brousseau for guidance in using electron microscopy. Many thanks to Cardiff University for funding this project.

My gratitude to Prof. Simon Cutting (Royal Holloway, University of London), who kindly provided some strains from his laboratory for this project.

Finally, my love and thanks to my family for their support and encouragement.

Publications and communications

Publications

Under review:

Dmitry Malyshev, Catrin F. Williams, Jonathan Lees, Les Baillie, Adrian Porch. Model of microwave effects on bacterial spores. *Journal of Applied Physics*

Malyshev D, Baillie L. Surface Morphology Differences in Clostridium difficile Spores, Based on Different Strains and Methods of Purification. *Anaerobe*

Conferences and communications

European Spores Conference 2018:

Oral presentation: “*Characterisation of Clostridium difficile spore surface morphology*”

European Spores Conference 2015:

Poster Presentation: “*Characterisation of Clostridium difficile*”

Society for Applied Microbiology 2016 calendar.

False Coloured SEM of *C. difficile* spores mixed with gold nanoparticles.

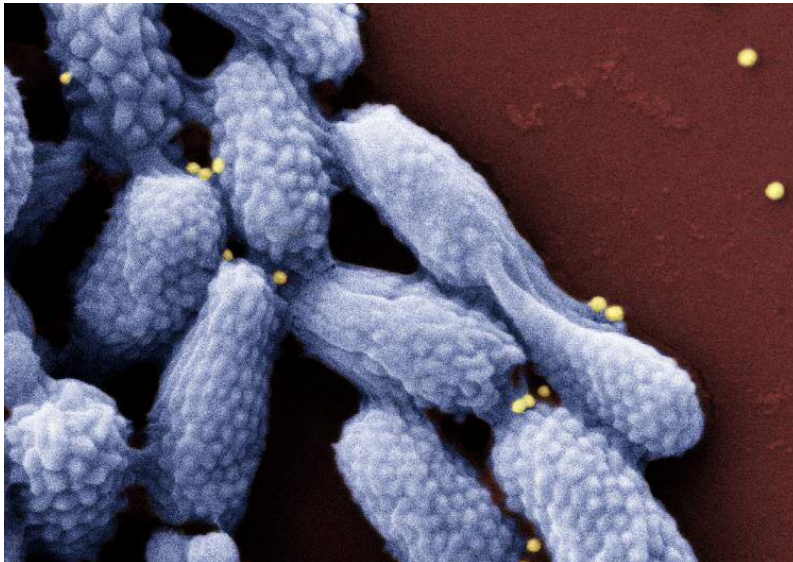


Image used in the SFAM 2016 calendar

Contents

Declaration	i
Summary	ii
Acknowledgements	iii
Publications and communications	iv
Contents	v
List of Figures	ix
List of Tables	xii
List of Abbreviations	xiii
1. Chapter 1. Introduction	1
1.1 Historical Background	1
1.2 <i>C. difficile</i> overview	2
1.2.1 Sporulation	3
1.2.2 Epidemiology of <i>C. difficile</i>	4
1.2.3 Toxins	6
1.2.4 Typing of <i>C. difficile</i>	7
1.3 Spore Structure	9
1.3.1 The exosporium and its naming debate	10
1.3.2 Spore surface proteins	12
1.4 Current <i>C. difficile</i> detection methods	14
1.4.1 Bacterial culture	14
1.4.2 Cell cytotoxicity assay	15
1.4.3 Enzyme immunoassays	15
1.4.4 PCR-based assays	15
1.5 Microwaves	16
1.5.1 Mechanism of action	16
1.5.2 Microwave cavity	17
1.6 Nanoparticles	18
1.6.1 Mechanisms of nanoparticle activity	18
1.6.2 Microwaves acting on nanoparticles	19
1.7 Microwave-based bacterial detectors	20
1.7.1 Microwave-accelerated metal-enhanced fluorescence	21
1.7.2 Low-power microwave system	21
1.7.3 Other microwave systems	24

1.8 Project Aims	25
1.8.1 Aims	25
1.8.2 Hypotheses being tested	26
2. Chapter 2. General Methods	27
2.1 Spore growth and purification methods	27
2.1.1 Strains and growth conditions	27
2.1.2 Lawley's method	28
2.1.3 Sorg's method	29
2.1.4 Heeg's method	29
2.2 Spore visualisation methods	30
2.2.1 Visualisation of spores by light microscopy	30
2.2.2 Visualisation of spores by SEM	30
2.2.3 DNA Visualisation by Fluorescence	31
2.3 Spore characterisation	31
2.3.1 Determination of spore density	31
2.3.2 Hydrophobicity test	32
2.3.3 Sonication	32
2.4 Spore microwave exposure	32
2.4.1 Electric field experiments	32
2.4.2 Electric vs Magnetic field experiments	33
2.5 DNA concentration measurements	33
2.5.1 DNase treatment of spores	33
2.5.2 DNA Quantification by Qubit	33
2.5.3 Spore disruption quantification by fluorescence	34
2.6 Statistical tools used	34
3. Chapter 3. Characterisation of the spore structure of <i>C. difficile</i>	35
3.1 Introduction	35
3.2 Aims and objectives	38
3.3 Results	39
3.3.1 Identification of the optimal growth and spore purification method	39
3.3.1.1 Lawley's method	39
3.3.1.2 Sorg's method	40
3.3.1.3 Heeg's method	41
3.3.2 Characterisation of spores by Scanning Electron Microscopy (SEM)	43
3.3.2.1 Physical dimensions of spores	43
3.3.2.2 The effect of individual spore production and purification methods on spore surface architecture	44
3.3.2.2.1 DS1748	44

3.3.2.2.2	DS1813	44
3.3.2.2.3	R20291	47
3.3.2.2.4	CD630	47
3.3.2.2.5	Summary of findings	50
3.3.2.3	Sonication of <i>C. difficile</i> strains and the effect on surface architecture	51
3.3.2.3.1	Sonication of DS1748 spores	51
3.3.2.3.2	Sonication of DS1813 spores	52
3.3.2.3.3	Sonication of R20291 spores	53
3.3.2.3.4	Sonication of CD630 spores	53
3.3.2.3.5	Summary of findings	54
3.3.3	Hydrophobicity of <i>C. difficile</i> spores	55
3.3.3.1	Characterisation of <i>C. difficile</i> spore coat mutants	56
3.3.3.2	Relative hydrophobicity	57
3.4	Discussion	58
4.	Chapter 4. Characterising DNA release from spores	63
4.1	Introduction	63
4.2	Aims and objectives	65
4.3	Results	66
4.3.1	Determining required stock concentration for Qubit	66
4.3.2	Removing surface DNA from purified spores	66
4.3.2.1	DNase Treatment	66
4.3.2.2	Staining <i>C. difficile</i> spores with DNA fluorophores	68
4.3.3	DNA released from spores after microwaving	70
4.3.4	Visual appearance of spores after microwaving	72
4.3.5	Spore disruption dependence on exposure time	72
4.3.6	Asymmetrical DNA fluorescence of spores	76
4.4	Discussion	78
5.	Chapter 5. Optimising the microwave generator setup	80
5.1	Introduction	81
5.2	Aims and objectives	84
5.3	Materials and methods	85
5.3.1	Microwave system components	85
5.3.2	Cavity Q-factor	85
5.3.3	Measuring sample heating	86
5.3.4	Measuring the effect of electric field strength	86
5.4	Results	87
5.4.1	Verifying system properties	87
5.4.1.1	Verifying the power output of the system	87

5.4.1.2 Cavity Properties	87
5.4.2 Designing a minimal heating microwave setup	88
5.4.2.1 Initial estimations of sample heating	88
5.4.2.2 Actual sample heating with initial setup	88
5.4.2.3 Optimising the system to eliminate power leaks . . .	89
5.4.3 Differences between electric and magnetic field effects . . .	91
5.4.3.1 Calculating field strength in the cavity	92
5.4.3.2 Electric and magnetic field effects	93
5.5 Discussion	95
6. Chapter 6. Nanoparticle and microwave spore disruption	97
6.1 Introduction	97
6.2 Aims and objectives	100
6.3 Methods	101
6.3.1 Nanoparticles used	101
6.3.2 Modelling of Nanoparticles and Spores	102
6.4 Results	103
6.4.1 Estimating nanoparticle heating	103
6.4.1.1 Particle heating basic model	103
6.4.1.2 Heating model results	104
6.4.2 Electric field model using COMSOL	105
6.4.2.1 Nanoparticles model	105
6.4.2.2 Spore model	106
6.4.3 Spore interaction with microwaves and nanoparticles	109
6.4.3.1 DNA release by microwaved spores	109
6.4.3.2 Characterisation of spores exposed to nanoparticles	110
6.5 Discussion	115
7. Chapter 7. General Discussion	119
7.1 Characterisation of the spore structure of <i>C. difficile</i>	119
7.2 Characterisation of DNA release from spores	121
7.3 Optimising the microwave generator setup	122
7.4 Nanoparticle and microwave spore disruption	123
7.5 Final Conclusions	125
8. Chapter 8. References	127
Appendix	140

List of figures

Figure 1.1 The infection cycle of <i>C. difficile</i> .	3
Figure 1.2. Schematic representation of spore formation from a vegetative cell	4
Figure 1.3. Transmission electron micrograph of a <i>C. difficile</i> CD630 strain spore.	10
Figure 1.4. Transmission electron micrograph of a <i>Bacillus cereus</i> spore.	11
Figure 1.5. Transmission electron micrographs of different <i>C. difficile</i> strains, showing the spore structure.	12
Figure 1.6. The bow-tie setup used for MAMEF.	20
Figure 1.7. A: the opened cylindrical (pillbox) microwave cavity	22
Figure 3.1. The initial yield of spores after growth in media and final yield of purified spores of clinical isolates of <i>C. difficile</i>	39
Figure 3.2. Phase contrast microscopy of <i>C. difficile</i> DS1748 spores following purification using the Lawley method.	40
Figure 3.3. Phase contrast microscopy of <i>C. difficile</i> DS1748 spores following purification using the Sorg's method.	41
Figure 3.4. Phase contrast microscopy of <i>C. difficile</i> DS1748 spores following purification using the Heeg's method.	42
Figure 3.5. The effect of production and purification methods on the physical dimensions of spores of four <i>C. difficile</i> isolates determined from SEM micrographs.	43
Figure 3.6. SEM of <i>C. difficile</i> spores of the DS1748 strain spores produced and purified using the Lawley (A) and Sorg methods (B).	45
Figure 3.7. SEM of <i>C. difficile</i> spores of the DS1813 strain spores produced and purified using the Lawley (A) and Sorg methods (B).	46
Figure 3.8. SEM of <i>C. difficile</i> spores of the R20291 strain spores produced and purified using the Lawley (A) and Sorg methods (B).	47
Figure 3.9. SEM of <i>C. difficile</i> spores of the CD630 strain spores produced and purified using the Lawley (A) and Sorg methods (B).	49
Figure 3.10. SEM of <i>C. difficile</i> spores of the DS1748 strain spores produced and purified using the Sorg method, before (A) and after sonication (B).	51
Figure 3.11. SEM of <i>C. difficile</i> spores of the DS1748 strain spores produced and purified using the Sorg method, after sonication.	52
Figure 3.12. SEM of <i>C. difficile</i> spores of the DS1813 strain spores produced and purified using the Sorg method, before (A) and after sonication (B).	52
Figure 3.13. SEM of <i>C. difficile</i> spores of the R20291 strain spores produced and purified using the Sorg method, before (A) and after sonication (B).	53
Figure 3.14. SEM of <i>C. difficile</i> spores of the CD630 strain spores produced and purified using the Sorg method, before (A) and after sonication (B).	53

- Figure 3.15.** Change in the relative proportion of spores with a the “pineapple-like” shape (for strains DS1748, DS1813) or loose exosporium with (R20291, CD630) within a population, before and after sonication. 54
- Figure 3.16.** Relative hydrophobicities of different *C. difficile* spores produced using the Lawley and Sorg methods before and after sonication 55
- Figure 3.17.** SEM of *C. difficile* spores of the structural gene mutants of CD630, showing no visible differences in morphology. 56
- Figure 3.18.** The relative hydrophobicity of spores of *C. difficile* strain CD630 and its mutants deficient in a structural proteins. 57
- Figure 4.1.** Level of dsDNA (red line) and ssDNA (blue line) detected in spore suspensions a function of the duration of spore treatment with DNase. 67
- Figure 4.2.** Images of the same field of view unpurified *C. difficile* CD630 spores (grown using the Sorg method, but not purified), viewed under phase contrast (A) or fluorescence microscopy with 0.1 µg/ml AO (B). 68
- Figure 4.3.** Fluorescence microscopy images purified spores of *C. difficile* of strains CD630 (A), DS1748(B) without DNase treatment. After DNase treatment, the fluorescence of the spores was reduced for both the CD630 (C) and DS1748 (D). 69
- Figure 4.4.** Fluorescence microscopy images of purified spores of *C. difficile* of strain DS1748. 71
- Figure 4.5.** SEM of *C. difficile* spores of the DS1748 strain spores. A: no microwaving. B: 120 sec (10% pulse) microwaving. 73
- Figure 4.6.** Fluorescence microscopy images of purified spores of *C. difficile* of strain DS1748 using PI following exposure to microwaves (10% duty cycle). 74
- Figure 4.7** Ratio of fluorescent spores to total spores for different strains of *C. difficile*. 75
- Figure 4.8.** Images R20291 spore suspension (same field of view) viewed under phase contrast (A) or fluorescence microscopy with PI (B). 76
- Figure 4.9.** Fluorescence microscopy images of purified spores of *C. difficile* of strain DS1748 using PI (A) or AO (B). 77
- Figure 5.1.** The schematic of the setup of the microwave generator. 82
- Figure 5.2.** Temperature increase of a 150 µl sample following microwaving for 10 seconds at a given duty cycle. 89
- Figure 5.3.** Summary of the changes to the initial microwave generator system (A) to the new setup (B) to minimise power leaks. 90
- Figure 5.4.** Temperature increase of a 150 µl sample following microwaving for 10 seconds at a given duty cycle. 91
- Figure 5.5.** The fluorescence of *C. difficile* spores under PI exposed to electric and magnetic fields at a duty cycle of 0.3%. 94
- Figure 5.6.** The fluorescence of the DS1748 *C. difficile* spores under PI exposed to variable electric field at a duty cycle of 0.3% 95
- Figure 6.1.** The temperature reached by 100 nm spherical nanoparticles in water, depending on the power absorbed by the nanoparticle. 104

- Figure 6.2.** 3D model showing the focusing of an electric field by metallic nanoparticles. 106
- Figure 6.3** A simple model of multiple spore layers under the effect of an electric field. 107
- Figure 6.4.** ssDNA release from *C. difficile* spores following a 0.3% duty cycle, 30 second microwave exposure 109
- Figure 6.5.** The effect of different nanoparticle suspensions on DNA release following microwave exposure. 110
- Figure 6.6.** SEM of *C. difficile* spores of the DS1748 strain spores exposed to microwaves in the presence of 100 nm spherical gold nanoparticles. 111
- Figure 6.7.** SEM of *C. difficile* spores of the R20291 strain spores exposed to microwaves in the presence of 100 nm spherical gold nanoparticles. 112
- Figure 6.8.** SEM of *C. difficile* spores of the DS1813 strain spores exposed to microwaves in the presence 30 nm spherical nanoparticles. 113
- Figure 6.9.** SEM of *C. difficile* spores of the CD630 strain spores exposed to microwaves in the presence 30 nm spherical nanoparticles. 113
- Figure 6.10.** SEM of *C. difficile* spores of the DS1813 strain spores exposed to microwaves in the presence 30 nm spherical nanoparticles. 114

List of Tables

Table 2.1. Strains of <i>C. difficile</i> used.	28
Table 3.1 Methods used to produce and purify of <i>C. difficile</i> spores	36
Table 6.1 Nanoparticle types used	100

List of Abbreviations

AO	acridine orange
BHI	Brain Heart Infusion
cfu	colony forming units
dB	decibel
dBm	decibel-milliwatt
dsDNA	double-stranded DNA
E-field	electric field
g	relative centrifugal force
H-field	magnetic field
min	minute
n	Number of replicates
nm	nanometre
OD ₆₀₀	Optical Density with 600 nm light
PI	propidium iodide
RF	radiofrequency
rms	root mean square
SEM	Scanning Electron Microscopy
sec	second
ssDNA	single-stranded DNA
TEM	Transmission Electron Microscopy
V/m	Volt per metre
° C	degrees Celsius
µg	microgram
µl	microlitre

Chapter 1

Introduction

1.1 Historical Background

Clostridium difficile was first isolated in 1935 under the name *Bacillus difficilis*, referring to difficulty of its isolation. At the time, little work was done on the newly discovered bacterium, as it was not thought to be a pathogen of humans (Bartlett, 1994). In the early 1970s, a new antibiotic, clindamycin began to be used to treat patients with anaerobic infections. Unfortunately, deaths of patients treated with clindamycin were reported (Tedesco *et al.*, 1974). Typically, the patients' symptoms started with diarrhoea, which later deteriorated. Inflammation of the colon resulted in the formation of pseudo-membranes filled with fibrin, leucocytes and dead cells which prevents the normal uptake of food. Initially, it was thought to be an adverse effect of the antibiotic and the disease was called "clindamycin colitis". However, no link between clindamycin and the disease was found, and the disease was renamed "pseudomembranous colitis" or PMC (Lyerly *et al.*, 1988). Finally, in 1978, *C. difficile* was identified as the causative agent of the disease (Bartlett *et al.*, 1978), countering earlier claims the disease may be caused by *Clostridium sordellii*. Interestingly, infants are usually asymptomatic to *C. difficile*, even though as many as 50% carry it in concentrations that would cause disease in adults. Lower sensitivity of the infant colon has been suggested as possible cause. It is thought that infants may lack the receptor protein for one of the toxins or part of the reaction cascade

necessary for toxin action (Pothoulakis & Lamont, 2001). *C. difficile* became the most common cause of hospital acquired diarrhoea in both the US and UK in the 90-s, (Kelly & LaMont, 1998; McNulty et. al. 1997).

1.2 *C. difficile* overview

C. difficile is an obligatory anaerobic Gram-positive bacterium. Under stress, low nutrients or following oxygen exposure, *C. difficile* vegetative cells sporulate (form spores). Vegetative *C. difficile* is very sensitive to oxygen and will die if it does not sporulate. Only spores survive in aerobic conditions (Dapa *et al.*, 2013).

C. difficile infection is an intestinal disease, ranging from asymptomatic, to mild diarrhoea to pseudomembrane colitis, which can lead to death (Voth & Ballard, 2005; Smits *et al.*, 2015). The disease is transmitted by the oral-fecal route, primarily among people with weaker immune systems and depleted gut flora. A person ingests the bacteria from a contaminated source and the spores pass through the digestive system. While vegetative bacteria die due to stomach acid, spores survive passage through the stomach and germinate and divide in the duodenum. Patients may asymptomatic, but still be carrying the disease. An infected person's faeces contain *C. difficile* spores, which then contaminate and survive in the environment (such as bed sheets and door handles) for a long time (Salyers & Whitt, 2002). The infection cycle of *C. difficile* is shown on Figure 1.1.

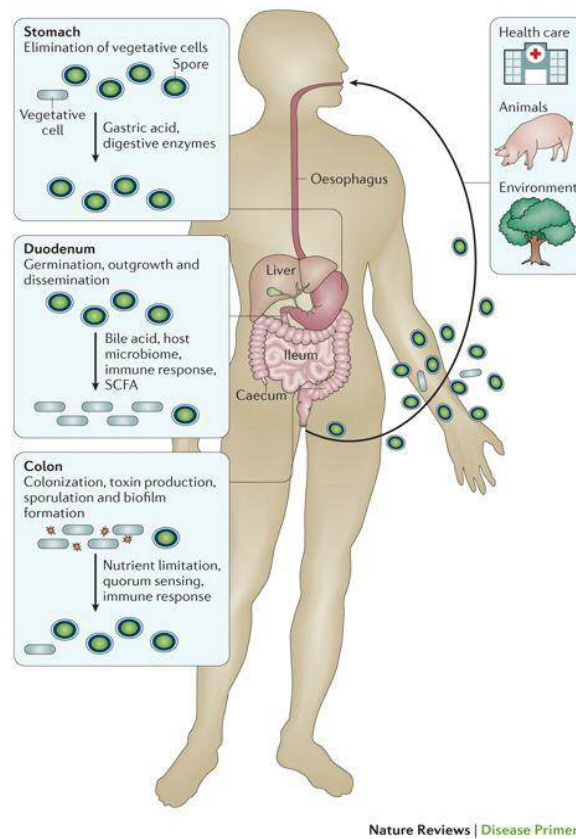


Figure 1.1 The infection cycle of *C. difficile* (Smits *et al.*, 2015). Spores allow the species to survive in the environment and stomach acid, before germinating in the duodenum.

1.2.1 Sporulation

Sporulation is process of forming the spore from the vegetative cell. Sporulation begins as a form of cell division. This division is asymmetric, with the future spore section being much smaller than the vegetative portion. The future is then engulfed by the mother cell and spore coat and exosporium assembly begins starting from the mother cell side (Higgins and Dworkin, 2012). The order of this assembly is governed by sigma-factors (σ -factors). In *C. difficile*, σ^F and σ^E control the formation of inner coat layers, while σ^G and σ^K control the formation outer coat layers and exosporium (Pereira *et al.*, 2012). Once the spore formation is complete, the vegetative cell lyses and the spore is released.

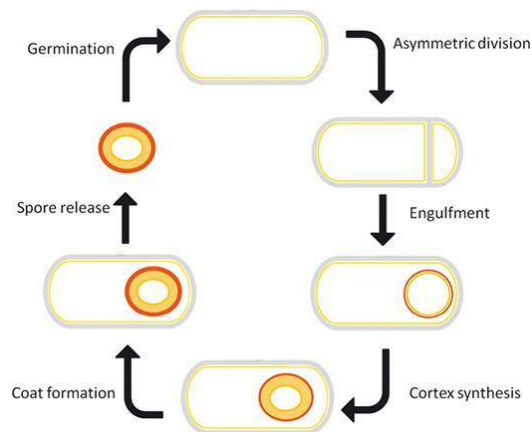


Figure 1.2. Schematic representation of spore formation from a vegetative cell (Higgins and Dworkin, 2012).

1.2.2 C. Difficile epidemiology

Spores are resistant to antibiotics, stomach acid, desiccation, temperatures of up to 95⁰C, alcohol-based cleaning agents and other chemical biocides and can survive for several months on surfaces and in the environment (Fordtran, 2006, Kim *et al.*, 1981). Notably, spores resist alcohol hand disinfectant and quaternary ammonium-based cleaning agents (Owens, 2006). Some cleaning agents (detergent and peroxide based) are thought to promote the sporulation of vegetative bacteria (Fawley *et. al.*, 2007).

Normally, gut flora prevents colonisation of *C. difficile* by producing modified bile salts. Chololate salts, such as taurocholate and glycocholate induce the germination *C. difficile*. However, bile salt derivatives produced by gut microflora actually inhibit either the spore germination or growth of germinated cells (Sorg & Sonenshein, 2009). Of particular interest is deoxycholate, a germinant, but vegetative growth inhibitor. Deoxycholate is produced by the bacterial reduction of cholic acid, a bile salt found in the gut. Microflora also break down glycine and taurocholate, which are germinants of *C. difficile* (induce germination of spores) (Giel *et al.*, 2010). An inhibitor of both taurocholate-induced germination and vegetative growth is chenodeoxycholate (competitive inhibitor). Some analogs of chenodeoxycholate are more effective at inhibiting germination and resist degradation by *C. scindens*, a species commonly found in the gut (Sorg & Sonenshein 2010). Thus, the gut microflora provides protection from *C. difficile* infection: ingested

spores may germinate in the duodenum but are unable to grow. Antibiotic treatment, such as clindamycin, removes the gut flora, which result in higher concentrations primary bile salts, while reducing concentration of modified salts, and this allows *C. difficile* to grow (Sorg & Sonenshein, 2008).

Vegetative *C. difficile* itself is resistant to many antibiotics. The CD630 strain, for example, is resistant to bacitracin (encoded by the CD0643-646 genes), tetracycline (Tn5397), ampicillin (beta lactamase CD0458, CD0470), cefoxitin, gentamycin, and several others. Similar genes were reported in other isolates, like the inferred beta-lactamase, undecaprenyl-diphosphatase and lysyltransferase in the R20291 strain (UniProt database C9YIK5, C9YQF6 and C9YPU7). That *C. difficile* both resists many antibiotics and easily colonises (with germinating spores) in patients who have had recent antibiotic treatment makes it a very large problem in hospitals (Sebaihia et. al., 2006).

The standard UK guidance for treating *C. difficile* infection is usage of metronidazole and vancomycin with doses of up to 500 mg four times daily, depending on disease severity (Kuipers & Surawicz, 2008). Resistance to these antibiotics has emerged across Europe, but is low as of 2015 (Freeman *et al.*, 2015). A more recent compound, fidaxomycin, has shown better performance in managing recurrent disease, there has been no observed resistance at the time of writing, but its very high cost precludes wide-scale usage. In general, metronidazole is used for milder cases, while vancomycin is used for more severe cases (Public Health England, 2013).

C. difficile infection causes thousands of deaths annually. Centers for Disease Control (CDC *C. diff* 2015) data from the USA for 2011 attributed approximately 500,000 cases and 29,000 deaths to the pathogen. Public Health England and Wales (PHE *C. diff* annual data 2015), (PHW monthly *C. Diff* update 2015) and Office of National Statistics (ONS *C. diff* 2015) data shows 14,993 confirmed cases in England and approx. 2,000 in Wales in 2012, with 2,053 deaths reported. While UK cases have reduced significantly from a peak in 2007 of 60,000 cases and 8,300 deaths, due to rigorous enforced hygiene in

hospitals, it remains a major problem and represents considerable financial burden, with each case incurring between £4,000 and £8,000 in additional costs (Wiegand *et al.*, 2012).

1.2.3 Toxins

The pathology of *C. difficile* is primarily due to the production of two toxins, named TcdA and TcdB. TcdA is an enterotoxin which targets the epithelium of the colon. TcdB is a cytotoxin, and responsible for cell pore formation. Both toxins are glucosyltransferases that target small GTP-ases, specifically Rho and Ras proteins. The toxins are absorbed into the cells by endocytosis. The acidic environment causes a conformational change, and the glucosyltransferase domain of the toxin is inserted into the endosome membrane and cleaved by autocatalytic cleavage. The glucosyltransferase glycosylates the Rho and Rac proteins, making them no longer work (Jank & Aktories, 2008). This leads to cell death, which results in the production of actin rich cell debris. In addition, the toxins increase vascular permeability leading to bleeding in the colon. The accumulation of cell debris filament proteins such as actin, results in the formation of small pseudomembranes that are filled with cell debris and leucocytes which have migrated to the inflammation site. (Poxton *et al.*, 2001). The resulting reduction in colon surface area available for absorption (in severe cases the pseudomembranes block most of the colon surface) can lead to death. Initially, there was confusion over which toxin was more significant in causing disease symptoms. Early experiments showed toxin A was causing disease (Voth & Ballard, 2005). However, following a paper in Nature by Lyras *et al.* (2009), toxin B was thought to be more important than toxin A in causing disease and toxin A alone was not virulent. Finally, in 2010, a study by Kuehne and colleagues, using individual gene knock out variants of *C. difficile*, were able to show that each toxin alone was capable of causing the symptoms associated with infection (Kuehne *et al.*, 2010).

The genes which encode the toxins and regulate their expression are located in a region of the genome called the pathogenicity locus (PaLoc). It is a 19.6 kb region that includes TcdA, TcdB and three regulatory genes. Non-virulent strains of *C. difficile* lack PaLoc completely, and as such, PaLoc is replaced with a short non-coding region. TcdR, which

was earlier known as TcdD is a positive regulator of toxin expression (Spigaglia & Mastrantonio, 2002). TcdC, on the other hand is a down regulator of toxin expression (Hinkson *et al.*, 2008). The third gene is TcdE, encoding a holin-like protein, which is thought to assist toxin release from the cell (Tan *et al.*, 2001). Hypervirulent strains have been found to have deletions in their TcdC gene and produce more toxin, notably, the NAP1/027 strain (McDonald *et al.*, 2005).

Separate from the PaLoc, a different toxin is produced by some strains of *C. difficile*. The Binary toxin, CDT is encoded on a separate locus, CdtLoc, and has two essential components. The first component, CDTa, is an ADP-ribosyltransferase which can modify actin and thus damage cell cytoskeleton. The second component, CDTb, is a binding protein which is responsible for transporting the toxin to the cells (Geric *et al.*, 2006). While the presence of the binary toxin genes in highly pathogenic strains of *C. difficile* has been reported, their contribution to pathogenicity has yet to be determined (Gerding *et al.*, 2014).

1.2.4 Typing of *C. difficile*

Typing bacteria is a way of grouping together strains of a bacterial species by common characteristics and aids in determining the source of an outbreak. It also helps identify genes that play a role in virulence of the disease. The two common way of typing *C. difficile* are toxinotyping and ribotyping.

The study of the PaLoc locus has resulted in the development of a DNA-based typing method for the categorisation of *C. difficile* strains. While toxinotypes do not directly correlate with disease severity, some toxinotypes have been associated with severe disease (Bruggeman & Gottschalk, 2009). Toxinotype categorises the strains by differences in the PaLoc, compared to the reference strain VPI 10463, which has been set as toxinotype 0. That strain produces restriction digest fragments of known size and location of the PaLoc. By comparing the fragment sizes between the reference strain and

the studied strain, addition mutation and deletion mutations can be found and located. Since examining the entire locus of every sample is too labour intensive, researchers focus on the DNA fragments B1 (covering the 5'-end of *tcdB*) and A3 (covering the 3'-end of *tcdA*) (Rupnik, 2008).

Another method commonly used to categorise *C. difficile* isolates is ribotyping, which identifies the differences in the 16S-23S rRNA non-coding region. The method is fast, reproducible, and has been used to build a library of over 100 different ribotypes (Stubbs *et al.* 1999). Although rRNA does not directly affect virulence, some ribotypes are associated with more virulent strains, such as the 027 hypervirulent ribotype, which includes strains with high mortality. In 2007-2008, during the peak of *C. difficile* infection in UK hospitals, the 027 ribotype accounted for nearly 65% of all analysed clinical samples (CRDN 2011-2013 report). The other major strains were the 001 and the 106 ribotypes. In 2013, following efforts to reduce cross contamination in hospitals, the 027 ribotype accounts for less the 10% of the analysed samples, and there was no single dominant strain in hospitals (CRDN 2011-2013 report). Among emergent strains is the 078 ribotype, which, like 027, has a deletion in TcdC gene. This strain is thought to have originated from animal husbandry, as isolates have been identified in cattle and pigs, and the 078 were more frequently found in patients from rural areas (Goorhuis *et al.*, 2008).

1.3 Spore structure

Spores are dehydrated inactive forms of a bacterium. Many *Bacillus* and *Clostridium* species sporulate under conditions unfavourable for vegetative cell growth. Transmission electron micrographs of spores show a multi-layer structure like the one shown in Figure 1.1. There are differences in the structure, shape and behaviour of spores between species, but key structural elements described below are common to all spore formers: (Setlow, 2007)

- At the centre of the spore is the core, containing the DNA and other essential cellular machinery. The core is dehydrated (20-25% wet weight), and inactive. The water in the core is replaced with Ca^{2+} -dipicolinic acid.
- Surrounding the core is a mostly impermeable membrane, which isolates the core from the cell wall. It serves as the base of the vegetative membrane and cell wall when the spore germinates.
- The next layer is the germ cell wall, which will become the cell wall of the germinated cell.
- The next layer of the spore is a cortex, composed of peptidoglycans, which is thought to aid the stability of inner layers and is rapidly degraded during spore germination.
- The next thick and dense layer of the spore is spore coat. It is primarily protein-based, and is composed of multiple layers of different proteins. The coat of *B. subtilis*, for example is composed of over 70 different proteins. The spore coat has several protective functions. First, it gives the spore structural strength. Second, the coat resists degradation by such as proteinases and hydrolases, which be found in the digestive systems of the host. Third, the coat regulates spore germination, as any germinants must pass through it (McKenney *et al.*, 2013).
- Some, but not all spore forming species possess the additional outermost layer, known as the exosporium. Different structural features are referred to by this name and so this layer is described in detail below.

A transmission electron micrograph of a *C. difficile* spore with all its layers is shown on Figure 1.3.

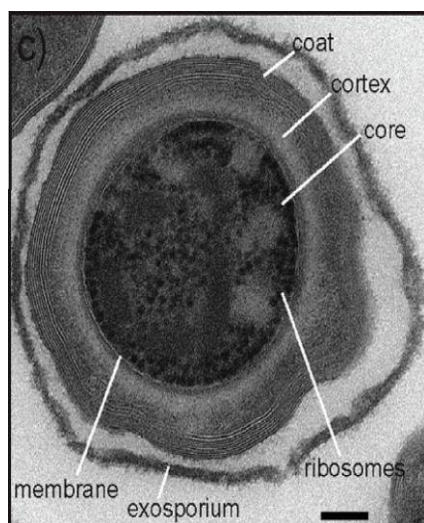


Figure 1.3. Transmission electron micrograph of a *C. difficile* CD630 strain spore, with the key structural layers identified from innermost to outer: core, membrane, cortex, coat and exosporium. Scale bar is 100 nm. (Lawley *et al.* 2009)

1.3.1 The exosporium and its naming debate

Some spore-forming bacterial species, like *Bacillus cereus*, have an extra layer, the exosporium, covering the spore. The exosporium is a less dense material layer surrounding the main coat protein and is somewhat less stable. Being the outermost layer of the spore and the first to interact with the environment, the exosporium may play a role in spore germination, and virulence of the strain (Panessa-Warren *et al.*, 2007). The exosporium of some *Bacillus* species is a loose “baggy” layer around the spore, with a base hexagonal structure around 8 nm in size (Ball *et al.*, 2008). It was later shown that CotY and CotE proteins can self-assemble into a similar honeycomb structure. X-ray crystallography a crystallisation pattern of CotY which formed the same hexagonal structure (Terry *et al.*, 2017). Hair-like appendages, which can be seen in extending from the exosporium have been proposed to be include of the CotW and BclA proteins (Jiang *et al.*, 2015). A high magnification TEM of the exosporium is shown on Figure 1.4.

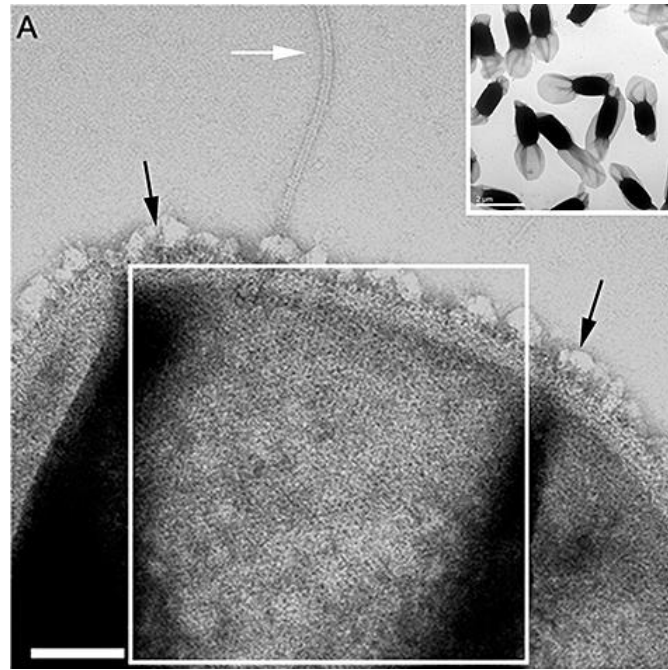


Figure 1.4. Transmission electron micrograph of a *Bacillus cereus* spore, with negatively stained spore image top right thumbnail, and a high magnification view on the exosporium on the main image (Ball *et al.*, 2008). Black arrow show the nap, white arrows show spore appendages. Scale bar is 100 nm.

In contrast to *B. cereus*, the outer layer of *C. difficile* is quite varied (Figure 1.4). Some stains show a very distinct exosporium, with no hair-like projections and the exosporium appears to be tightly bound to the spore coat. Other stains have hair-like projections, but still have a tightly bound layer, which can be removed by intense sonication and proteinase treatment (Barra-Carrasco *et al.*, 2013, Pizarro-Guajardo *et al.*, 2016). Other stains possess a baggy exosporium (Joshi *et al.*, 2012).

The large variety in the outer layer structure of spore forming species has led to recent attempts to no longer use the word “exosporium” for the outermost layer of *C. difficile*, or split the term “exosporium” into separate sub-structures. Thus, when discussing *B. subtilis* and some *B. anthracis* strains, McKenney *et al.* use the term “crust” (McKenney *et al.* 2013). When describing the outer layer of unpurified *C. difficile* spores from biofilms, Semenyuk *et al.* describe a new outer layer, which they call the “shroud”. And

when describing the well characterised 630 strain, Díaz-González *et al.* refer to the outer layer as “exosporium-like” (Díaz-González *et al.*, 2015).

None of the new terminology is official or finalised, so for the purposes of this report, the term “exosporium” will still be used with regards to the outermost layer of *C. difficile*, unless otherwise stated.

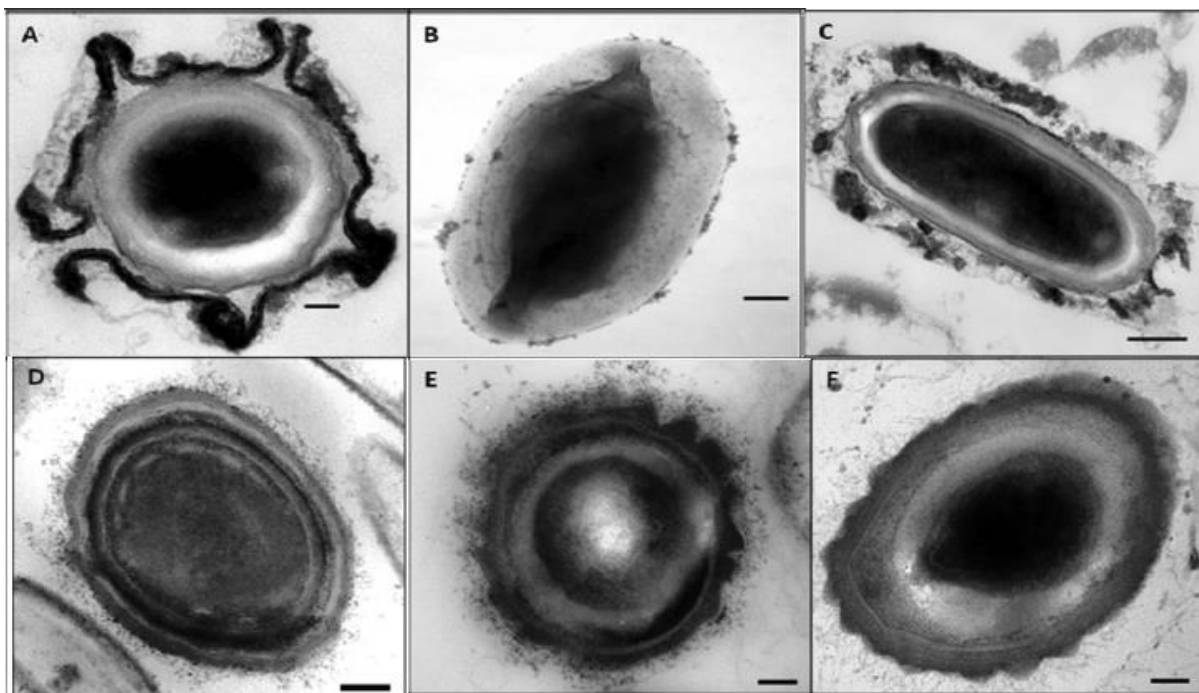


Figure 1.5. Transmission electron micrographs of different *C. difficile* strains, showing the spore structure. Scale bars are 100 nm. A, B and C are DS1813 spores, showing a less dense exosporial layer. D is DS1771, E is DS1684, and F is DS1748. D, E and F show the same concentric structure, but no reported exosporial layer (Joshi *et al.*, 2012)

1.3.2 Spore surface proteins

Several *C. difficile* structural coat and exosporium proteins have been identified and described over the past few years, but it was confirmed the proteins involved in *C. difficile* spore formation are very different from *Bacillus* species. Sebahia *et al.* (2006) reported that 52 of the 70 known *Bacillus* spore coat genes have no *C. difficile* homolog, indicating that composition of the spore coat differs significantly.

The *C. difficile* BclA proteins have *Bacillus* homologs. They are primarily exosporium glycoproteins, originally identified in *B. anthracis*, hence the name: *Bacillus* collagen-like protein of *Anthraxis*. In *Bacillus* species, BclA are surface proteins, composing a part of the hair-like projections seen on the *B. cereus* and *B. anthracis* (Stewart, 2015). Although *C. difficile* does not show the same hairlike projections, it still expresses three BclA protein homologs: BclA1, BclA2, and BclA3. Inactivation of either BclA1 or BclA2 in *C. difficile* 630 strain resulted in visible changes in spore structure, with spores becoming malformed. It was also noted that while the spores without BclA germinated faster, they showed reduced infectivity than spores of the wild-type strain, suggesting that BclA may contribute to virulence. The precise role is unclear, but hypervirulent 027 ribotype strains have been found to have a truncated version of the BclA1 gene, and as a consequence produce an incomplete protein of only 6 kDa compared to a normal size of 90 kDa (Phetcharaburanin *et al.*, 2014).

Cot proteins are a family of outer spore coat of *C. difficile* which were first isolated in 2011. Five proteins, named CotA to CotE have been identified (not equivalent to *B. subtilis* proteins with the same name). Some of these have homologs in other species, such as CotB structural protein and CotD manganese catalase, which was similar to CotJC inner spore coat protein found in *B. subtilis* (Permpoonpattana *et al.*, 2011). Of great interest are the CotA structural protein, and the CotE bifunctional protein. Knockout of CotA result in malformed spores suggesting an essential role in coat assembly, similar to CotE found in *B. subtilis*. The CotE protein of *C. difficile* has no homologs in other species. It is a bifunctional protein with C-terminal chitinase activity and with N-terminal peroxiredoxin activity and is thought to be partially located in the exosporium (Permpoonpattana *et al.*, 2013). The conserved chitinase activity is unusual as *C. difficile* spores do not encounter chitin in the gut.

Another protein of interest is the CdeC protein. This exosporium protein has been identified as a key component in the exosporium assembly, and without it the exosporium does not form a layer around the spores.

1.4 Current *C. difficile* detection methods

Detecting *C. difficile* infection fast is very important. Not only does early detection allow earlier treatment and better prognosis for the patients, early detection is important in ensuring hospitals are clean and minimising the risk of acquiring the disease. It is also important that the number of false-positives and false-negatives is minimised (Aslan *et al.*, 2008, Joshi *et al.*, 2014). False-negatives delay essential treatment and waste time on testing for possible other causes of the symptoms investigated. False-positives result in unnecessary antibiotic usage, potentially leading to resistance, as well as discontinuation of existing antibiotic treatment (Planche & Wilcox, 2010). Thus an ideal system will be fast-acting, with low cost and with a minimum number of false negatives and false positives.

1.4.1 Bacterial culture

Direct culture is the oldest method to detect *C. difficile* infection. However, growing *C. difficile* requires an incubation of up to 48 hours in anaerobic conditions, making this method slow and expensive. Cycloserine cefoxitin fructose agar (CCFA) is the most common agar, which has been used for several decades, but it allows non toxinogenic species to grow just as easily as *C. difficile* (Delmee *et al.*, 2005). As a result, the strain will need to be additionally tested to verify that the strain is toxinogenic (Goldenberg & French, 2011). A two-step process to selectively grow the bacteria and then test for toxin production can take up to 5 days.

An alternative agar for growth is Clostridium Difficile Moxalactam Norfloxacin agar (CDMN), which is selective for *C. difficile* and prevent the growth of even the closely related *C. sporogenes* (Aspinall *et al.*, 1992).

1.4.2 Cell cytotoxicity assay

The cell cytotoxicity assay (CCTA) is commonly used to identify *C. difficile*. The method uses a sterile filtrate of a sample (for example, a clinical faecal sample) on a monolayer of HeLa cells. The cells are examined using a microscope before and after a 48 hour incubation with the filtrate for changes in cell morphology (Delmee *et al.*, 2005). Vero or Hep2 can also be used (Planche & Wilcox, 2011). After a cytotoxic effect on the cells is confirmed, the cells are exposed to a combination of filtrate and the toxin antibody for 24 hours to see if the effect has been neutralised. While this method is highly sensitive (94%) and specific (99%) (Snell *et al.*, 2004), it is expensive and time consuming due to tissue culture requirement.

1.4.3 Enzyme immunoassays

Enzyme immunoassays detect the presence of toxins A and B. There are several commercial testing kits, which allow results in under 1 hour but they are not routinely performed at the bedside and thus there are delays while the sample is shipped to a local laboratory for processing. A key drawback of these tests is insufficient sensitivity (Tenover *et al.*, 2010; Tenover *et al.*, 2011). Another limitation is the cost of the kits. Some kits combine toxin testing with an immunoassay for the enzyme glutamate dehydrogenase (GDH), a common antigen of *C. difficile* infection. This improved the sensitivity of the test to 78%, however a number of test results was contradictory, with positive GDH, but negative toxin, with some false positives among these (Sharp *et al.*, 2010).

1.4.4 PCR-based assays

PCR assays amplify the target DNA, such as the genes encoding *C. difficile* toxins, like *TcdB*. Existing systems, such as Cepheid Xpert promise detection in 45 minutes from the clinical sample with high sensitivity (99%) and specificity (95.1%) (Barbut *et al.*, 2009). However, 45 minutes of laboratory time is still a large time requirement for a diagnostic system. In addition, there is the added cost in proprietary kits. Finally, the problem with

DNA assays is the requirement for DNA. PCR works well with stool samples of patients, where there is DNA of lysed vegetative cells, but this will not work for testing surfaces or early stages of infection as the DNA will be locked in the spore and inaccessible for PCR.

1.5 Microwaves

A new approach in detecting bacteria and extracting usable DNA from samples is in using microwaves. Microwaves provide a way to accelerate the detection process from 45 minutes in immunoassays, to as little as 1 minute (Aslan *et al.*, 2008).

1.5.1 Mechanism of action

Microwaves are electromagnetic waves with the wavelength of 1-1,000 mm. They provide a cheap, simple and reliable method of delivering energy towards a target (Sorrentino *et al.*, 2010). Like all electromagnetic waves microwaves have two components: the electric field and magnetic field, perpendicular to each other. These fields affect the materials around them. The electric field will accelerate charged particles along the field lines. The magnetic field induces an electric current in electrical conductors and can cause inductive heating (Feynman, 1964).

In poorly conducting materials, such as protein, there would be no induction. The charge to mass ratio of molecules is too low to cause any acceleration of particles from the material. Instead, the molecules realign themselves to match the field with their polar region, and as the field alternates rapidly (a kitchen microwave operates at around 2.4 GHz), the resulting vibration of molecules generates heat. The heating is called dielectric heating (Piyasena *et al.*, 2003).

Typically, microwave action in biological applications is assumed to be heating alone. Indeed, microwaves have been used since the 90-s to deactivate bacteria and spores, for both hospital applications (Pellerin, 1994) and industrial food treatment (Vaid and Bishop, 1998). Microwaves are capable of inactivating both vegetative bacteria and spores,

including *Bacillus anthracis*, *Bacillus subtilis* (Celandroni *et al.* 2004), *Bacillus licheniformis* (Kim *et al.*, 2009) and *C. sporogenes* (Vaid and Bishop, 1998). Since nothing except electric power and the microwave device is required, the procedure is very cheap.

However, the effect of microwaves is not limited to heating alone. A spore structure contains polar molecules (such as polar groups on proteins) within the tightly packed spore coat. The movement of the polar regions in response to the alternating electric field can cause structural damage to the coat, without any required heating. These effects were seen in high power microwave exposure by Celandroni *et al.* (2004). *B. subtilis* spores were disrupted with structural changes that appeared different from effects of directly heating the spores. Similar results were later obtained by Kim, 2009 with *B. licheniformis*. High power microwaves cause spore damage distinct from heating.

These experiments used high power microwave sources (kW range), making it difficult to separate the electric field heating and non-heating effects. A high electric field can be generated at low power, without high sample heating, by focusing the microwaves using a specialised microwave cavity.

1.5.2 Microwave cavity

A radiofrequency (RF) cavity is simply a metal chamber containing an electromagnetic field. For example, an ordinary kitchen microwave is a microwave cavity, where the energy from the alternating electric field is absorbed, and this heats up the food. Microwave cavities work by creating standing waves with fixed field values at a given location. Due to the nature of standing waves, a cavity will have an optimum resonant frequency where the field values are the highest at the desired location (Pozar, 1998). Since the field is trapped in the cavity, all power is ultimately either absorbed by the materials or reflected back. Resonant cavities are very efficient at delivering targeted energy to a sample.

More specialised cavities can focus and direct the electric and magnetic field depending on the purpose. While in a common microwave, the field is spread out to ensure heating of food, in a specialised cavity, the electric field can be focused in a small volume. The electric field in an RF cavity can be used to accelerate and realign charged particles. This movement generates heat in materials. The ability of a cavity to maintain high field values with low power (in other words the ability to store energy) is referred to as the Q-factor (Gerigk, 2011).

1.6 Nanoparticles

Nanoparticles are particles with a diameter of 1-100 nm. Numerous nanoparticles exist, made of materials, including, but not limited to gold, silver, carbon, and magnesium. The antimicrobial potential of nanoparticles has been recognised for a few years, with wide research into the direct antimicrobial action of nanoparticles of different materials. For example, zinc oxide nanoparticles were effectively used against *B. subtilis* (Gunalan *et al.*, 2012), while gold against *E. coli* (Hayden *et al.*, 2012).

1.6.1 Mechanisms of nanoparticle activity

Nanoparticles have several mechanisms by which they can they cause their effects.

Silver particles have been of particular interest due to the production of silver ions by the nanoparticles and due to the formation of reactive oxygen species (ROS). Silver nanoparticles were shown to degrade the ultrastructure of bacteria *E. coli* and *P. aeruginosa* with concentration of 2.7 µg/mL (Ramalingam *et al.*, 2016). Metal ion absorption leads to release of groups, such as carboxyl- (COOH) and mercapto- (SH), inhibition of enzymes, which ultimately leads to bacterial cell death (Wang *et al.*, 2017).

Non-metallic nanoparticles like graphene work via oxidative stress without metal ions and radical species production. At sufficiently high doses, the nanoparticles also lead to DNA degradation (Gurunathan *et al.*, 2012).

Finally, some nanoparticles can produce an antibacterial effect without any ROS or oxidative stress. MgO nanoparticles were shown to inactivate *E. coli* and damage the membrane without ROS release, with effects attributed to nanoparticle attachment and pH change (Leung *et al.*, 2014). Another study noted that silver nanoparticles can physically break the bacterial cell wall at concentrations of 180 $\mu\text{g/mL}$, and that this effect is based on shape of the nanoparticles (Acharya *et al.*, 2018).

1.6.2 Microwaves acting on nanoparticles

Metallic nanoparticles will focus an electric field, producing a localised high field on the surface. Conductive nonmagnetic particles will not heat from electric field, as they will not be subject to dielectric heating, they will focus electric field on their surface. On the other hand, semiconductive particles will be subject to dielectric heating and will produce a localised heating effect. As for magnetic particles, they will similarly absorb the magnetic field (Porch *et al.*, 2013).

This effect has been investigated for medical applications. For example, 70 nm magnetite (Fe_2O_3) nanoparticles were used recently as an in-vitro demonstration of localised hyperthermia of biological tissue for cancer treatment (Kim *et al.*, 2016). In this experiment, nanoparticle-treated tissue reached higher temperatures than non-treated tissue, allowing for targeted energy delivery for killing cancer cells. This allowed to limit the microwave source power to below 1W. Heating occurs due to normal dielectric heating in the tissue, and the nanoparticles merely enhance the local tissue properties, rather than providing the heat directly (Pearce *et al.*, 2016).

These properties of nanoparticles make them very good tools for delivering energy to the spores. As nanoparticles are much smaller than spores, only a small part of the spore will be subjected to the physical and microwave-induced effects.

1.7 Microwave-based bacterial detectors

1.7.1 Microwave-accelerated metal-enhanced fluorescence (MAMEF)

A technology described by Aslan *et al.* in 2008, it demonstrated the ability to detect *B. anthracis* spores in under 1 minute. This was achieved by detecting the DNA released from the spores. Spores were placed on glass slides with a bow-tie shaped metal structure (Figure 1.5), deposited to focus the microwaves and maximise the effect. Spores were exposed to a short microwave pulse, which was sufficient for spores to release DNA. Afterwards the solution containing the DNA was mixed with a fluorophore-labeled oligonucleotide and was deposited on a silver island film (SIF nanoparticles) containing an anchor for the target (in this case anthrax) DNA. The mixture was briefly heated using a 2.45GHz microwave source. Nanoparticles are important as they serve as a platform for fluorophore binding. They also amplify fluorescence. Finally, they are not directly heated by microwaves and so form a temperature gradient, ensuring molecular movement towards them (Aslan *et al.* 2009).

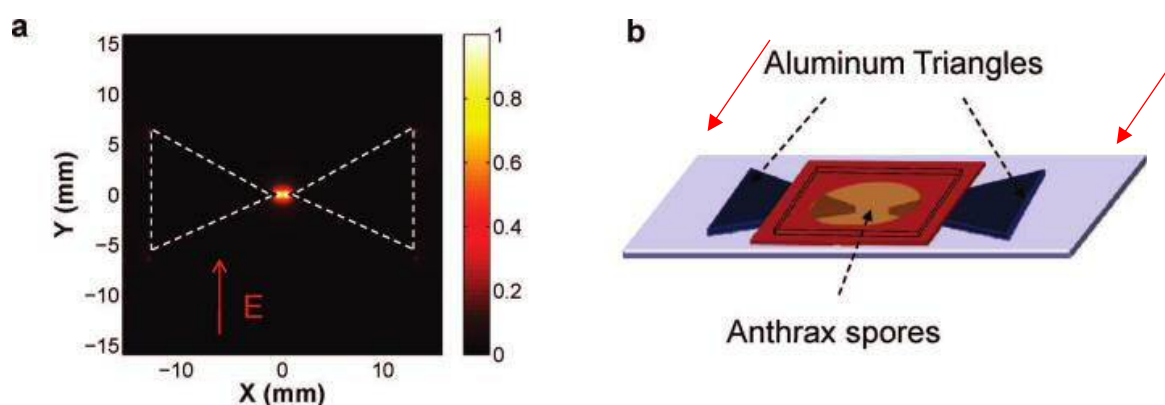


Figure 1.6. The bow-tie setup used for MAMEF. A 140 W power was used to generate an electric field along the surface of the slide for 30s with an unspecified duty cycle. a: the aluminium triangles are used to focus the microwave electric field in the space between the two tips, the electric field outside the area being minimal. b: the setup with spore sample on top of the triangles. The overall heating of the bulk liquid sample was reported to be from 23° C to 28° C. Image from Aslan *et al.*, 2008

The results successfully demonstrated that the released DNA could be detected within 1 minute and thus confirm the presence of the pathogen. In this scenario, microwave induced spore disruption may have been caused by induced electric fields in combination with heating or by the expansion of heated water. Changes to the spore structure, after microwave exposure were visible under transmission electron microscopy.

The technology was further developed by Joshi (2014), and adapted for the detection of *C. difficile* DNA, specifically the conserved regions within toxins A and B. Detecting the toxin genes was considered a better target than the detection of the toxins themselves for 2 reasons. First, it allowed the detection of spores, which do not produce any toxin until they germinate. Secondly, by detecting the spores, and not just vegetative bacteria, it was possible to identify patients who are carrying the pathogen and thus are at risk of developing the disease. The technology is able to detect less than 1000 cfu (colony forming units) of *C. difficile* in faeces in 10 min, an improvement over the initial demonstration by Aslan *et al.* in 2009 in which used 10^5 spore/ml concentrations.

1.7.2 Low power microwave system

The limitations of the MAMEF system described above were the need for a commercial high-power (kW range) microwave cavity, which made the system bulky and the use of a single microwave frequency which limited its flexibility.

To address these issues a pillbox type microwave cavity was developed at the Cardiff School of Engineering (Figure 1.5). The cavity input power was set to be no higher than 30 W, as opposed to the earlier high power experiments using 700 W and more. The cavity was a TM_{010} cylindrical cavity, meaning the electric field is axial (“up/down” on Figure 1.6), while the magnetic field is azimuthal (circular).

This system uses a low power signal generator (1 mW rms) and the signal is then amplified with a power amplifier to 30W. This power is then applied to a 170 μ l sample. To further control the power input and to avoid overheating the sample (which would present a hazard due to spore samples), power could be applied in short pulses, limiting

undesired heating. For example, at 1% duty cycle, the effective power is only 0.3 W so a 0.2 ml aqueous sample would only heat up by 0.36°C in one second.

The system is controlled with an in-house program written in LabVIEW. The user-friendly program allows a someone who is not an electrical engineer to operate the system without much difficulty.

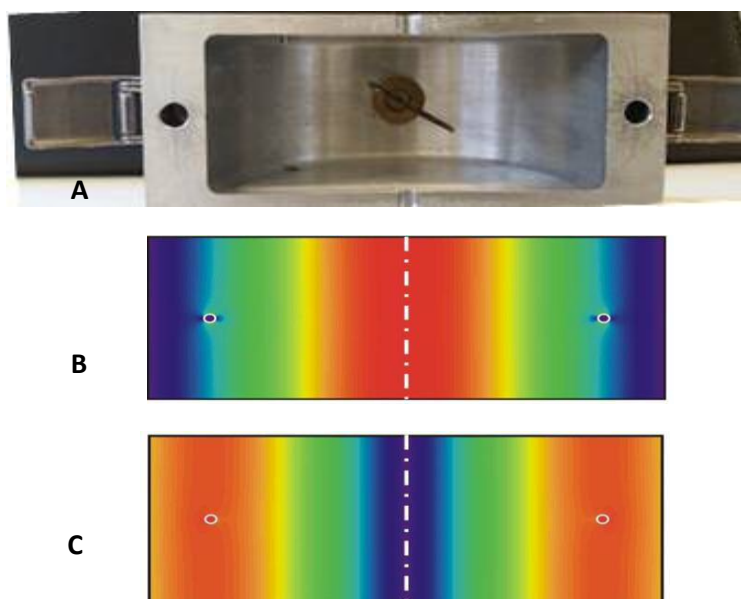


Figure 1.7. A: the opened cylindrical (pillbox) microwave cavity. B: The electric field distribution in the cavity. C: The magnetic field distribution in the cavity (Williams *et al*, 2016). Red light indicates higher values (actual value depending on power input). Deep blue indicates zero.

The cavity focuses the microwaves at a small area at the sample holder, where a high electric field (10^5 V/m) is generated. This meant that despite low heating, electric field effects (if they are distinct from heating) will be maximised.

A second cavity was made with the same properties, but with additional sample holes. One at the peak electric field as before, one near the edge maximum magnetic field, and one where both electric and magnetic fields were at approximately 50% of their maximum value (Williams *et al*, 2016). This cavity could be used to compare and contrast the electric and magnetic field effects.

It was hypothesized that by combining nanoparticles with spores and microwaves it may be possible to enhance spore disruption and the release of DNA but at a further reduced power requirement. The reduction in the energy needs of the system to that of a mobile phone would create the possibility of developing a handheld bacterial detector.

1.7.3 Other microwave systems

Of note is a detection system for various bacterial clinical samples, developed by Chung *et al*, 2014, which also used nanoparticles and oligonucleotides. 16s ribosomal RNA from target bacteria was amplified using PCR. The amplified single strand DNA would bind to two oligonucleotides, one to each end. One of the oligonucleotides is conjugated to a bead, the other to a magnetic nanoparticle. As a result, the DNA would be what was called a “magnetic sandwich complex”. The sample would then be exposed to a micro-NMR. The result could be interpreted as a bacterial species and it was possible to differentiate between several different species (improving specificity is ongoing work). The PCR required time, but results could be obtained in two hours, which is faster than existing testing methods for those species.

1.8 Project aims

1.8.1 Aims

The principal aim of this project was to investigate the mechanisms by which microwaves affect bacterial spores and cause the release of DNA and to determine whether this is due to the effect of the electric field, the heating of trapped water particles or a combination of both.

This project had several objectives:

- i. To characterise the spore structure of *C. difficile* and to determine how different elements of the spore interact with microwaves. To do this, a standardised spore production method must be developed, which will allow for the generation of reproducible results and to fully characterise the spore diversity which has been observed in clinical isolates of this pathogen.
- ii. Characterise the interaction of spore with microwaves in terms of physical structures and determine the relative contribution of heating, electric field or magnetic field effects to spore disruption.
- iii. Characterise the interaction of nanoparticles with spores and with microwaves. To determine if the chemical composition and the size and shape of the nanoparticle amplify the sporicidal activity of the microwaves.
- iv. Develop a computer model of spore-nanoparticle interactions, which will match experimental results, and will ultimately be able to predict experimental results.
- v. To develop a nanoparticle-based strategy which will increase the sensitivity of the point of care assay.

1.8.2 Hypotheses being tested

- The hypothesis regarding spore structure: the variation within spore structure correlates to different clinical isolates and correlates with different spore properties.
- The hypothesis regarding microwaves: the variation within the spore structure correlate with different rates of DNA release from the spore.
- The hypothesis regarding microwave mechanism action: the microwaves cause release of DNA from spores by electric field effects, and not by heating.
- The hypothesis regarding the spore DNA release: the microwave cause the release of DNA from inside the spore.
- The hypothesis regarding nanoparticles: nanoparticles amplify the effect of microwaves on the spores.

Chapter 2

General Methods

2.1 Spore growth and purification methods

2.1.1 Strains and growth conditions. The clinical isolates of *C. difficile* used in this study are shown in Table 2.1 and were obtained from the National Anaerobic Reference Unit, Cardiff, Wales. The CD630 strain and its knockout strains were obtained from the laboratory of Prof. Simon Cutting, University of Royal Holloway. The R20291, DS1748 and DS1813 originated from the National Anaerobic Reference Unit, Cardiff, Wales. Unless otherwise stated, all organisms were stored as spores at 4° C in sterile water.

To study and compare spore structure, a method which produced pure spores was needed, in large quantity with minimal damage to their outer surface. Three published purification methods were compared with regards to their ability to produce intact spores. Spores were compared on several factors: the concentration of spores produced, the spore to vegetative cell ratio, and the time required to produce spores.

Table 2.1. Strains of *C. difficile* used.

Strain	Ribotype	Description
R20291	027	Hypervirulent ribotype, Stoke-Mandeville strain (Joshi <i>et al.</i> , 2012)
DS1813	027	Relatively high hydrophobicity of 87%, no visible exosporium (Joshi <i>et al.</i> , 2012)
DS1748	002	Relatively low hydrophobicity of 12% (Joshi <i>et al.</i> , 2012)
CD630	012	The first isolate of <i>C. difficile</i> to be genome sequenced (Lawley, 2009)
CD630 BclA1 ⁻	012	Knockout of BclA homolog 1 (a collagen-like spore coat glycoprotein)
CD630 BclA2 ⁻		Knockout of BclA homolog 2 (Phetcharaburanin <i>et al.</i> 2014)
CD630 BclA3 ⁻		Knockout of BclA homolog 3
CD630 CotE ^{N-}	012	N-terminal deletion of spore coat protein CotE (Permpoonpattana <i>et al.</i> 2013).
CD630 CotE ^{C-}		C-terminal deletion of the spore coat protein CotE.

Cultures were incubated at 37° C in a BugBox Plus anaerobic workstation (Ruskin Technology Ltd., Bridgend, United Kingdom) using an 85% nitrogen, 10% carbon dioxide, and 5% hydrogen gas mix.

Unless otherwise stated, all reagents were purchased from Sigma Aldrich, Dorset, UK.

2.1.2 Lawley's method. The following method is based on the work of Lawley and colleagues, 2009 and was employed to produce *C. difficile* spores. To produce spores, a single colony harvested from a Brain Heart Infusion (BHI) agar plate was used to inoculate 25 ml of Wilson's broth, which was then incubated for 10 days at 37° C in anaerobic conditions.

To purify the spores, the cultured broth was centrifuge at 16,800 g for 15 min using a Beckman Coulter J-20 centrifuge, the supernatant was discarded, and the pellet was resuspended in 1.5 ml distilled water. This washing step was repeated 4 more times using the Eppendorf 5417R centrifuge and the final pellet was resuspended in 1.5ml PBS. The

spore suspension was then subjected to sonication for 90 seconds using a tapered probe set at an amplitude of 35%. Following sonication, the sample was mixed with 1.5 ml of 10% Sarkosyl and incubated for 1 hour at 37° C with agitation. Samples were then pelleted at 3,400 g for 10 min and the pellets were resuspended in 1.5 ml of PBS + 0.125 M Tris buffer (pH 8) + 10 mg/ml lysozyme and incubated overnight at 37 °C with 120 RPM agitation. The suspensions were then sonicated again as described above, but with 1% Sarkosyl instead of 10% Sarkosyl prior to the 1-hour incubation.

The suspensions were then layered onto a 50% sucrose solution and centrifuged at 3,400 g for 20 min. The pellets were resuspended in 2 ml of PBS containing 200 mM EDTA, 300 ng/ml proteinase K + 1% Sarkosyl and incubated for 1 hour at 37 °C with agitation. The suspensions were then layered on 50% sucrose and centrifuged as described above. The resulting pellets washed with sterile distilled water (SDW) twice and finally resuspended in SDW and stored at 4° C.

2.1.3 Sorg's method. Described by Sorg, this method differs from that of Lawley in that the spores are produced on agar rather than in broth and the purification process is less complex (Sorg & Soehnshein, 2008; Sorg & Soehnshein, 2010). Bacteria were incubated in BHIS agar anaerobically at 37° C for 4 days. Following incubation, cells were collected from the surface of the plate, using a 10 µl inoculating loop and suspended in 1 ml SDW in a sterile Eppendorf tube. The suspension was incubated at 4° C overnight and then centrifuged at 5000 g for 5 min, the supernatant was discarded, and the pellet was resuspended in 1ml ice cold water. This washing step was repeated 4 times. The suspensions were then layered onto a 50% sucrose solution and centrifuged at 3,400 g for 20 min and the pellet was resuspended in 1ml ice cold water. The suspension was then centrifuged at 5000 g for 5 min, the pellet was resuspended in 1ml ice cold water. This washing step was repeated 4 times. The resulting final pellet was resuspended in SDW and stored at 4° C.

2.1.4 Heeg's method. The following method is based on the work of Heeg and colleagues 2012. Bacteria were incubated on BHIS agar supplemented with 250 µg/ml cycloserine

and 8 µg/ml cefoxitin anaerobically at 37° C for 4 days. Following incubation, cells were collected from the surface of the plate, using a 10 µl inoculating loop and suspended in 1 ml SDW in a sterile Eppendorf tube. The suspension was incubated at 4° C overnight and then centrifuged at 16,000g for 4 min, with the supernatant and top layer of the pellet carefully removed after centrifugation. The rest of the pellet was resuspended in SDW and the washing step repeated 10 times. The resulting final pellet was resuspended in SDW and stored at 4° C.

2.2 Spore Visualisation Methods

2.2.1 Visualisation of spores by light microscopy

A standard Gram staining method was used to stain the spores (Beveridge, 2001). 10 µl of spore suspension was placed on a glass slide and dried under a flame. The slide was subsequently flooded in crystal violet, Gram's iodine and Safranin for up to 30 seconds in each step. Slides were washed with water following crystal violet and Gram's iodine flooding, and with ethanol following Safranin. Vegetative cells, if any, stained were stained and would appear as long purple rods. A Leica DM2500 microscope was used to visualise the spores, using ×64 objective lens with oil immersion. Spores were then visualised using phase contrast settings in the microscope, with the slide under oil immersion

2.2.2 Visualisation of spores by Scanning Electron Microscopy (SEM)

A 10 µl aliquot of the purified spore suspension from stock was dried on a glass slide. The slide was then coated with a film of Gold-Palladium using the Agar Scientific Sputter Coater in three 15-second coating runs, using argon plasma. SEM images were captured using a Zeiss 1540 Crossbeam Scanning Electron Microscope using Inlens and SE2 imaging modes. Spore dimensions were measured from SEM images using ImageJ software. To determine spore characteristics, at least 30 individual spores were used from at least 6 fields of view.

The analysis of spore samples by electron microscopy was undertaken under the direction of Dr. Emmanuel Brousseau in the Cardiff School of Engineering.

2.2.3 DNA Visualisation by Fluorescence

A fluorescence and microscopy method using Acridine Orange (AO) and Propidium Iodide (PI) was adapted from Schichnes *et al.* (2006).

A 10 µl sample drop was dried on a glass slide. 10µl of 0.1µg/ml of either AO or PI were added to the same spot and covered with a cover slip. The slide was then imaged using an Olympys IX50 fluorescence microscope, using a ×64 objective lens with oil immersion. A phase contrast image was taken to confirm the presence of spores in the field of view, then a fluorescence image of the same field of view was taken. This was repeated 3 times for each sample. A green light source (500 nm) was used for PI and AO. In addition, the light source was changed to blue light with AO to differentiate ssDNA from dsDNA.

2.3 Spore Characterisation

2.3.1 Determination of spore density

10 µl aliquots of the sample were heat shocked at 90° C for 10 min, using a heating block, (Dri-Block, Techne, UK) to kill any vegetative cells. The aliquots were then 10-fold serially diluted down to 10⁻⁷ dilution. The dilutions were then plated on BHI agar with 0.1% sodium taurocholate. From each dilution, 3 separate 10 µl drops of liquid was pipetted onto the surface of a BHI agar plate containing 0.1% sodium taurocholate. Plates were incubated under anaerobic conditions at 37° C for 2 days. Colonies were counted, and the initial spore concentration determined from the dilution. The concentration of the original sample is given by the following formula:

2.3.2 Hydrophobicity test

The Microbial Adhesion to Hydrocarbons (MATH) test was employed to determine the hydrophobicity of spores examined in this study (Rosenberg, 1984). A 3 ml spore suspension in distilled water with an OD₆₀₀ 0.4-0.6 was prepared in a McCartney bottle. (Ultrospec 1100 *pro* UV/Visible spectrophotometer, Biochrom, Cambridgeshire, UK). A 300 µl aliquot of hexadecane was then added to the suspension and vortex mixed (VortexGenie, Fisher Scientific, UK) for 1 min at room temperature. The mixture was incubated for 15 min at room temperature, allowing the layers to separate. After this, the OD of the aqueous (bottom) layer was measured and change in OD recorded as a percentage from original to the final OD.

2.3.3 Sonication

To determine the feasibility of removing the exosporium, the methods of Escobar-Cortes *et al.* (2013) and by Alyousef *et al.* (2013) were adapted. These studies reported that intense sonication can remove the exosporium in spores. For this investigation, 1 ml spore suspensions with 10⁷ spores each, were treated with 16 sonication cycles at 15 µm amplitude for 50 seconds each, and cooling on ice for 1 min between each cycle.

2.4 Spore microwave exposure

2.4.1 Electric Field Experiments

Spores were exposed to microwaves using the pillbox microwave cavity described in 1.6.2. A 170 µl sample, at a concentration of 10⁷ spores/ml for spore samples, was placed in a 200 µl capped eppendorf. The eppendorf was placed in the cavity sample hole. The cavity with the sample was checked using a N1996A Agilent CSA Spectrum analyser, to verify that the resonance peak is matching the input frequency and verify that there is no noise in the system. After confirming this (tuning the cavity if necessary), the sample was exposed to microwaves, with duration, power and duty cycle selected.

2.4.2 Electric vs Magnetic Field Experiments

A modified microwave cavity, described by Williams *et al.*, 2016 was used in this experiment. The cavity contains 3 sample holes, with the axial sample hole as before, and the extra sample holes at 27.6 mm and 46 mm along the radius of the cavity. Three identical 170 μ l samples were placed in the holes and run simultaneously as previously described in section 2.4.1.

2.5 DNA concentration measurements

2.5.1 DNase treatment of spores

DNase treatment was adapted from Herman *et al.* (1995). 40 ng of DNase I in 0.067 M phosphate buffer (pH 7) and 15 mM MgCl₂ incubated at 37° C with a spore sample of 1 ml in volume, containing 10⁸ spores, with aliquots taken every 24 hours. These aliquots had the concentration of DNA measured using Qubit dsDNA and ssDNA as detailed in section 2.5.2 below.

For the samples to be stored as stocks for later experiments, the DNase was deactivated by heating the sample to 70° C for 15 min and then the samples were washed by centrifuging at 5000 g and resuspending the pellet in SDW.

2.5.2 DNA Quantification by Qubit

The first was the usage of the Qubit 3.0 fluorometer for a simple immediate result. The Qubit assay kits for measuring double stranded (ds) and single stranded (ss) DNA were purchased from ThermoFisher. To measure the concentration of DNA, the Qubit fluorophore was added to the provided buffer at a ratio of 1:200. 10 μ l of the provided “DNA standard” was then mixed with 190 μ l of the buffer to calibrate the device. For sample runs 20 μ l of the spore suspension was then mixed with 180 μ l of the buffer and used in the fluorometer.

2.5.3 Spore disruption quantification by fluorescence

To compare the level of disruption in spores in different samples, fluorescence microscopy as detailed in section 2.2.3 was used. This method had the advantage of identifying individual disrupted spores but had the disadvantage of not giving a simple number like Qubit.

Spores were counted, ignoring areas with clumped spores and using fields of view with at least non-clumped 50 spores. The ratio of spores which were fluorescent to the total number of spores was determined and this was repeated 3 times. This ratio was compared in samples in different test conditions.

2.6 Statistical tools used

For simple statistical tests like t-test and standard deviation, Microsoft Excel was used. For statistical tests where more than two data sets were compared, tests were done using Graphpad Prism 5.0. 1-way and 2-way ANOVA was used to determine overall significance of results, with post-tests, such as Dunnett's Multiple Comparison Test (for 1-way ANOVA) and Bonferroni post-tests (for 2-way ANOVA) being used to compare individual samples to each other.

Chapter 3

Characterisation of the spore structure of *C. difficile*

3.1 Introduction

The overall goal of this project was to investigate how spores interact with microwaves and nanoparticles. To do this, it was necessary to develop a standardised spore production method which would allow generation of reproducible results and to fully characterise the spore diversity which has been observed in clinical isolates of this pathogen (Joshi *et al.*, 2012, Pizarro-Guajardo *et al.*, 2014, 2016). Notably, it was necessary to characterise the differences in genetically related strains belonging to the same ribotype (Stubbs *et al.* 1999). As was described in chapter 1 (section 1.2.2), some ribotypes, such as the 027, are associated with hypervirulence and with increased mortality. In 2007-2008, during the peak of *C. difficile* infection in UK hospitals, the 027 ribotype accounted for nearly 65% of all analysed clinical samples (CRDN 2011-2013 report). It was also important to characterise the spore surface architecture to understand the effects that microwaves, and nanoparticles have on the spores.

Various methods have been employed to produce and purify *C. difficile* spores in published literature (Table 3.1). They vary in the choice of media to grow the vegetative cells in and stimulate sporulation as well as the techniques to purify the spores and remove vegetative debris.

Table 3.1 Methods used to produce and purify of *C. difficile* spores

Growth medium	Purification	Example
Wilson's Broth	Sonication + Lysozyme + Proteinase + Density Gradient	Lawley <i>et al.</i> , 2009.
TY Agar	Density gradient	Pizarro-Guajardo <i>et al.</i> 2016.
BHI + Taurocholate agar	Water wash	Joshi <i>et al.</i> 2012.
BHIS Agar	Density Gradient	Sorg & Sonenshein, 2008.
BHIS+ Agar	Water wash + manual removal	Heeg <i>et al.</i> , 2012.
SMC	Density Gradient	Phetcharaburanin <i>et al.</i> , 2014.

As a consequence of these differences in methods, the results presented in different studies are not directly comparable. Thus, it was important to identify a standard method capable of giving reproducible result for different strains. The disruptive nature of some of these approaches raises the possibility that the properties of the spores produced using these methods may be different to those of spores found in clinical samples.

To develop a standardised method which minimized culture- and purification-induced modifications to the spore surface, the physical properties of spores produced using the methods of Sorg *et al.*, 2008, Lawley *et al.*, 2009 and Heeg *et al.*, 2010 were compared. Structural differences were identified using scanning electron microscopy (SEM), which gives very high resolution (up to 10 nm) images of the surface of the spore. The advantage of SEM is that it provides more information about the 3D shape of the structure which is extremely useful when attempting to characterise the surface architecture of spores. The sample preparation for SEM is also less invasive (consisting of only coating the sample with a thin metal film), while the TEM sample preparation (immersion in tannic acid, glutaraldehyde, osmium tetroxide) may in itself change the spore architecture.

In addition to employing electron microscopy spore hydrophobicity was also measured with the goal of detecting more subtle differences in spore properties. The microbial adhesion to hydrocarbons test (MATH) test was used to determine the hydrophobicity and gives an indication of the overall charge of the spores. Hydrophobic spores have fewer polar groups on the surface than hydrophilic ones. It was previously reported that

different clinical isolates have varying hydrophobicity, and this may be connected to the structure of their outer layers (Joshi *et al.*, 2012). However, this study was done with unpurified spores, which could have changed the results of the MATH test due to the vegetative debris.

To test this hypothesis and to ensure that the data generated in this study was representative of *C. difficile* as a species, four different clinical isolates were examined (Table 3.1). Two of these belonged to the same 027 ribotype.

In addition to characterising clinical isolates, the contribution of individual spore structural proteins to surface architecture was explored, using mutants of the CD630 strain. The following gene knock outs were examined: *BclA1*, *BclA2*, *BclA3*, *CotEc*, *CotEn* (see section 1.3.2. for details on the *BclA* and *Cot* proteins). The *BclA* mutants, *BclA1* and *BclA2* in particular, were of interest as they have been shown to substantially affect spore properties; notably it was reported that that *BclA1* and *BclA2* knockout strains have lower hydrophobicity, show malformed spore coats (under TEM) and were less virulent than regular spores, suggesting that protein may play a role in attachment (Phetcharaburanin *et al.*, 2014). The *CotE* mutants were of interest as it was previously reported that *CotE* is located on the surface of the spore and mutation of the gene can lead to the release of sheet-like material from the spore surface (Permpoonpattana *et al.* 2013).

3.2 Aims and Objectives

The aims of this chapter were:

- To identify an “optimal” spore production and purification method which minimised spore surface disruption, while still removing vegetative debris
- To employ this method to characterise and compare the spore surface of clinical isolates of *C. difficile*.
- To determine the contribution of individual spore proteins to the spore surface properties.

3.3 Results

3.3.1 Identification of the optimal growth and spore purification method.

The initial experiments sought to determine the ability of individual growth media to support the production of spores. The concentration of viable spores harvested from the growth media, before and after the purification was determined using the drop count method and is summarised in Figure 3.1.

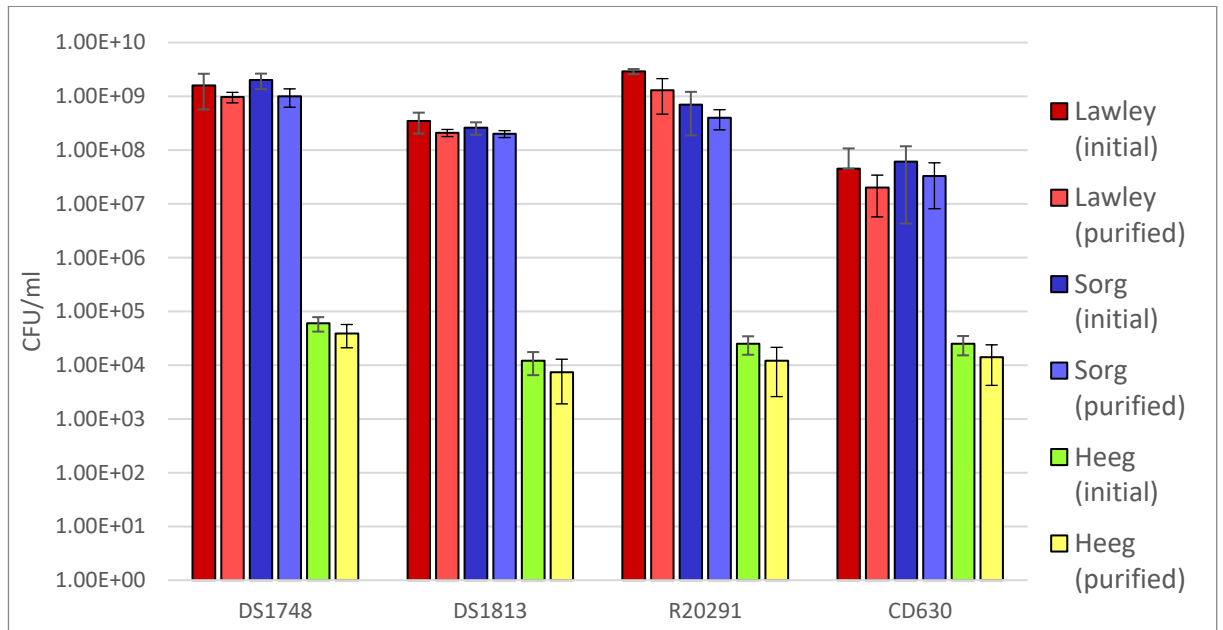


Figure 3.1. The initial yield of spores after growth in media and final yield of purified spores of clinical isolates of *C. difficile* obtained using three different production and purification methods (n=3). Error bars indicate the standard deviation of results.

3.4.1.1 Lawley's method

The concentration of unpurified spores harvested was comparable to those achieved by Lawley (2009), where up to 10^{10} spores were recovered from a 500ml culture. The culture volume in this investigation was only 25 ml per sample (20 times lower), so approximately $10^8 - 10^9$ unpurified spores were expected. The ratio of purified spores to those harvested at the end of culture was lower than the 90% reported by Lawley, ranging from 47.5% to 64%, suggesting that either the culture conditions were not optimal or that clinical isolates of *C. difficile* differ widely in their ability to produce spores. The purity of final spore preparations was determined using phase contrast microscopy (Figure 3.2.)

which showed that the preparation comprised more than 99% spores and less than 1% vegetative cells.

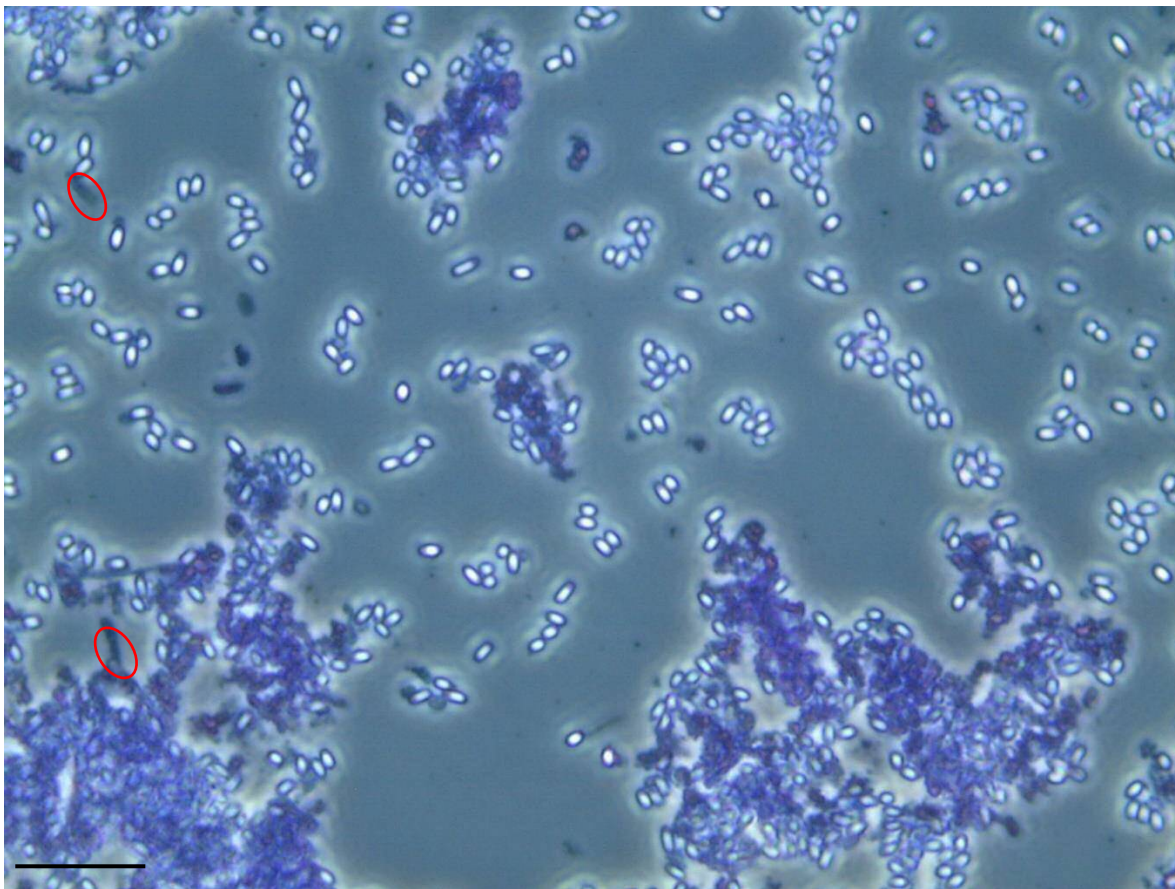


Figure 3.2. Phase contrast microscopy of *C. difficile* DS1748 spores following purification using the Lawley method. This image is representative of all of the isolates examined in this study. More than 300 separate phase bright spores are visible in the field of view, with 2 possible vegetative cells. Several large spore clumps can also be seen (omitted from the count). Scale bar is 10 μm .

3.3.1.2 Sorg Method:

The concentration of spores obtained from each isolate, before and after purification was comparable ($p=0.64$) to that seen using the Lawley method, as can be seen from Figure 3.1. This suggests that the ability of individual isolates to form spores is similar in these two growth conditions. The ratio of purified spores to those harvested at the end of culture was from 55% to 79%.

The purity of final spore preparations was determined using phase contrast microscopy (Figure 3.3) which showed that the suspension comprised more than 99% spores and less than 1% vegetative cells.

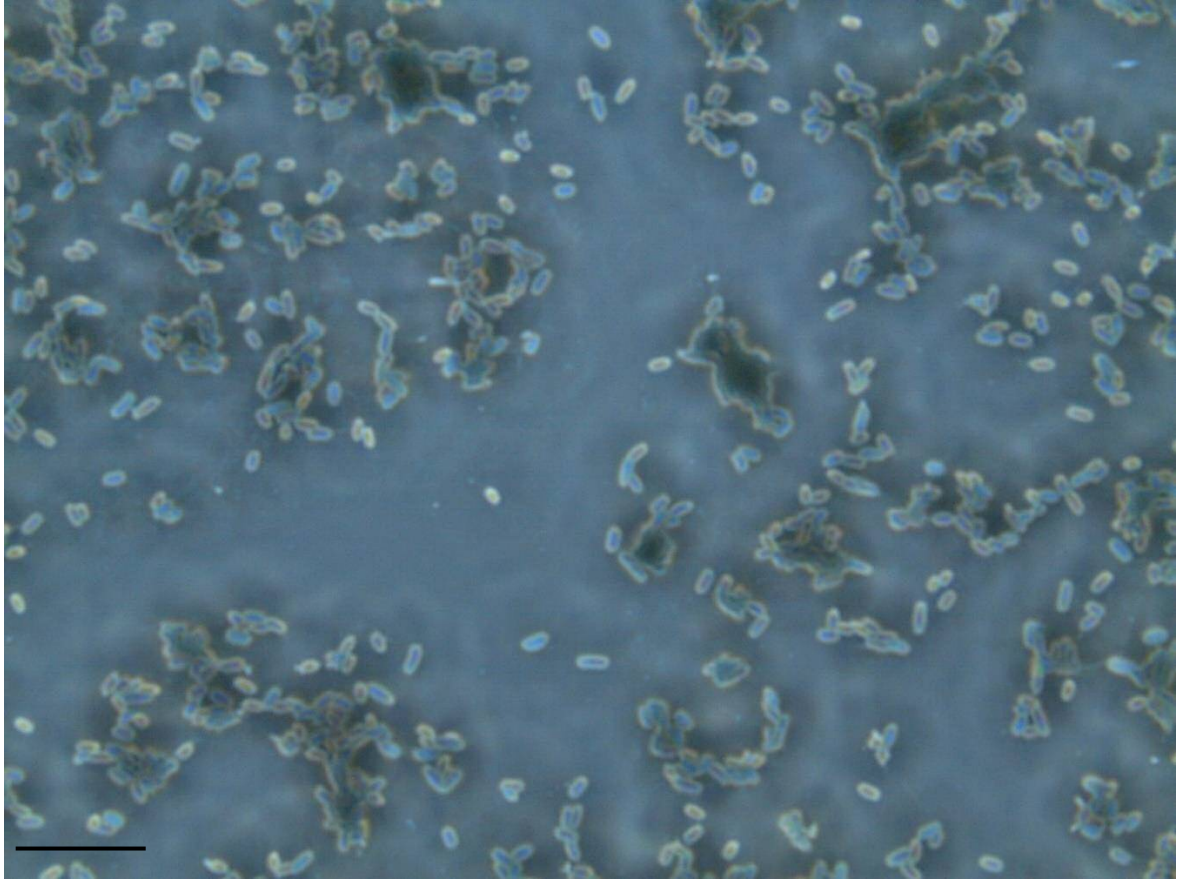


Figure 3.3. Phase contrast microscopy of *C. difficile* DS1748 spores following purification using the Sorg's method. This image is representative of all of the isolates examined in this study. More than 300 spores are visible in the field of view, with no obvious vegetative cells. Scale bar is 10 μm .

3.3.1.3 Heeg's method

Although the growth of all the *C. difficile* strains on the agar plates appeared typical, with creamy irregular-shaped colonies, sporulation was poor, with only 10^4 - 10^5 viable spores/ml in the final suspension. This was true for all strains, which was significantly different to the other methods ($p < 0.0001$).

The large number of vegetative cells and lack of spores were confirmed using microscopy (Figure 3.4). This failure to sporulate efficiently suggests that the antibiotic interfered

with vegetative cell sporulation, and similar spore yields were seen in Phetcharaburanin *et al.*, 2014 when using erythromycin for selection. Due to the low spore yields, at least 10^3 times lower than that of other methods, it was decided not undertake any form of purification or use this method in future experiments.

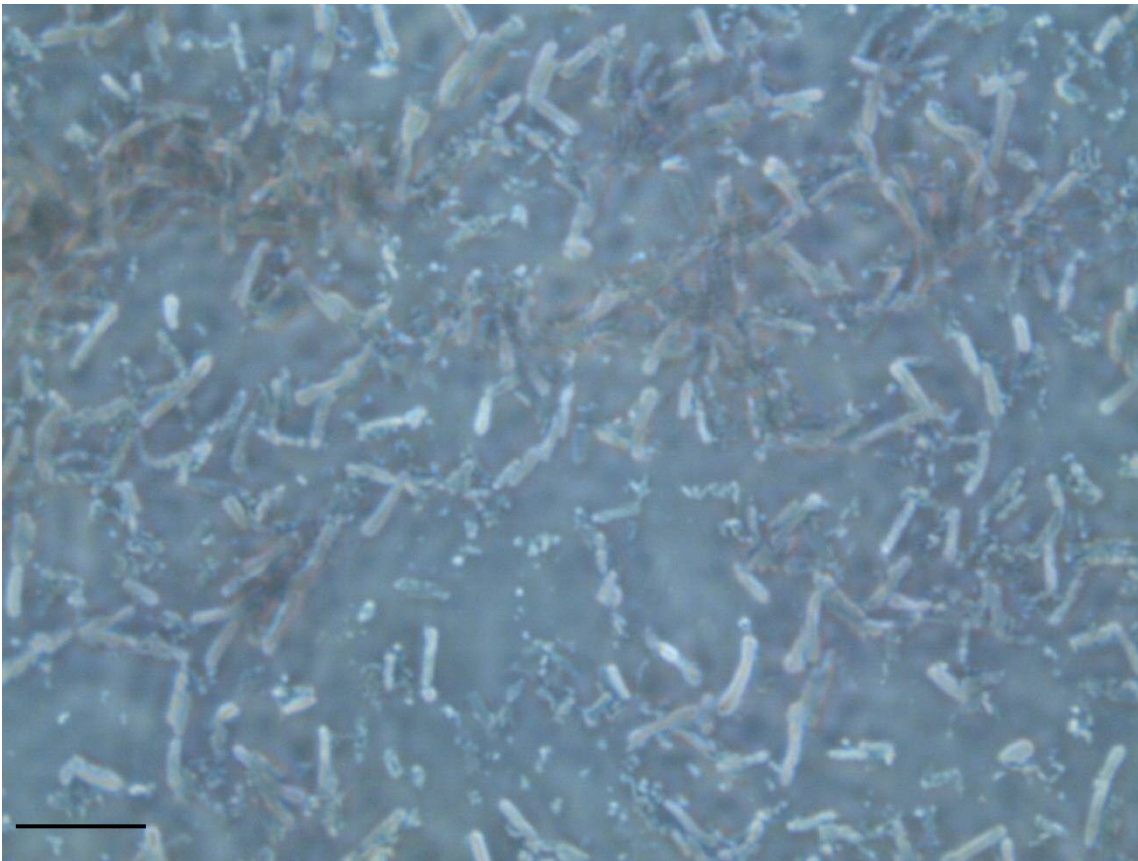


Figure 3.4. Phase contrast microscopy of *C. difficile* DS1748 spores following purification using Heeg's method. This image is representative of all the isolates examined in this study. More than 100 vegetative cells are visible in the field of view, with no obvious spores. Debris is also present around the cells. Scale bar is 10 μm .

3.3.2 Characterisation of spores by Scanning Electron Microscopy (SEM)

Suspensions of purified spores from different isolates (DS1748, DS1813, R20291 and CD630) produced using the Lawley and Sorg methods were observed using SEM to determine their surface characteristics.

3.3.2.1 Physical dimensions of spores

To determine the effect of the different production and purification methods on the gross morphology of the spores, the length and width of individual spores was determined by analysing SEM images. Physical dimensions varied markedly, ranging from 1.2 μm to 2.6 μm in length and from 0.7 μm to 1.15 μm in width (Figure 3.5).

Overall, spores produced using the Lawley method were larger than the spores produced using the Sorg method. This difference was not significant for DS1813 and CD630 ($p > 0.05$, Tukey's multiple comparisons) but was significant for strains DS1748 ($p = 0.011$ for width) and R20291 ($p < 0.001$ for length).

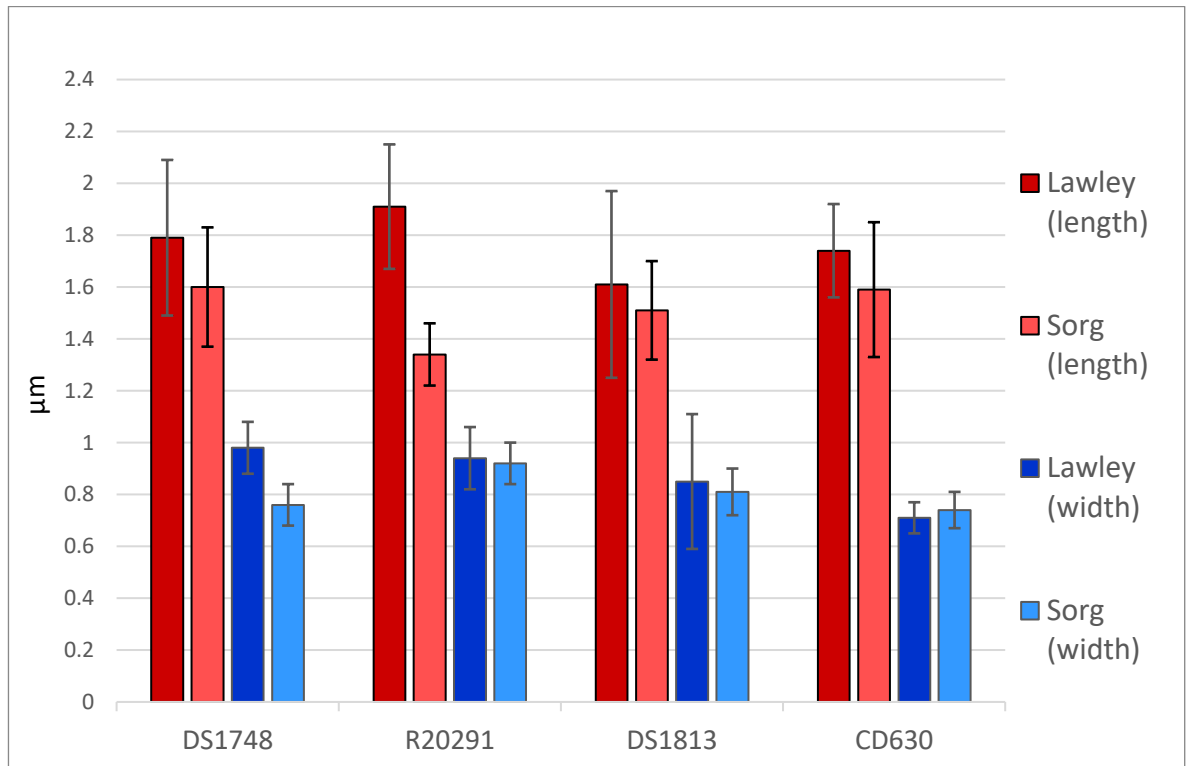


Figure 3.5. The effect of production and purification methods on the physical dimensions of spores of four *C. difficile* isolates determined from SEM micrographs. 30 spores of each strain were measured. Error bars indicate the standard deviation of results.

3.3.2.2 The effect of individual spore production and purification methods on spore surface architecture

Once the basic dimensions of the spores had been determined, the next step was to characterise the effect of spore production methods on the surface architecture of the spores of same four clinical isolates of *C. difficile*.

3.3.2.2.1 DS1748

Following purification using the Sorg or Lawley method, two spore morphotypes were observed. The most common form consisted of a cylindrical shape with “spikes” protruding from the surface, resulting in a “pineapple-like” structure (Figure 3.6). The second morphotype was the same cylindrical shape, however no “spikes” were observed.

Depending on the purification method employed differences were seen in the ratio of the two morphotypes. While the Lawley method yielded primarily pineapple-like spores (99%) the Sorg method produced a lower percentage of these structures (75% of those observed).

3.3.2.2.2 DS1813

Spores of DS1813 were also observed to form two distinct morphotypes; the first were ridged and similar in appearance to the “pineapple like” morphotype of DS1748, while the second were smooth and featureless (Figure 3.7). Both morphologies were present in Sorg and Lawley purified spores. While 70% of the spores purified using the Sorg method were “ridged” in appearance (Figure 3.7B). only 21% of the spore produced using the Lawley method showed these features (Figure 3.7A).

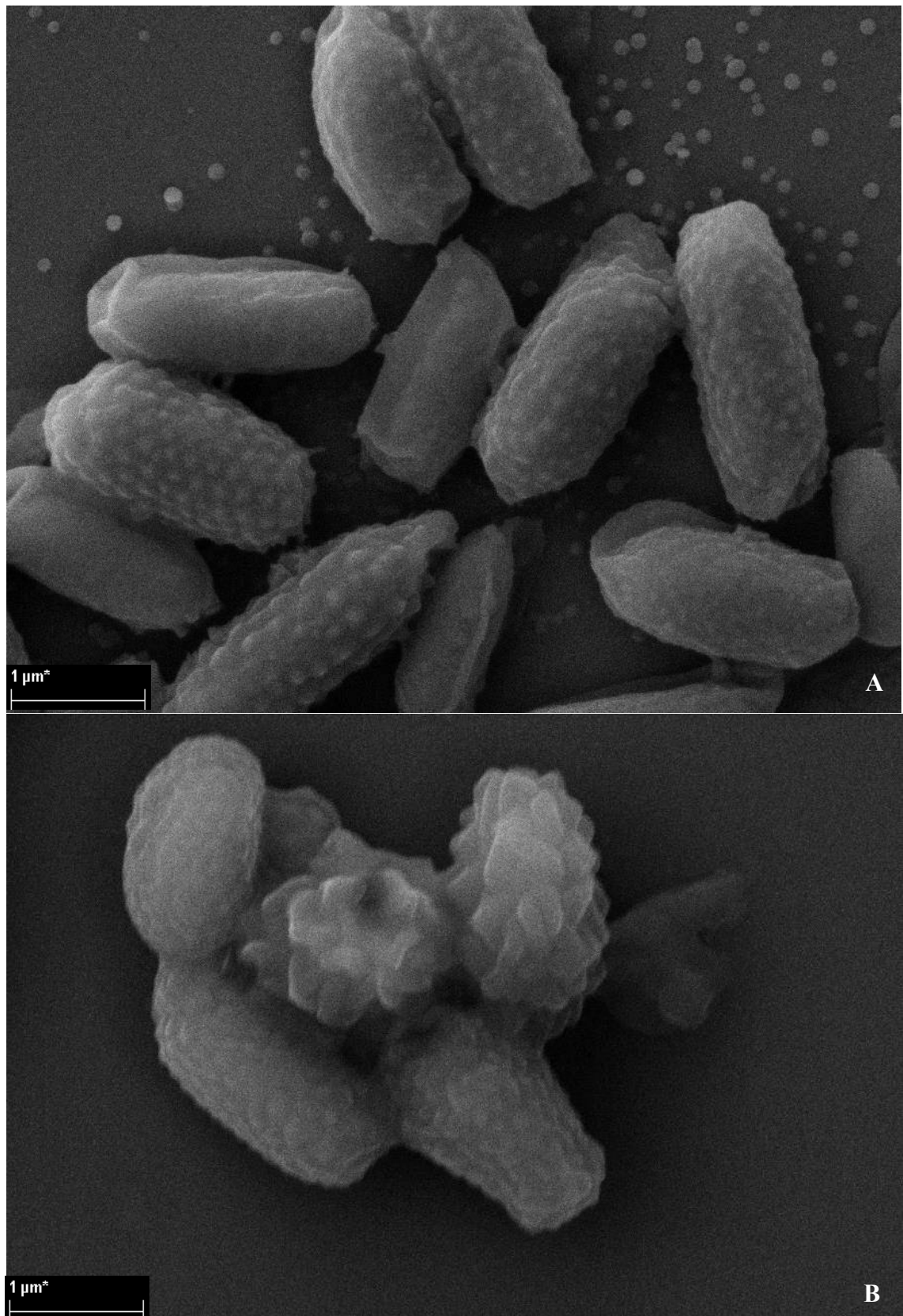


Figure 3.6. SEM of *C. difficile* spores of the DS1748 strain spores produced and purified using the Lawley (A) and Sorg methods (B). The magnification was x34,140. These images are representative of 10 fields of view.

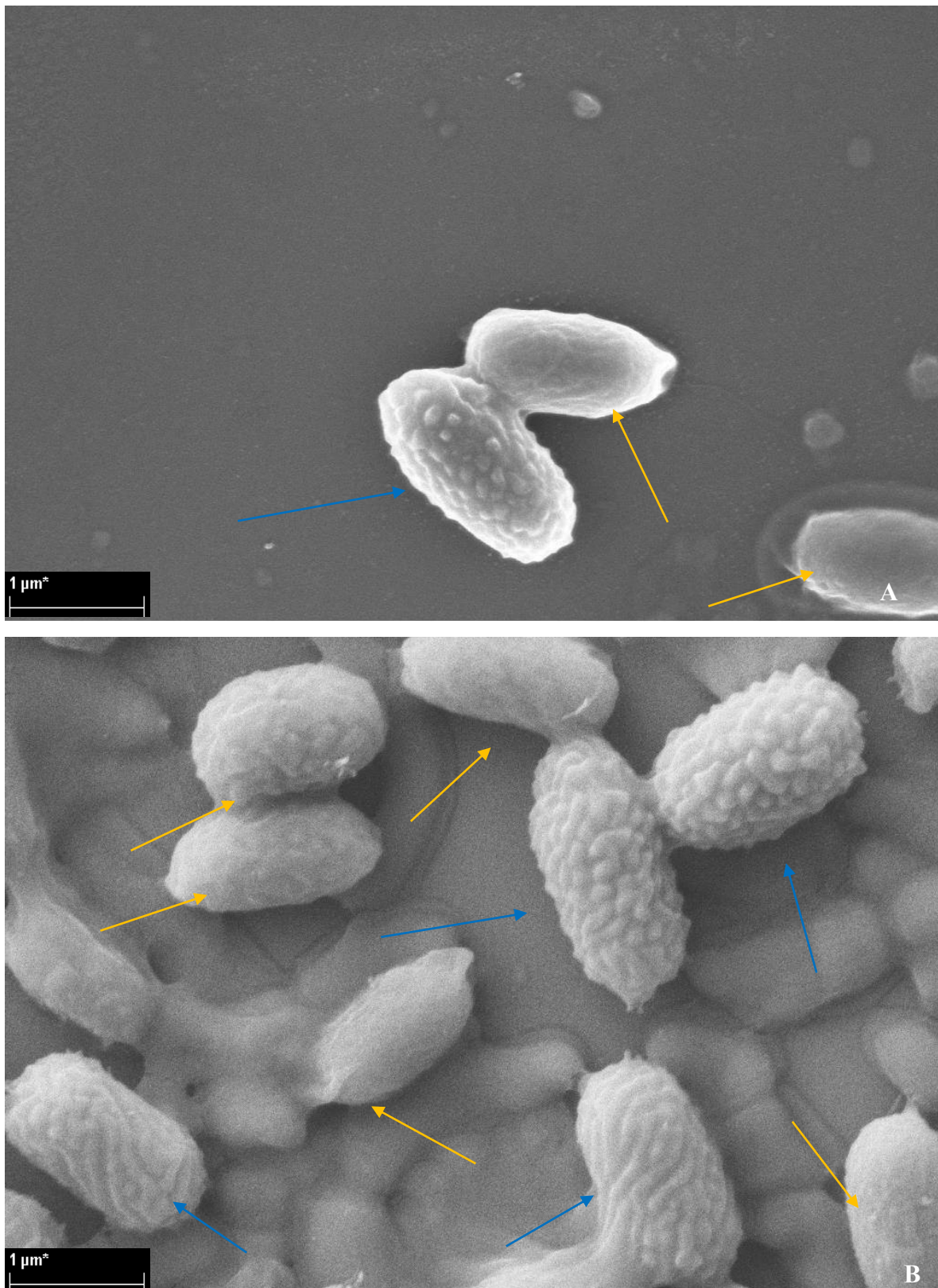


Figure 3.7. SEM of *C. difficile* spores of the DS1813 strain spores produced and purified using the Lawley (A) and Sorg methods (B). The blue and yellow arrows highlight the different morphotypes. The magnification was x34,140. These images are representative of 10 fields of view.

3.3.2.2.3 R20291

The primary morphology of R20291 spores differed markedly from those produced by DS1748 and DS1813 in that they appeared to be surrounded by a loose layer, which may represent an exosporium (Figure 3.8, yellow ovals). The majority of spores (97%) purified using the Sorg method were surrounded by a loose layer. In contrast, only 44% of the spores produced using the Lawley method were surrounded by a loose layer

The second morphotype lacked this layer and were featureless in appearance. The presence of sheet like structures distinct from spores suggests that this outer layer may be relatively fragile. In addition to this loose layer, what appeared to be filaments, approximately 80 nm in width, were seen extending from the spore surface (Figure 3.8, blue circles). While these filaments were present in spores purified using the Lawley method they were absent of Sorg purified spores.

3.3.2.2.4 CD630

The primary morphology of CD630 strain were smooth without any ridges or bumps (Figure 3.9). The majority of spores (85%) purified using the Sorg method had a loose layer surrounding the spore, but it was different and smaller than in the R20291 strain. Spores purified with the Lawley method lacked the loose layer and were featureless.

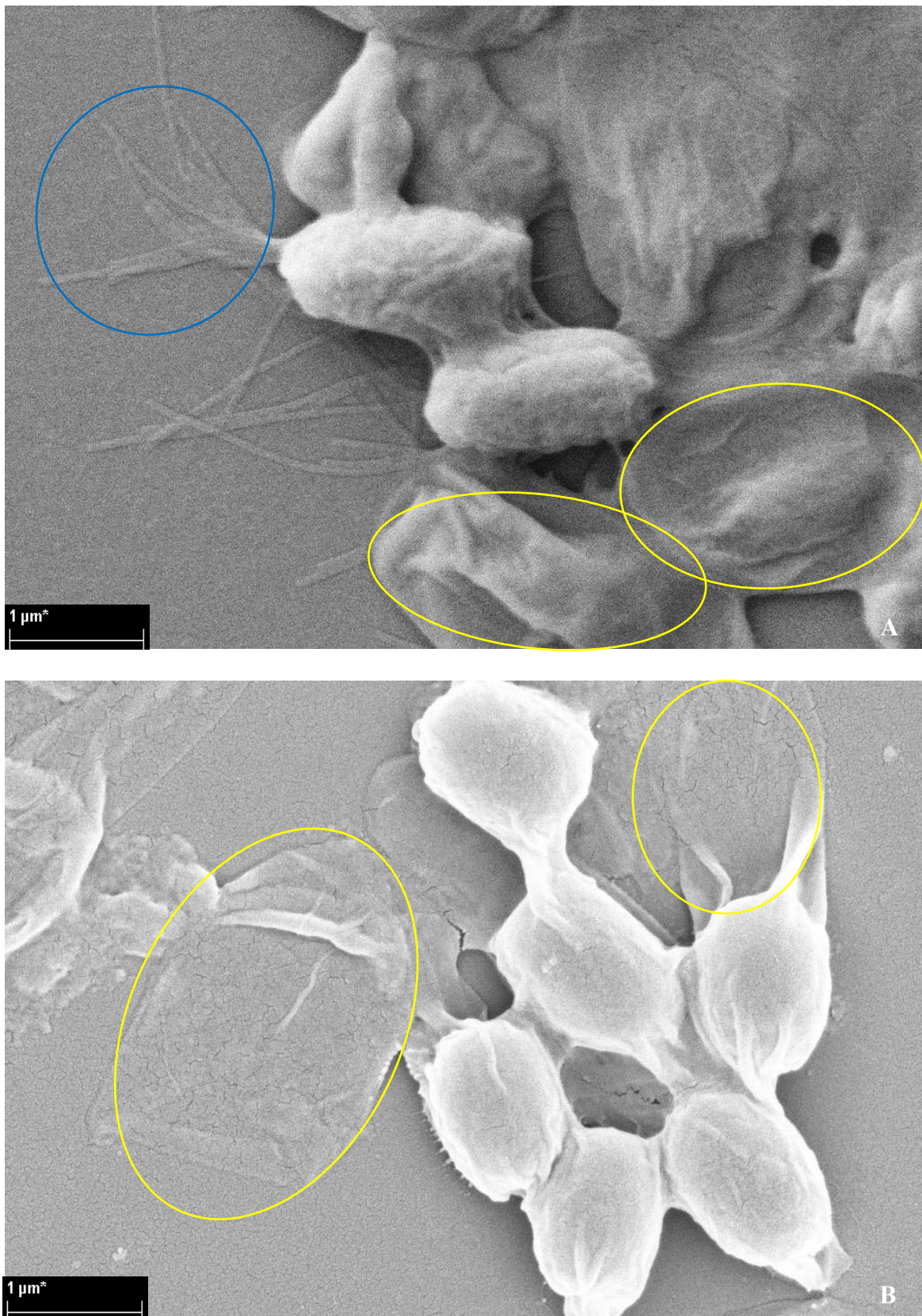


Figure 3.8. SEM of *C. difficile* spores of the R20291 strain spores produced and purified using the Lawley (A) and Sorg methods (B). The magnification was x34,140. These images are representative of 10 fields of view. The yellow ovals highlight the loose layer on the spores.

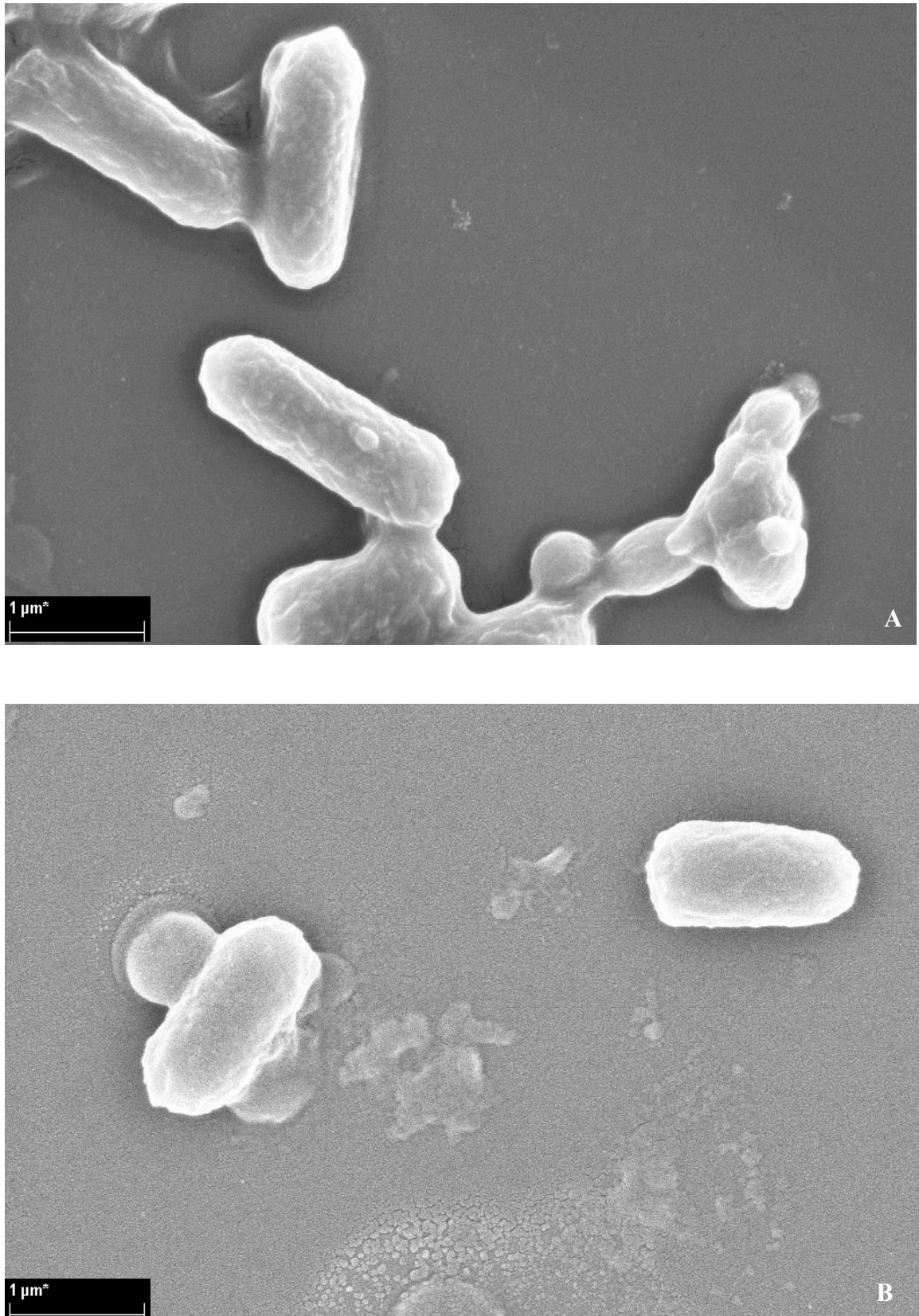


Figure 3.9. SEM of *C. difficile* spores of the CD630 strain spores produced and purified using the Lawley (A) and Sorg methods (B). The magnification was x34,140. These images are representative of 10 fields of view.

3.3.2.2.5 Summary of findings

Overall, it was observed that spores produced by different clinical isolates of *C. difficile* differed in their morphology depending on the method used to produce them. They could broadly be grouped into three morphotype groups which were: pineapple-like (DS1748 and DS1813), surrounded a bag-like layer (R20291 and CD630) and smooth (DS1748, DS1813, R20291 and CD630). There were differences within these groups too, such as between the DS1748 “pineapples” and the DS1813 “ridges”, but these were difficult to differentiate. The ratio of each morphotype in the population varied depending on the clinical isolate and the purification method. Interestingly, clear differences in the appearance of spores from clinical isolates DS1813 (pineapple) and R20291 (bag-like) were observed, despite belonging to the same hypervirulent 027 ribotype.

3.3.2.3 Sonication of *C. difficile* strains and the effect on surface architecture

Sonication has been used across a number of studies, including those using *C. difficile* to disrupt the bacterial spore structure (Escobar-Cortes *et al.*, 2013). The Lawley spore purification method includes a sonication step to prevent spore clumping, raising the possibility that this process could alter the spore surface architecture. To determine if this was the case, spores purified using the Sorg process were subjected to intense sonication and the effects on spore structure were observed using SEM.

3.3.2.3.1 The effect of sonication on DS1748 spores

Sonication of DS1748 spores resulted in the loss of the “pineapple” layer from 20.3% of the total spores observed (Figure 3.10). The resulting spores were smooth in appearance.

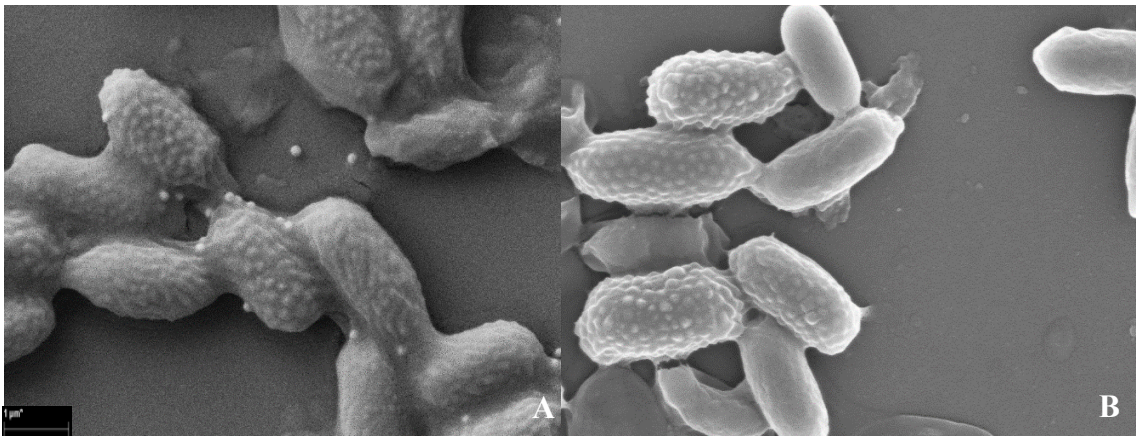


Figure 3.10. SEM of *C. difficile* spores of the DS1748 strain spores produced and purified using the Sorg method, before (A) and after sonication (B). The magnification was x34,140. These images are representative of 10 fields of view.

Interestingly, the detached outer “pineapple” layer was observed (Figure 3.11), covered in bumps which may correspond to the bumps seen on the surface of non-sonicated spores.

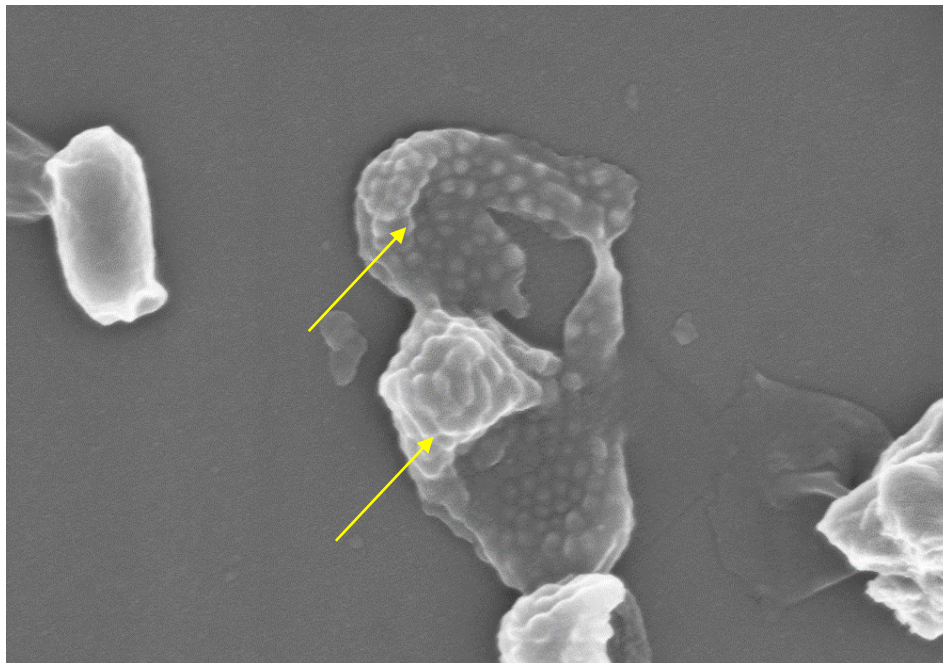


Figure 3.11. SEM of *C. difficile* spores of the DS1748 strain spores produced and purified using the Sorg method, after sonication. The magnification was x34,140. The arrows highlight the detached “pineapple-like” layer.

3.3.2.3.2 The effect of sonication on DS1813 spores

Sonication of DS1813 spores resulted in the loss of the “pineapple” layer from 39% of the observed spores (Figure 3.12), resulting in smooth spores. Unlike DS1748, this removed outer layer was not seen separately.

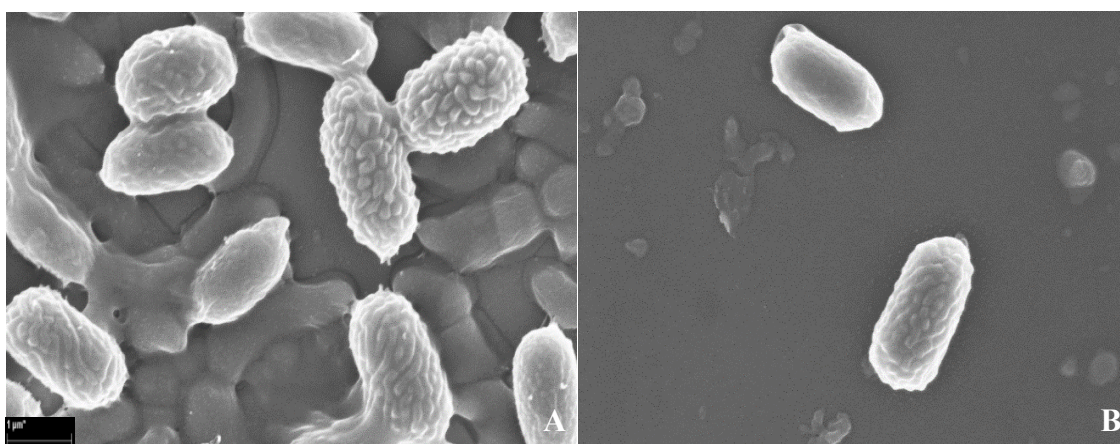


Figure 3.12. SEM of *C. difficile* spores of the DS1813 strain spores produced and purified using the Sorg method, before (A) and after sonication (B). The magnification was x34,140. These images are representative of 10 fields of view.

3.3.2.3.3 The effect of sonication on R20291 spores

Sonication of the R20291 strain resulted in the removal of the loose layer from 39% of the observed spores (Figure 3.13). Unlike DS1748, this removed outer layer was not seen separately.

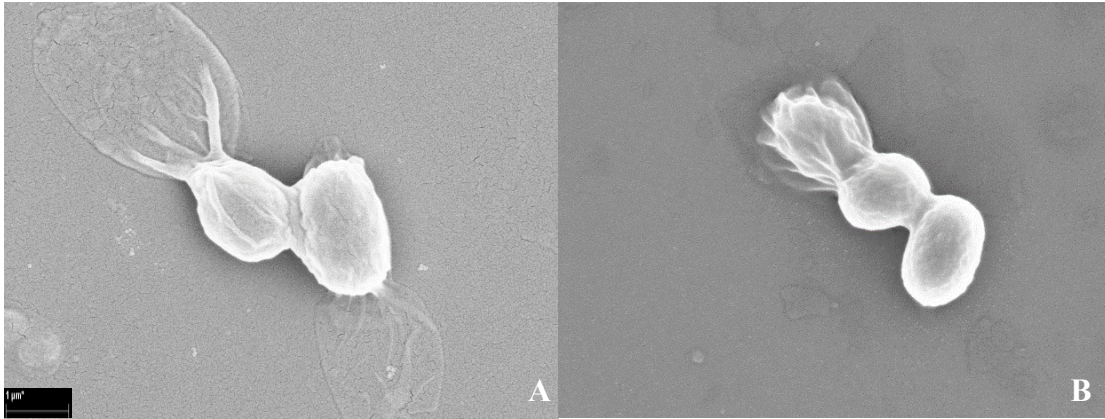


Figure 3.13. SEM of *C. difficile* spores of the R20291 strain spores produced and purified using the Sorg method, before (A) and after sonication (B). The magnification was x34,140. These images are representative of 10 fields of view.

3.3.2.3.4 The effect of sonication on CD630 spores

Sonication of the CD630 strain resulted in the removal of the loose layer from 49% of the observed spores (Figure 3.14). This resulted in spores which are smooth in appearance. Unlike DS1748, this removed outer layer was not seen separately.

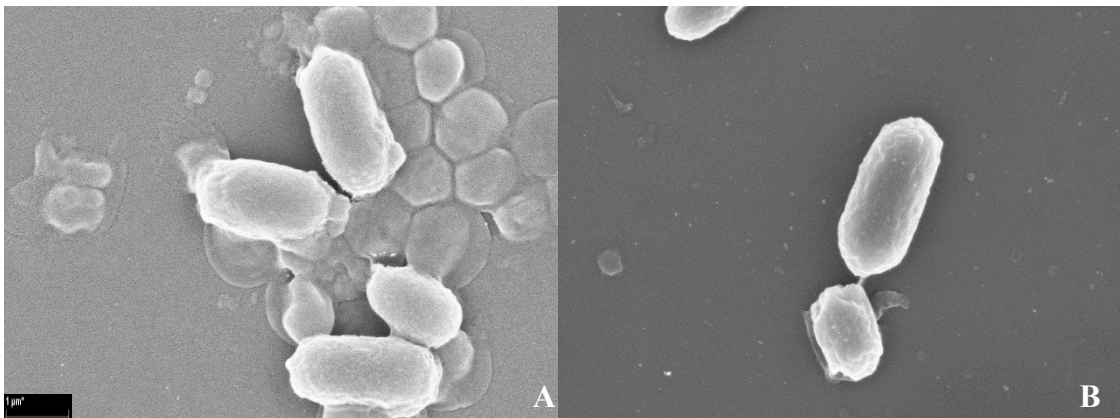


Figure 3.14. SEM of *C. difficile* spores of the CD630 strain spores produced and purified using the Sorg method, before (A) and after sonication (B). The magnification was x34,140. These images are representative of 10 fields of view.

3.3.2.3.5 Summary of findings

Sonication resulted in the loss, to varying degrees, of the outermost surface features of the spores of all four clinical isolates, as could be seen from the SEM images 3.10 – 3.14. The change in morphology was significant for all 4 strains ($p=0.005$ for 1748; $p=0.004$ for 1813; $p<0.001$ for R20291; $p<0.001$ for 630).

Sonication of DS1813, CD630 and R20291 resulted in a larger proportion of plain smooth spores, similar to using the Lawley method (Figure 3.15). Sonication of DS1748 spores resulted in the removal of the outer layer, which could be observed separately from the spore. This suggests that this layer is more robust than in other strains.

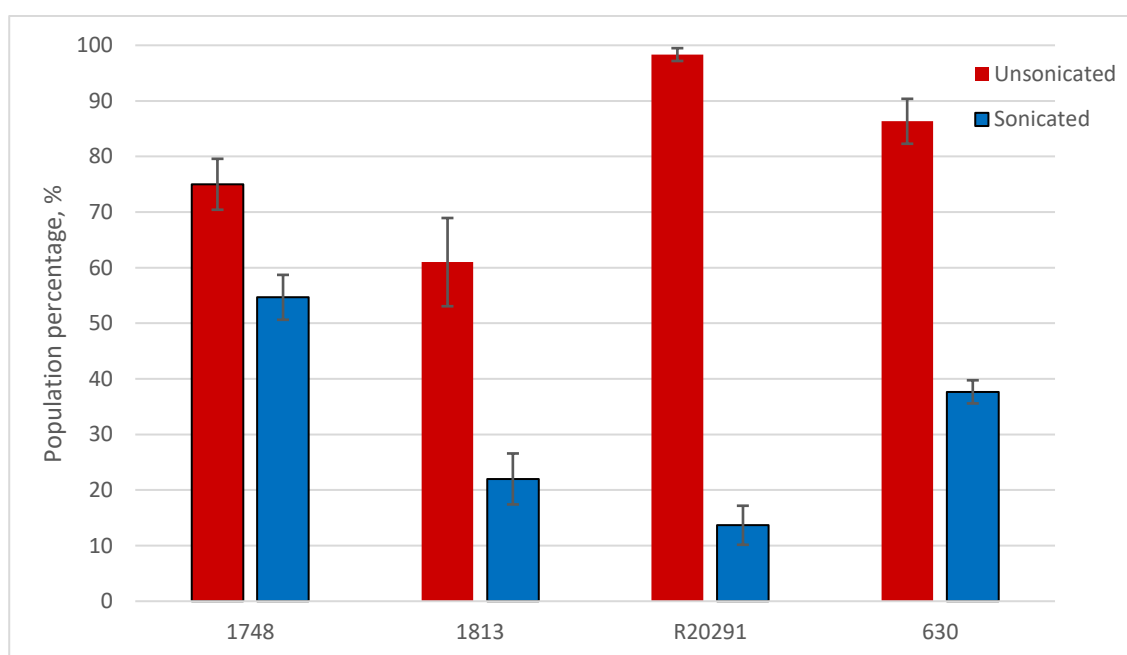


Figure 3.15. Change in the relative proportion of spores with a the “pineapple-like” shape (for strains DS1748, DS1813) or loose exosporium with (R20291, CD630) within a population, before and after sonication. Each result is the average of 3 separate samples, with 50 spores observed in each sample. Error bars indicate the standard deviation of results.

3.3.3 Hydrophobicity of *C. difficile* spores

In addition to employing electron microscopy, the spore hydrophobicity was also measured with view to detecting more subtle structural differences. The (MATH) test was employed to determine relative hydrophobicity (RH) of spores. The relative hydrophobicities (RH) of the different strains are shown on Figure 3.16. Comparison of the RH values of spores produced using the Lawley method revealed no statistically significant difference (ANOVA $p=0.67$), suggesting that all four strains possessed similar levels of hydrophobicity (Figure 3.16).

In contrast, when the spores from the same clinical isolates were produced and purified using the Sorg method, a statistically significant difference in RH values was observed across all of the strains (ANOVA $p=0.0001$), with the spores of the DS1748 and DS1813 strains having the highest hydrophobicity and the R20291 strain having the lowest.

Sonication of spores produced using the Sorg method caused a significant reduction in RH values of all isolates when compared to the unsonicated Sorg spores ($p<0.0001$), suggesting that the process had modified spore surface properties. For the DS1813, CD630 and R20291, the sonicated strain also had lower RH values than the spores purified with Lawley method.

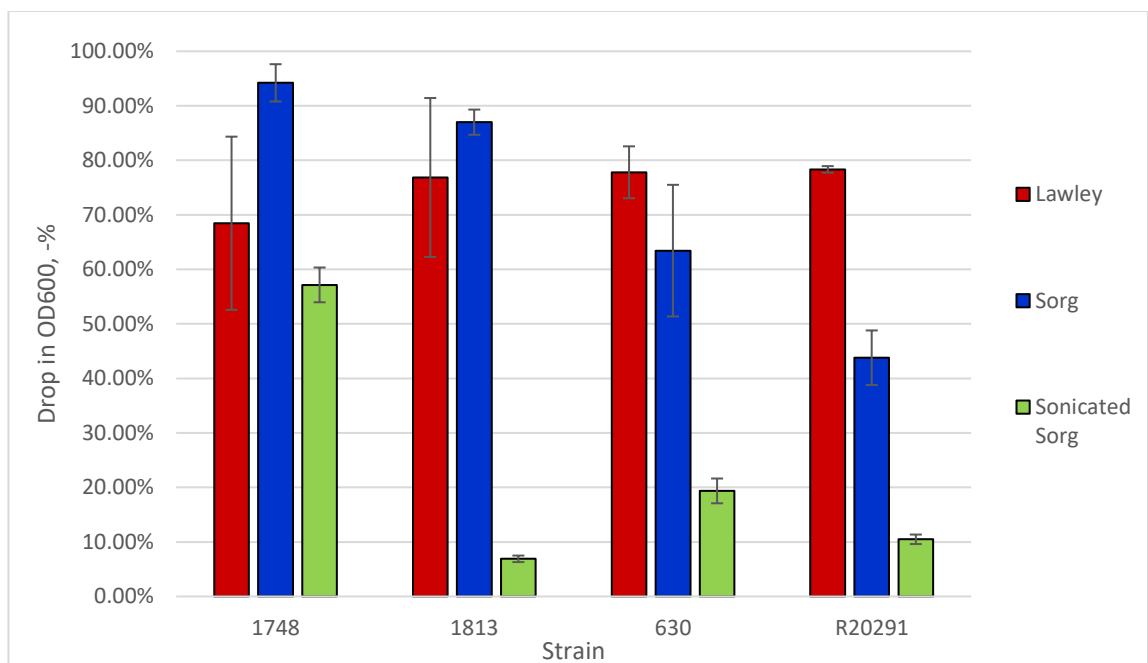


Figure 3.16. Relative hydrophobicities of different *C. difficile* spores produced using the Lawley and Sorg methods before and after sonication ($n=3$ replicates of each strain). Error bars indicate the standard deviation of results.

3.3.3.1 Characterisation of *C. difficile* spore coat mutants

Neither “pineapple-like” shapes like those of the DS1748 or the R20291 related structures (balloon like structures and filament projections) were seen. Typical spore images for each mutant strain can be seen below (Figure 3.17). Overall, no clearly identifiable visual difference was seen between the mutant stains.

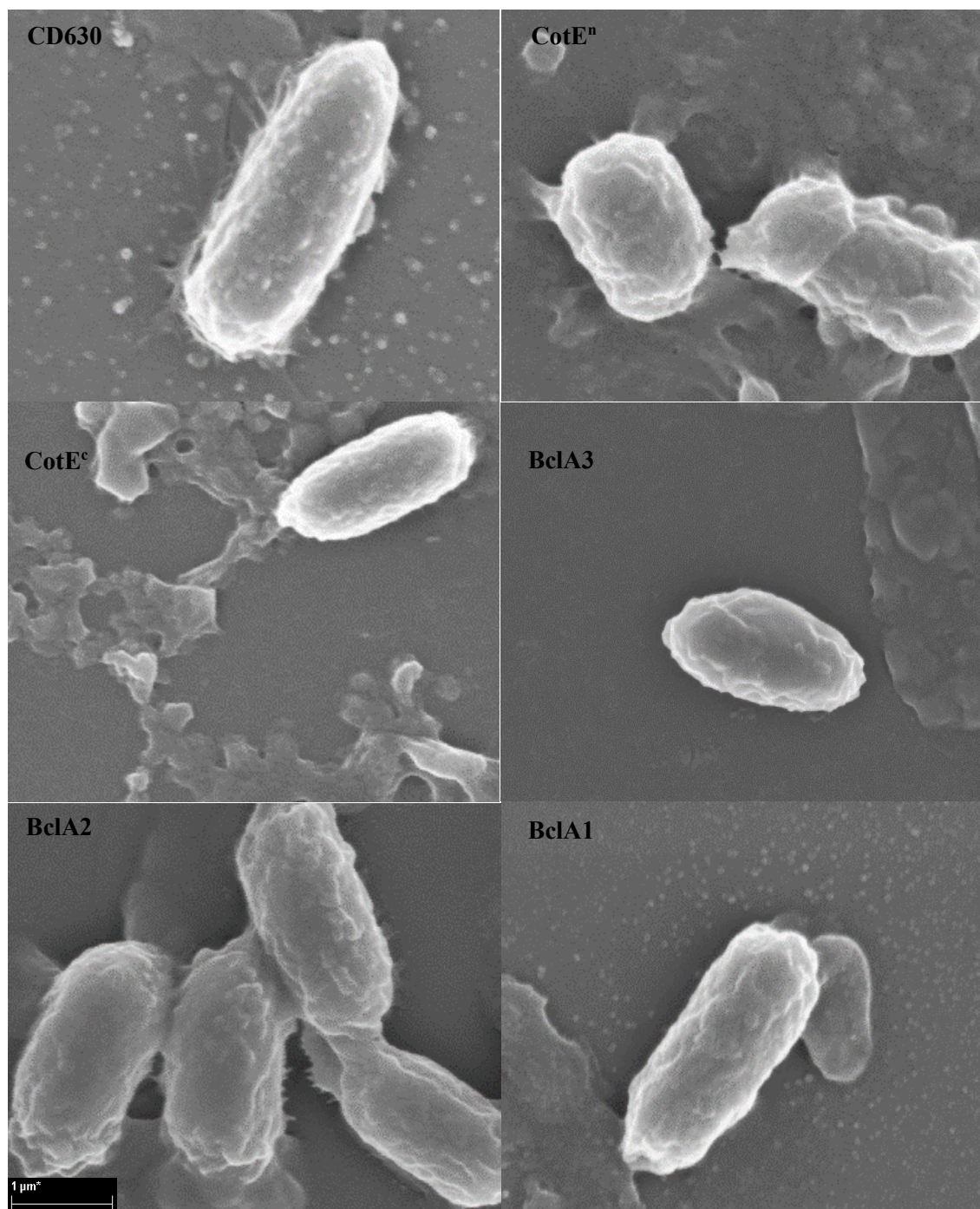


Figure 3.17. SEM of *C. difficile* spores of the structural gene mutants of CD630, showing no visible differences in morphology. The magnification was x34,140. These images are representative of 10 fields of view.

3.3.3.2 Relative hydrophobicity

The hydrophobicity of the spore forms of the structural protein strains (knockouts) was determined and compared to that of the parent CD630 strain. As can be seen from in Figure 3.18, values varied significantly ($p=0.0004$) with the *CotEn* and *BclA3* variants showing the greatest difference when compared to the parent strain. The greatest differences were seen in the *CotEn* and *BclA3* strains. *CotEn* is significantly higher in hydrophobicity than other strains ($p=0.001$). *BclA3* was the lowest in hydrophobicity ($p=0.006$).

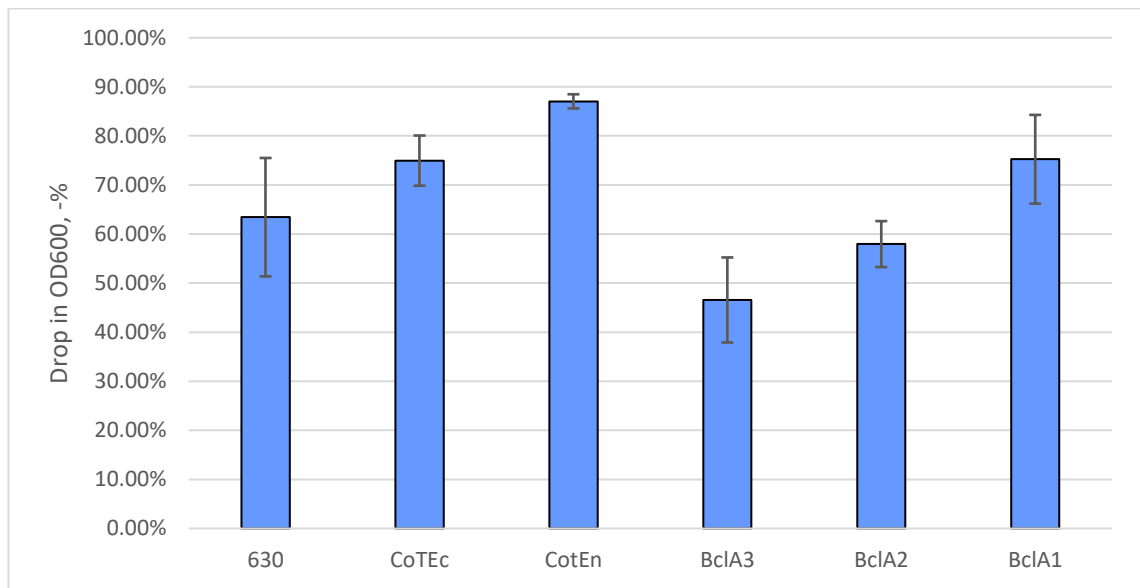


Figure 3.18. The relative hydrophobicity of spores of *C. difficile* strain CD630 and its mutants deficient in structural proteins. All spores produced and purified using the Sorg method ($n=3$ replicates of each strain). Error bars indicate the standard deviation of results.

3.4 Discussion

The results suggest that the Sorg method is the most suitable for future studies as it produces purified spores with a small number of steps and least damage to spore structure. Indeed, Pizarro-Guajaro and colleagues reported that the Sonication and Proteinase K step in the Lawley method may remove the outer layer of the spore (Pizarro-Guajardo *et al.*, 2014). As for the Heeg purification method, the low spore yields can be explained by the addition of antibiotic. A similar 10^4 - 10^5 spore yield per ml was observed by Phetcharaburanin *et al.* 2014 when using erythromycin selection for the mutants of *C. difficile* CD630. While the addition of antimicrobials to the culture media reduces the risk of contamination it can adversely impact on spore numbers.

The method used to grow *C. difficile* and purify the spores appears to affect spore size. The somewhat larger spores produced during the Lawley method could be due to both differences in the media composition and due to the fact that it was a liquid culture, as opposed to growth on agar.

The spores of different clinical isolates had clear differences in surface architecture. They could broadly be grouped into three morphotypes which were: pineapple-like (DS1748 and DS1813), surrounded a bag-like layer (R20291 and CD630) and smooth (DS1748, DS1813, R20291 and CD630). The ratio of each morphotype in the population varied depending on the clinical isolate and the purification method. Interestingly, clear differences in the appearance of spores were seen, from clinical isolates DS1813 (pineapple) and R20291 (bag-like) which belong to the same hypervirulent 027 ribotype.

In general, the Lawley method yielded the highest level of smooth morphotype spores with the exception of DS1748. The fact that the pineapple layer can be removed by sonication leaving behind a smooth surface suggests it might be a different form of the exosporium, a layer which surrounds many spore-forming organisms (Ball *et al.*, 2008). The ability of sonication to detach this layer may explain why the Lawley method which includes a sonication step, yields a higher proportion of smooth spores. This appears to be the first report of pineapple-like structures on the surface of *C. difficile* spores. They may be related to the “bumps” observed on the surface of the spores of TL176, TL178 and R20291 which have been linked to the “thick” exosporium morphotype (Pizarro-Guajardo *et al.*, 2016). However, unlike Pizarro-Guajardo *et al.*, the presence of short hair-like structures surrounding our spores was not seen, instead with long hair-like

features projecting from R20291 spores produced using the Lawley method. This may be due to the differences in the methods or the differences between TEM and SEM microscopy.

The differences between the isolates are not just visual, but also correlate with different properties. The strains purified with the Sorg method show significantly different hydrophilicities, with the strains lacking the loose exosporium having higher hydrophobicity. It must be noted the hydrophobicity of spores seems heavily dependent on the method used to purify the spores, as shown by the significantly different hydrophobicities in three of four the strains purified with the Lawley method, compared to Sorg method. A possible explanation is the inclusion of an extra minor sonication step as well the Proteinase K treatment in the Lawley method. However, even similar methods result in very different results in published literature. For example, the hydrophobicity of the 630 wild-type strain has been reported to be from 57% (Escobar-Cortes *et al.* 2013) to over 95% (Phetcharaburanin *et al.*, 2014), despite using very similar methods for growing and purifying spores as well as using the same hydrophobicity test.

Sonication resulted in the removal of the outermost layers of the spores and generally made them visually more similar to those purified by the Lawley method. Population statistics show the loose exosporium was effectively removed from the R20291 and 630 strains, making spores without a loose layer the most common in the sonicated spore population.

It was unexpected, that the removal of the outer layer from the spores of DS1748 and DS1813 strains would reveal a familiar smooth spore structure underneath, as the “pineapple” shape was initially thought to be the spore coat, as the DS1748 strain was reported to lack an obvious exosporium (Joshi *et al.* 2012). There is no indication in literature that sonication can remove solid spore coat layers. An alternative explanation is to follow the explanation by (Barra-Carrasco *et al.*, 2013) and treat the layer around DS1748 as a different “tightly bound” form of the exosporium. In this case, the question remains as to what causes such different states of the exosporium, given that the DS1813 strain and the R20291 strain belong the same hypervirulent ribotype. The appearance of spores with a loose exosporium in the sonicated DS1813 population, but not the non-sonicated suggests that these are different forms of the same structure, rather than separate structures.

Sonication drastically reduced the hydrophobicity of *C. difficile* spore suspensions, far more so than the Lawley method. This may be due to both exposed polar groups on the surface and due to remaining smaller exosporium fragments in the suspension.

Comparing the structural mutant strains, none presented the DS1748 or R20291 like structures. Nor was there any identified single clear unique characteristic that could reliably be seen on any of the mutant strains. Some spores had a different shape or appeared to have a different surface, but this was seen on some, not all spores of the same mutant strain. It was hoped that the spore structure deficiencies that were described by Phetcharaburanin *et al.* would be clearly visible, but this was not the case. Differences between SEM and TEM may make these malformed spores difficult to observe as they could look like debris.

At the same time, hydrophobicity measurements clearly show, that despite visual similarities, the strains are clearly different. Similar, but not directly comparable results for just the *BclA* mutants exist in Phetcharaburanin *et al.* The results for the *BclA* mutants obtained in this project seem to be in agreement, with *BclA1* having the highest and *BclA3* having the lowest hydrophobicity. However, the results for the non-mutant 630 strain are different. As mentioned earlier, reported results for the hydrophobicity of the wild type strain of 630 differs in published literature from less than 60% to over 95%, despite similar methods of purification and measurement. In this case this can lead to different conclusions. The Phetcharaburanin *et al.* results indicate that all *BclA* mutants have significantly lower hydrophobicity than the wild type strain. However, the results obtained here do not show a significant difference between the wild type, *BclA1* and *BclA2*, with only *BclA3* having significantly lower hydrophobicity.

The hydrophobicities of *CotE* mutants are significantly higher than the wild-type 630 and are similar with the DS1748 and DS1813 strains. This would be consistent with *CotE* being an important protein for exosporium formation, and lack of it leaving the hydrophobic spore coat exposed. However, these differences are not visually seen under SEM, suggesting that the differences are related to surface groups, and not overall exosporium layer stability.

In conclusion, the Sorg method was selected as the optimal method for spore production in other stages of this project. Significant variation in the spore morphology of clinical isolates of *C. difficile*, both in visual appearance and in hydrophobicity, was observed and

characterised. This is due in part to the methods used to sporulate and purify them. Sonication in particular can significantly change spore appearance and properties. This highlights the need for a common “standard” growth and purification method for *C. difficile* spores to allow for comparisons of results obtained by different research teams.

Chapter 4

Characterising DNA release from spores

4.1 Introduction

As was previously discussed in Chapter 1, *C. difficile* sporulates when growth conditions become unfavourable. Spores form a multilayer structure, with the core at centre containing the DNA, and isolated from the outside environment by the membrane, coat and exosporium layers. In previous studies it was shown that exposure of bacterial spores to microwaves results in the release of DNA, but the location from which the DNA was released was not established (Aslan *et al.*, 2008; Joshi *et al.*, 2014). The DNA detected in these preliminary experiments could have been derived from a number of sources:

- The spore core. Being the source of the entire bacterial genome, it is a likely source of *C. difficile* toxin genes.
- From fragments of vegetative bacteria in the suspension. Any spore suspension will contain fragments of vegetative cells that did not sporulate. These will also contain *C. difficile* toxin genes.
- Attached to the surface of the spore. Free-floating DNA may attach itself to the surface of spores. Due to the different surface properties of spores, DNA may attach more easily to different clinical isolates.
- From within the outer spore layers.

Having established the optimal method for the production and purification of spores, the next step was to determine the mechanism by which microwave exposure leads to the release of DNA from the spore. For this, it was important to remove extraneous DNA

from the suspension. This was important for several reasons. First, to confirm that the microwave treatment leads to release of DNA, and not just detection of DNA already in solution or debris. Second, to establish that the release of DNA is statistically significant, which will be easier in a sample that is free of DNA in solution. Finally, this will allow testing where the DNA comes from in the spore and determine the effectiveness of the chosen approach.

The working hypothesis was that the DNA observed comes from the spore core and is released due to microwave disruption. To determine if this is the case, the extraneous DNA was eliminated from the spore suspension. To achieve this, spore suspensions were treated with DNase which was then inactivated by heating and tested for DNA release after microwaving.

Spore disruption that causes the release of DNA could result in major structural changes in the spore. To investigate if this was the case, SEM was employed to compare microwaved spores to non-microwaved ones correlating any structural changes with DNA release. If the DNA is released from the core, as per the working hypothesis, then the spore will likely be damaged to provide route for DNA release.

The final point to address in this chapter was the nature of the DNA released from the spores following microwave treatment. In the context of a DNA based, rapid detection system, the DNA released needs to be in a form that is easily recognised by the detector systems. Based on the hypothesis about DNA release from the core, the expectation was that the DNA released is double-stranded (dsDNA), and not single-stranded (ssDNA), as this the form it is found in. To determine if this was the case, microwaved spores were stained by DNA-binding fluorescence dyes: Acridine Orange (AO) and Propidium Iodide (PI). With the green light excitation source used, AO would be fluorescent when bound to dsDNA, not ssDNA, while PI would be fluorescent with both dsDNA and ssDNA. PI is also a larger molecule (MW=668, compared to MW=235 for AO) and may have more difficulty permeating past the spore surface.

In the context of a rapid detection system, it was important that the DNA release from spores be as high as possible, at a level which will optimize its subsequent detection. Therefore, spore suspensions were tested on the relationship between exposure time and DNA release, to identify any plateau time value beyond which further application is not practical.

4.2 Aims and objectives

The aims of this chapter were:

- To develop a method which yields bacterial spores free of extracellular DNA
- To determine the conditions under which microwave exposure results in the release of DNA from the spores
- To determine the nature of DNA release, single or double-stranded

4.3 Results

4.3.1 Determining required stock concentration for Qubit

Qubit is a quantitative fluorometer system used to determine the concentration of DNA in a sample. It is sold as complete kits with all necessary ingredients, with different fluorophores selective for dsDNA, ssDNA or RNA. The limit of sensitivity of the Qubit assay is 100 pg/ μ l for the broad range (BR) assay and 10 pg/ μ l for the high sensitivity (HS) assay, in 200 μ l of solution. The maximum sample size for the assay is 20 μ l diluted in 180 μ l of buffer. The minimum weight of detectable DNA is therefore 20 ng (2×10^{-8} g) for the BR assay, and 2 ng (2×10^{-9} g) for the HS assay. To ensure that the samples contained sufficient DNA to give a measurable result, the number of bacterial spores which would be needed to yield sufficient DNA was calculated.

The *C. difficile* 630 genome is 4,290,252 base pairs long, in other words 4.3×10^6 . The average weight of a base pair is 650 daltons. 1 dalton is 1.67×10^{-24} grams. The weight of the *C. difficile* genome is therefore 4.7×10^{-15} g.

Each spore contains one copy of the genome, so number of spores needed to yield sufficient DNA for the HS assay, assuming 100% efficiency of release and no extraneous DNA would be 4×10^6 CFU/ml. It was therefore decided that bacterial spore stocks would be normalised to 1×10^7 CFU/ml to be well within the detection limit.

It was important to first estimate what spore concentration would be necessary to work with the Qubit system, so the assay has sufficient DNA to measure when spores are disrupted.

4.3.2 Removing surface DNA from purified spores

4.3.2.1 DNase Treatment

One of the principal aims of this project was to use microwaves to release the DNA trapped within the structure of the spore, so that it can be detected using the experimental diagnostic platform. Due to the way in which spores are produced from vegetative cells, it was likely that DNA is also attached to outer surface of the spore in a non-specific manner.

Given the level of sensitivity of the system used in the project, it is conceivable that the prototype detector system is detecting the presence of this external DNA rather than DNA

within the spore. To determine the efficacy of the microwaves at disrupting spore structure, it was necessary to remove this external DNA (see section 2.5.1). The level of residual spore surface DNA contamination was determined using two methods: the Qubit system (Figure 4.1), and fluorescence microscopy using acridine orange (Figure 4.2).

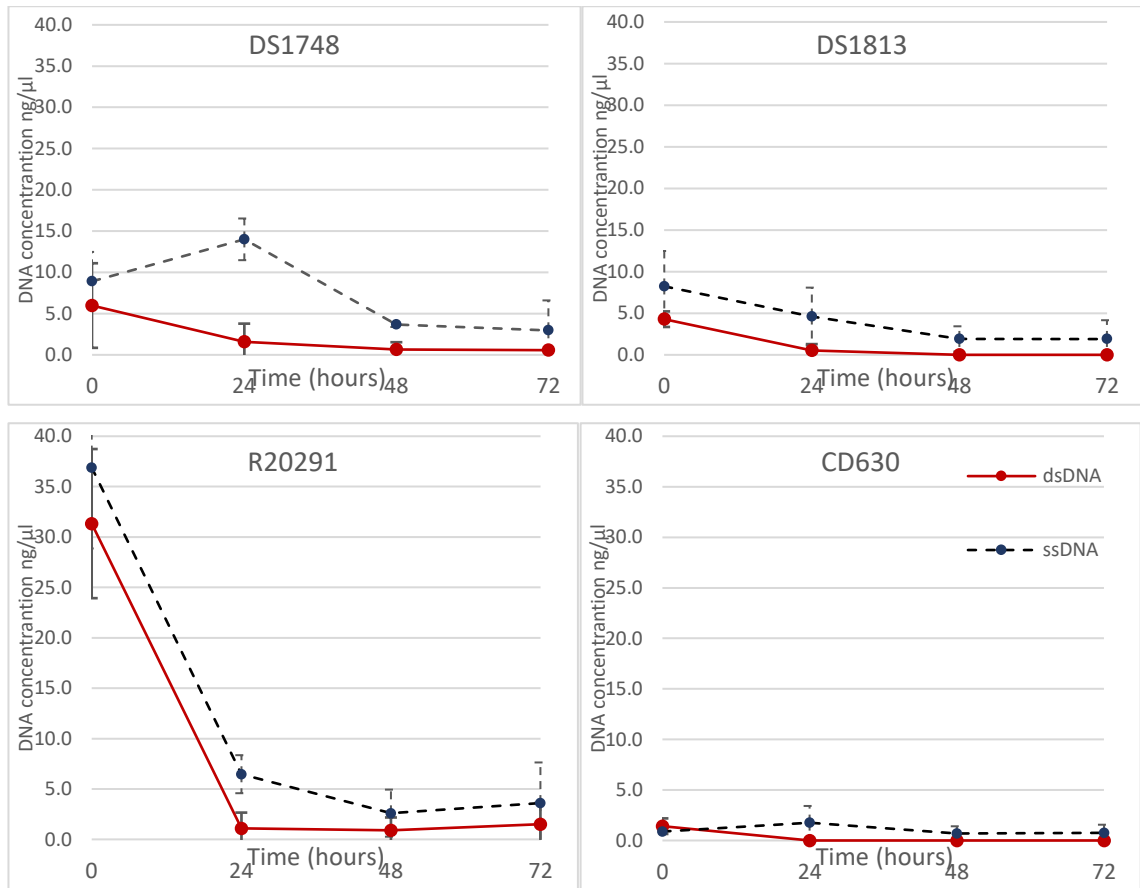


Figure 4.1. Level of dsDNA (red line) and ssDNA (blue line) detected in spore suspensions as a function of the duration of spore treatment with DNase. Quantification was done using the Qubit system in 24-hour intervals ($n=3$ for each data point). Error bars indicate the standard deviation of results. The different strains have different DNA concentrations initially but are all reduced after DNase treatment, reducing to below detection limit for dsDNA for all strains.

As can be seen in Figure 4.1, the DNase digest removed dsDNA to below detection limits. ssDNA signal remained at low concentration just above detection limits in all samples. It was notable that the DNA concentration in the R20291 strain was much higher than in other strains. This may be due to the presence of the loose baggy layer in the spores observed in Chapter 3. This layer may trap more DNA than the outer layers of other strains. ssDNA was not possible to completely remove due to fundamental limits of the DNase.

4.3.2.2 Staining *C. difficile* spores with DNA fluorophores

Acridine orange staining of unpurified spores was used as a positive control, to verify that the unpurified spores are covered in loose DNA. Observing samples directly can give more information than using Qubit, since it allows looking at individual spores to see the percentage of the population that is affected. As can be seen from Figure 4.2, the spore suspensions were fluorescent with both the spores and the non-spore material, indicating the presence of DNA both on the spore surface and on cellular debris.

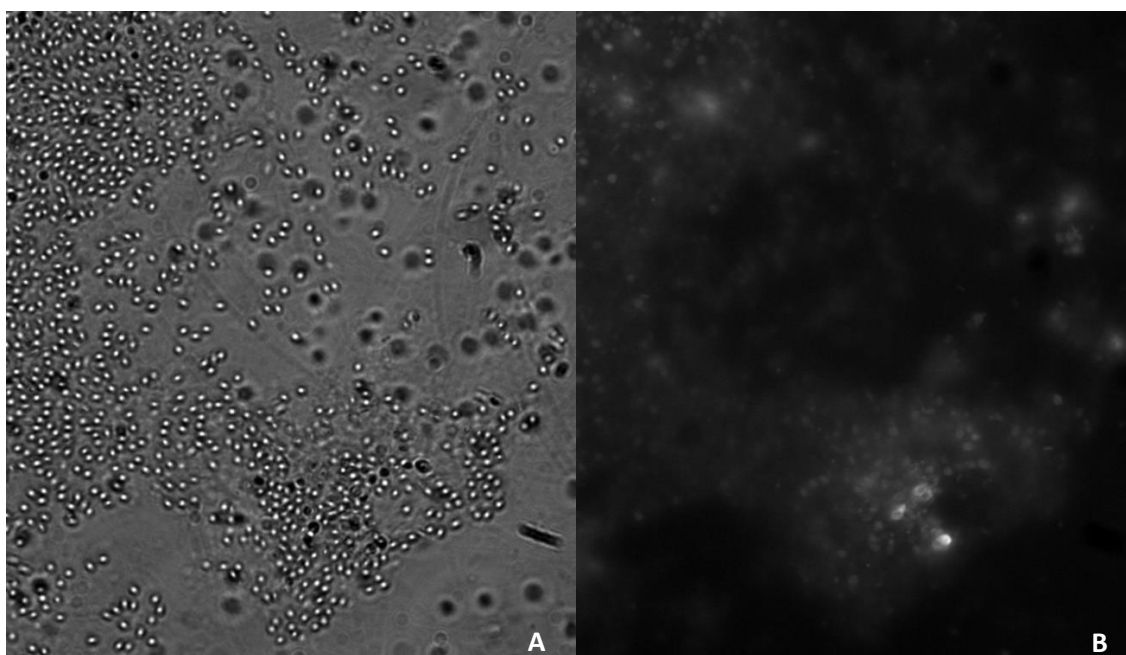


Figure 4.2. Images of the same field of view unpurified *C. difficile* CD630 spores (grown using the Sorg method, but not purified), viewed under phase contrast (A) or fluorescence microscopy with 0.1 µg/ml AO (B). Spores and the surrounding solution are fluorescent, indicating DNA is present there. This image is representative of 10 fields of view.

Next the purified spores (Sorg method) were tested to see if they retained DNA on the surface, by also staining them with acridine orange as before and viewing the spores by using fluorescence microscopy. As can be seen in the Figure 4.3A, there is no background fluorescence compared to unpurified spores shown earlier in Figure 4.2B. This is not limited to CD630, and other strains such as DS1748 on Figure 4.3B show a similar appearance. The spores themselves can be seen, with a resulting oval shape similar to *B. subtilis* spores (Schichnes *et al.*, 2006). This indicates that the DNA is present on the surface of the spores and the fluorophore does not penetrate into the core.

After DNase treatment, spores were less visible under fluorescence, indicating far less DNA on the surface of the spores Figure 4.3 (C, D). Due to rapid fluorescence decay of AO, it was not possible to quantify the decrease in fluorescence however, the camera exposure time to take the images was increased from 10 ms for sample not treated with DNase, to 100 ms for samples which were treated with DNase, indicating a 10-fold decrease or more in fluorescence, which agrees with Qubit data.

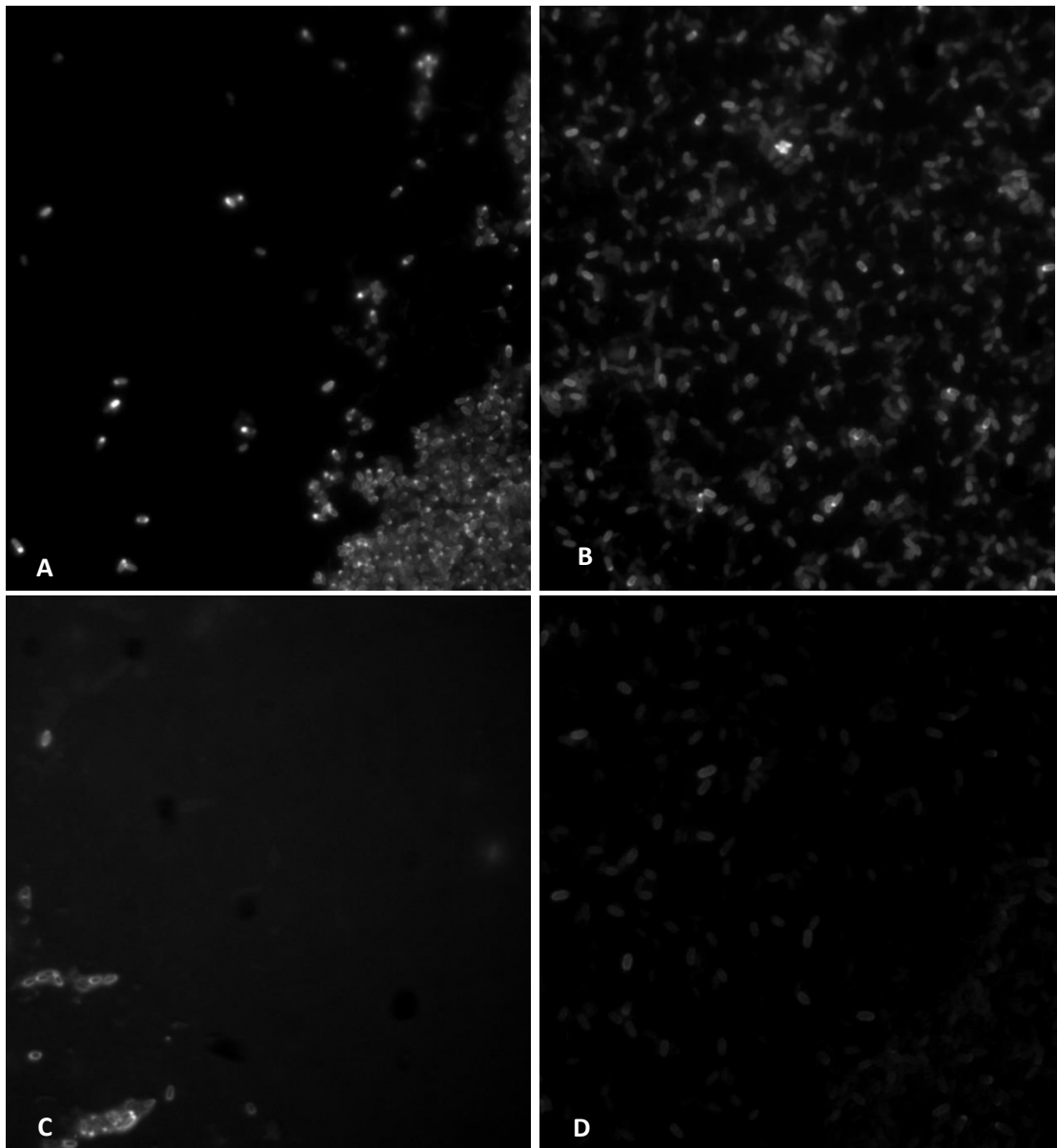


Figure 4.3. Fluorescence microscopy images of purified spores of *C. difficile* strains CD630 (A), DS1748(B) without DNase treatment. After DNase treatment, the fluorescence of the spores was reduced for both the CD630 (C) and DS1748 (D). Spores were stained with 0.1 µg/ml AO. These images are representative of 10 fields of view.

4.3.3 DNA released from spores after microwaving

The next step was to discover the nature of the previously reported release of DNA from microwaved spores. By comparing how a sample is stained with propidium iodide (PI) and with acridine orange (AO), the type of DNA released could be confirmed as well as making sure that the observed fluorescence is due to DNA and not due to non-specific binding.

Both stains are intercalating agents, capable of binding dsDNA, and ssDNA easily. However, AO forms different complexes with dsDNA and with ssDNA, resulting in different absorption and emission spectra (Rigler, 1966). With the excitation source used, dsDNA would have been visible, but not ssDNA. By contrast, PI forms the same complex with ds- and ss-DNA and its absorption and emission spectrum are identical for both (Cosa *et al.*, 2001). PI will not show non-specific binding, as unbound PI has a lower excitation and emission wavelength.

As can be seen from Figure 4.4, spores stained with AO remained pale and not very visible after microwaving, with only outlines seen, indicating there was no dsDNA on the surface of the spore. By contrast, part of the spores stained with PI did become brightly fluorescent. Therefore, the spores fluorescent under PI but not AO, are fluorescent in response to ssDNA and therefore microwaving causes spores to release ssDNA.

To confirm that this staining was representative of what would be seen in the presence of ssDNA, DNase treated spores of the DS1748 were mixed with ssDNA (20 ng/ml ssDNA from the Qubit calibration reference) and stained with AO and PI. As can be seen from Figure 4.3E and F, the same pattern was observed in the absence of extraneous ssDNA suggesting that ssDNA had indeed been released from inside the spore.

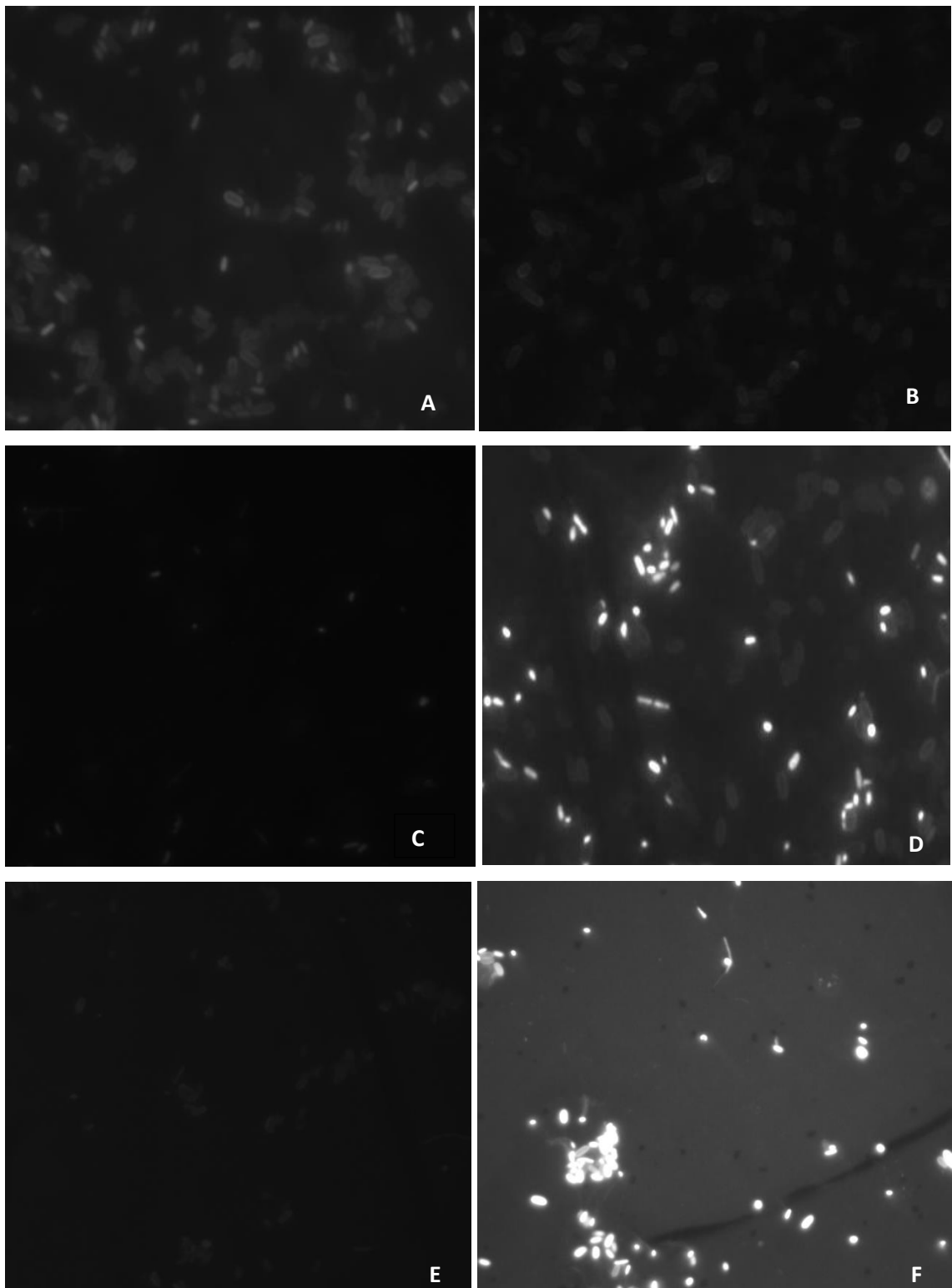


Figure 4.4. Fluorescence microscopy images of purified spores of *C. difficile* strain DS1748. A: no microwaving, stained with AO (1 ug/ml). B: 120 sec (10% duty cycle) microwaving stained with AO (1 ug/ml). C: no microwaving stained with PI (1 ug/ml) D: 120 sec (10% duty cycle) microwaving stained with PI (1 ug/ml). E. Control: spores vortex mixed with 20 ng/ml ssDNA for 1 min, washed and stained with AO (1 ug/ml). F. Control: spores vortex mixed with 20 ng/ml ssDNA for 1 min, washed and stained with PI (1 ug/ml).

4.3.4 Visual appearance of spores after microwaving

After establishing that the spores do release DNA, the next step was to check for any changes in spore appearance that could be correlated to the release of DNA. Using SEM, the spores were imaged before and after microwave exposure. As can be seen on Figure 4.5, the spores of the DS1748 strain looked visually intact after 120 seconds of microwaving. There was no visual difference in the appearance of spores compared to the appearance of non-microwaved spores in Figure 4.5A or to the images taken when characterising the spores in Chapter 3 (Figure 3.6). This was also true for other strains.

This means that while microwave exposure leads to DNA release, this effect is not destructive to the spores. This also indicates that the DNA does not come from the core of the spore. The likely source of the DNA is therefore one of the spore layers.

4.3.5 Spore disruption dependence on exposure time

The next step was to investigate how the number of fully fluorescent spores increases depending on exposure time to determine if increasing or decreasing the exposure time would give better results. As can be seen on Figure 4.6, there are no fluorescent spores before the microwave exposure, fluorescent spores increased in number following microwave exposure and their number increased with longer microwave exposure times, reaching 22% of the population after 120 sec.

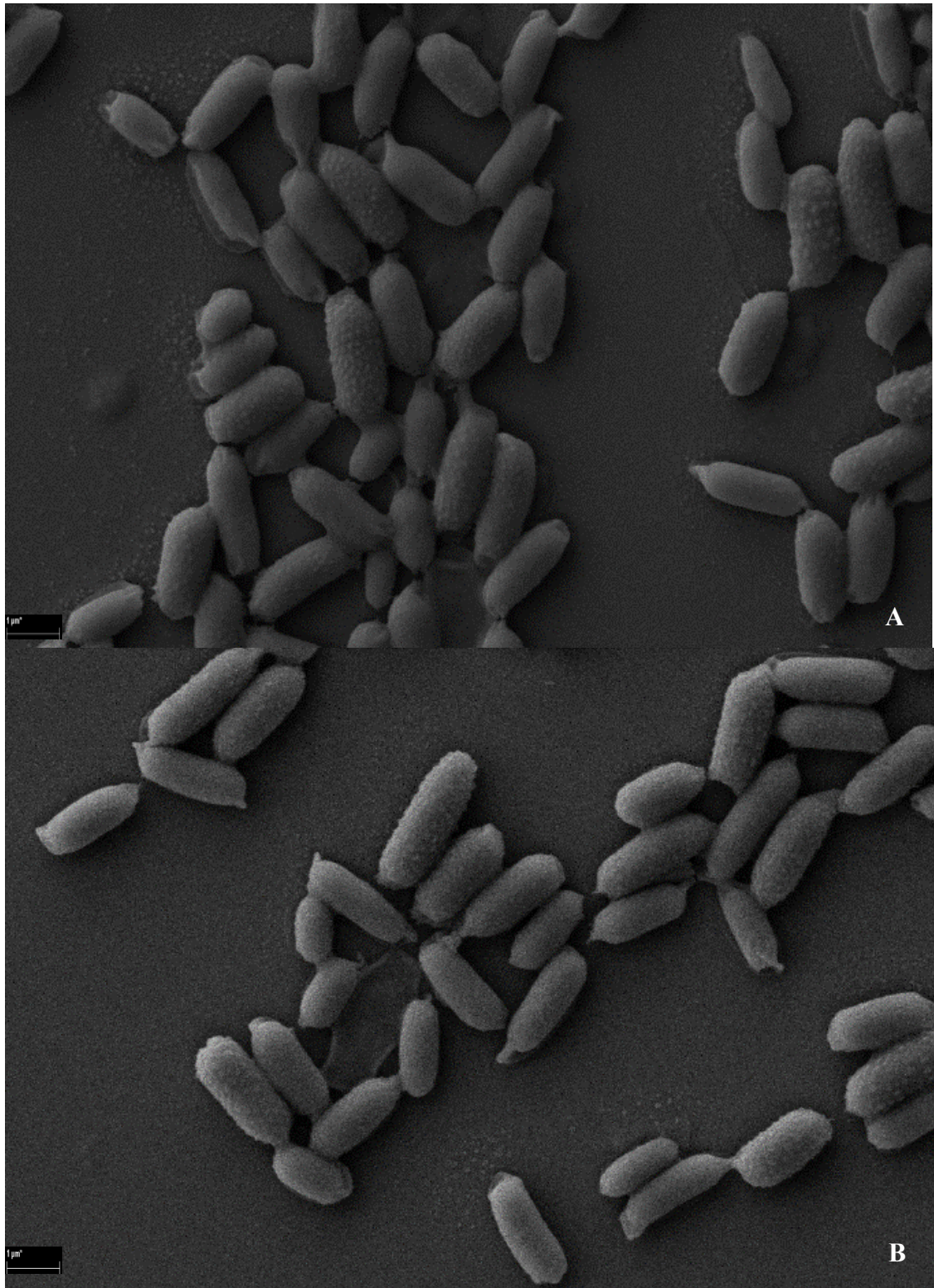


Figure 4.5. SEM of *C. difficile* spores of the DS1748 strain spores. A: no microwaving. B: 120 sec (10% pulse) microwaving. There was no visual difference between the two populations after looking at more than 200 spores across 10 fields of view in each sample. The magnification was x15,000.

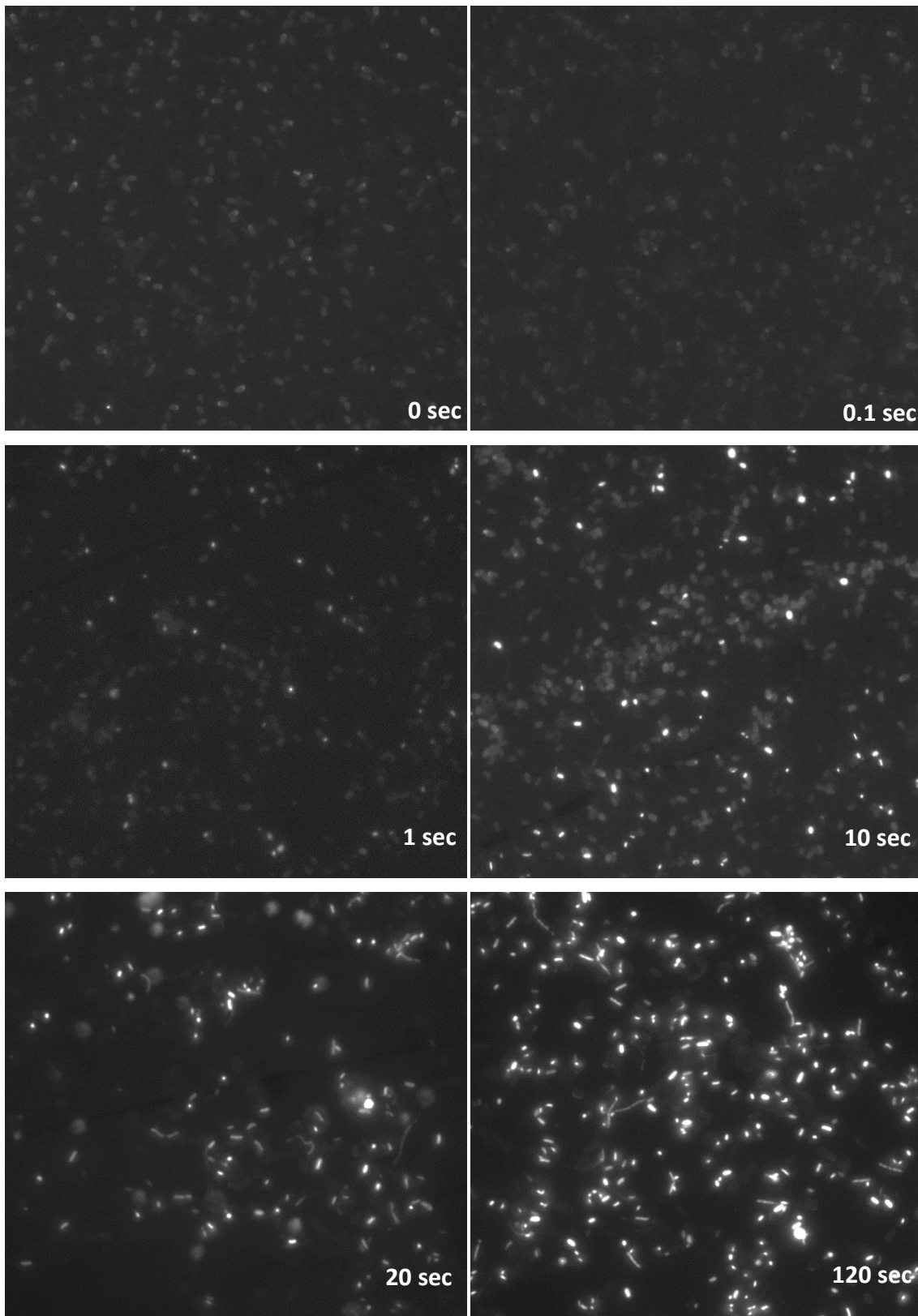


Figure 4.6. Fluorescence microscopy images of purified spores of *C. difficile* DS1748 using PI following exposure to microwaves (10% duty cycle). Bright fluorescent spores begin to appear at 1 sec microwaving and are most abundant at 120 sec.

This apparent increase in the percentage of fluorescent spores was quantified for the different clinical isolates (Figure 4.7). The increase in fluorescent spores is significant over time (ANOVA $p < 0.0001$), and proportional to the \log_{10} of the exposure time.

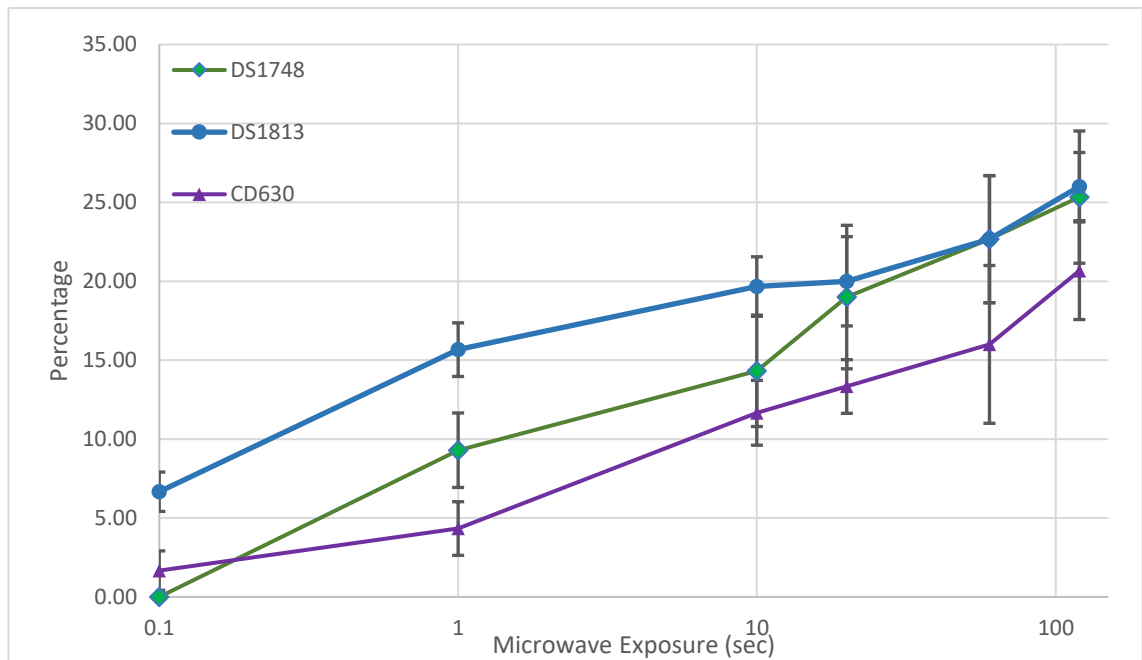


Figure 4.7 Ratio of fluorescent spores to total spores for different strains of *C. difficile*. The increase in fluorescent spores appears to increase logarithmically with exposure time. The log x-axis means there is no $t=0$ on it, but in all 3 strains, the percentage of fluorescent spores at $t=0$ is $<1\%$ of the population. $n=3$ for each data point, error bars indicate the standard deviation of results.

It was not possible to gather similar data in the for the spores of the R20291 strain in this experiment. The loose layer which is present in the R20291 strain can itself be brightly fluorescent (see Figure 4.8). This makes it difficult to tell apart the fluorescent spores from the fluorescent loose layer. So fluorescence microscopy was unsuitable for determining the increase in fluorescent spores in the R20291 due to microwaving. However, this fluorescence was an important result, which showed that DNA can be found in the loose layer and that this layer could be a source of DNA detected by Qubit.

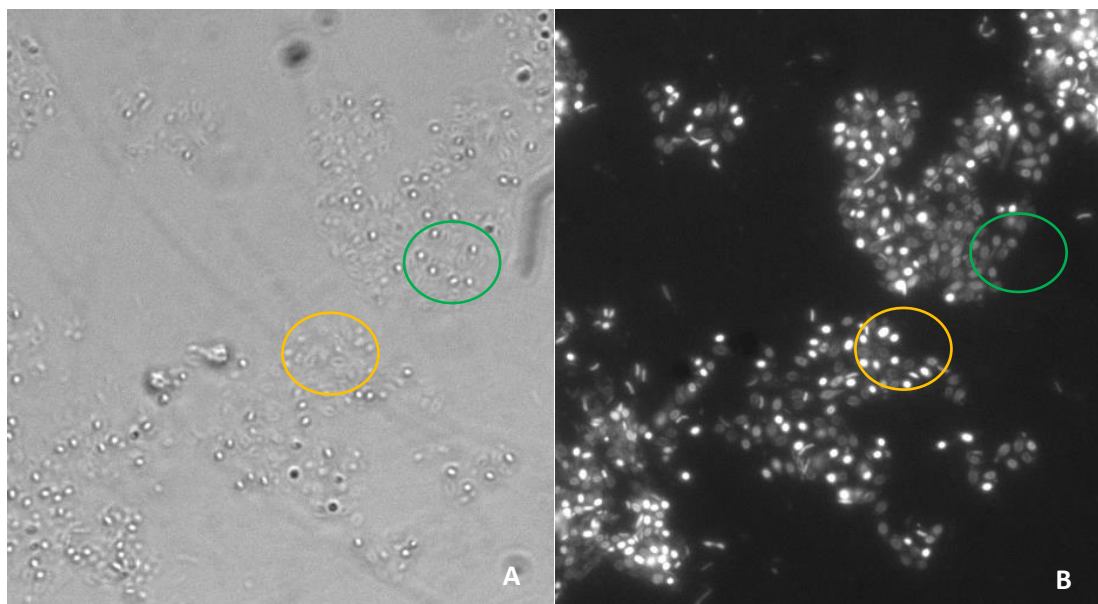


Figure 4.8. Images R20291 spore suspension (same field of view) viewed under phase contrast (A) or fluorescence microscopy with PI (B). The green area has 6 phase bright spores, none of which are fluorescent under PI. The orange area has no phase-bright spores, but the baggy layer is fluorescent. Due to this fluorescence, counting the number of fluorescent spores only is not possible.

4.3.6 Asymmetrical DNA fluorescence of spores

When staining *C. difficile* spores with DNA-binding dyes, some spores were noted to be asymmetrically stained. These spores had a fluorescent region at one pole of the spore only (Figure 4.9). This differential fluorescence was seen in spores of DS1813, DS1748 and CD630, when stained with AO or with PI. It was not seen in the R20291 strain, but this may be due to fluorescence from the loose exosporial layer (Figure 4.8) masking the effect. The fluorescence with acridine orange indicates that there is dsDNA in this region, which is notable, since dsDNA was not released in the microwaved samples. It is possible that what small amount of dsDNA is released is broken in to single strands under the effect of microwaves.

This effect was seen in in spores both before and after microwaving and was seen in $3.7 \pm 2.3\%$ of spores. There was no statistical difference between the different strains or microwave exposure (ANOVA $p=0.28$). This indicates that this is a common feature of the spores that is unaffected by microwaving.

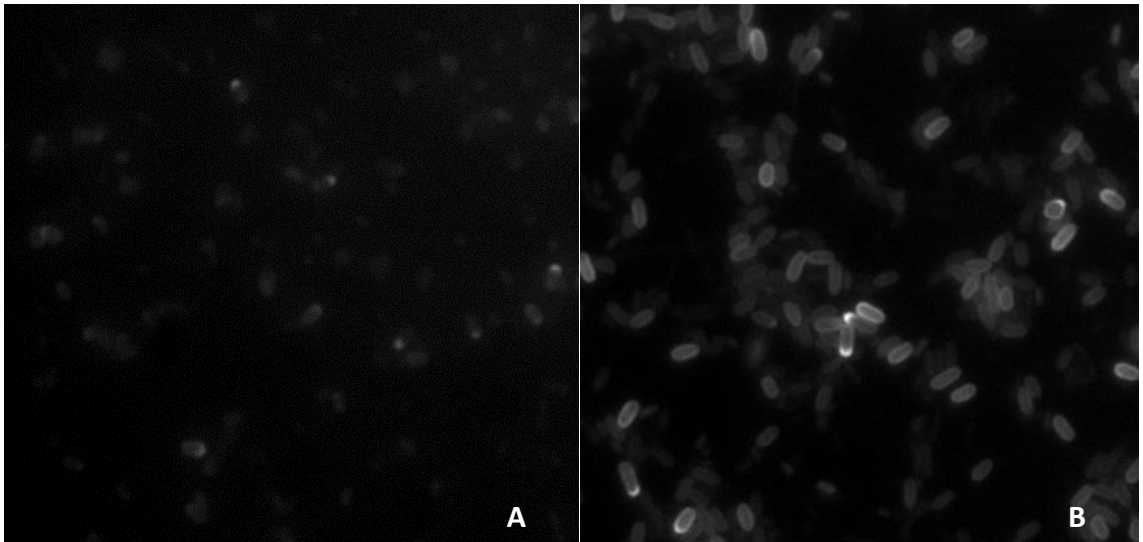


Figure 4.9. Fluorescence microscopy images of purified spores of *C. difficile* of strain DS1748 using PI (A) or AO (B). The brighter localised fluorescence can be seen in both case on a small number of spores.

4.4 Discussion

The results obtained with fluorescence microscopy show that purification does remove DNA from spores, although not equally effectively from different strains. Without DNase treatment, all purified spores still have both dsDNA and ssDNA on the surface and in solution. With DNase treatment, dsDNA was removed below Qubit detection limits and the fluorescence using AO was very low. ssDNA was more difficult to remove, and trace amounts could be detected by Qubit even after a 72 hour incubation, even though these spores were also not fluorescent using PI (see Figure 4.4C). There are multiple reasons for this difference:

1. The Qubit reagent binding to non-DNA components
2. The reagent not binding well to DNA bound on the spore surface
3. The reagent binds less well to shorter DNA strands
4. For a spore clump, may a lower result than separate spores

It is important to highlight that the different fluorophores have different sensitivities. The Qubit dsDNA reagent does not bind well to strands below 20 b.p. in length. By contrast, acridine orange binds to all nucleotides down to the fragments as short as a couple of base pairs long, which means it could still detect the tetramers digested by the DNase I. As such, it was important to use all the different methods, to be able to tell what is being detected. Overall, DNase treatment did effectively remove DNA from the suspension so new DNA detected afterwards did come from the spores.

It was confirmed that the spores release ssDNA and no dsDNA after microwaving. This meant that the DNA was unlikely to be coming directly from the core of the spore as hypothesised, since the core contains the genome in dsDNA form. SEM imaging has shown that microwaving does not appear to change the surface features or shape of the spore. Nor could any features of microwaved spores be correlated to the percentage of which were fluorescent when stained with PI. This further reinforces the conclusion from the fluorescence data, that the detected DNA does not come from the spore core. Any disruption sufficient to cause leakage of DNA from the spore, would have caused visible changes to the spore. Therefore, it is most likely that the ssDNA detected comes from the outer layers of the spore, like the exosporium and microwaving causes it to be released. A possible explanation is that the DNA was trapped during exosporium formation step in sporulation.

To optimise the setup for the experiments with the nanoparticles, it was important to identify the amount of time for the exposure. Initially, there appeared to be no statistical difference between exposure times of 20 and 120 seconds (Figure 4.6) based on the number of fluorescent spores, indicating that the effect happens over a shorter exposure period. Further experiments have shown that the number of fluorescent spores increases logarithmically with exposure time. This indicated that a short exposure time, around 10 seconds would be sufficient to produce DNA for detection.

When observing spores stained by AO and PI, some spores were noted much brighter stain on one end of the spore, indicating a high DNA concentration there. Pronounced staining was observed at the one of the two poles of the spore in different clinical isolates. This feature could not be correlated to any part of the spores visible under SEM. This feature could be related to “apertures” reported on *C. sporogenes* (Brunt *et al.*, 2015). These were protrusions on the exosporium, aligned with the location where the cell would emerge during germination, located on the pole of the spore. The exosporium of *C. difficile* is different, with “pineapple” structures on DS1748 and DS1813, with loose layer on R20291, and no visible exosporium on CD630. This means the equivalent structure to the *C. sporogenes* apertures may not be visible under SEM, but nevertheless still exist as a more permeable area of the spore, allowing fluorophores to bind there.

In conclusion, in this part of the investigation, it was established that the release of the DNA does happen from the spore and specifically that this ssDNA being released from the outer spore layers. This information allowed for optimisation of the microwave generator setup, detailed in Chapter 5. In addition, the presence of DNA trapped near spore surface raises questions on the biological purpose and significance.

Chapter 5

Optimising the microwave generator setup

5.1 Introduction

As was previously described in Chapter 1, microwaves are a form of electromagnetic radiation. Microwaves typically refers to waves 1-1,000 mm long (this corresponds to frequencies of 300 GHz – 300 MHz). The electric and the magnetic field components can be used as ways to deliver energy to the sample as a way of heating it. This has been previously used with spore forming organisms (Kim *et al.*, 2009; Celandroni *et al.* 2004; Vaid & Bishop, 1998). However, the nature of microwave heating, which happens under reorientation of charged groups of a molecule (a form of “friction” to heat up the surroundings) is different from that of simply heating the sample directly and athermal effects have been widely documented (Banik *et al.*, 2003). For that reason, microwaves have been used for changing and enhancing biochemical reactions, which happens with microwaves, but not under heating alone (Chen *et al.*, 2014; Collins & Leadbeater, 2007).

For this project it meant that the fundamental cause microwave-based disruption that was previously carried out in Cardiff University (Aslan *et al.*, 2008; Joshi *et al.*, 2014) may have been electric and magnetic field effects too, rather than temperature gradients or localised heating. Taking this as a working hypothesis, this meant that high microwave power was not necessary for the disruption. Instead, a high electric or magnetic field concentration for a brief period of time would be needed instead. This led to the design of a microwave cavity and microwave system for this project.

The microwave generator is a custom-built piece of equipment built in the Cardiff School of Engineering in 2013, prior to the start of this project, as a test bed for rapid microwave-based spore detection. Preliminary experiments at the time, as well as the results from Chapter 4 show that DNA can be released from spores using this setup. However, to be able to optimise the system, it was important to understand how the system works, rather than just running experiments with the system as a user. The schematic diagram for the system, as it was at the start of the project (in 2014), is shown on Figure 5.1.

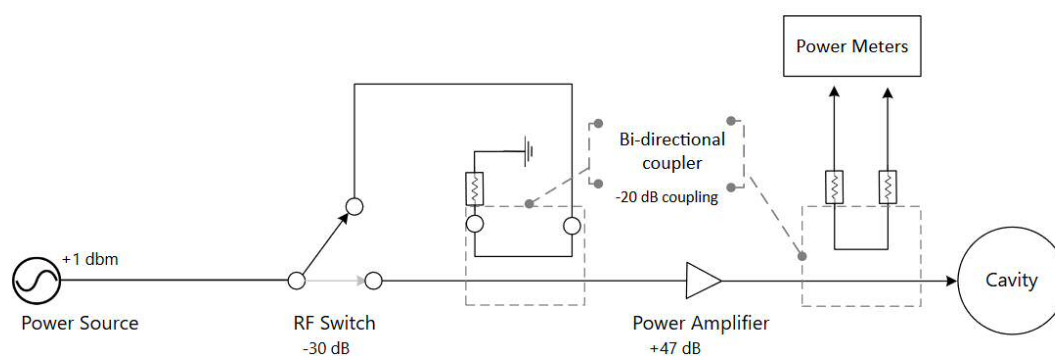


Figure 5.1. Schematic of the setup of the microwave generator. The generated signal passes through an RF switch where, depending on the switch state it either goes directly through to the power amplifier, or first passes through a bi-directional coupler where it is attenuated. The power amplifier increases the signal by approximately +47 dB, and this signal then enters the cavity. A second bi-directional coupler has the coupled outputs going to the power meter to allow monitoring of the signal strength. The theoretical full power output, after cable and equipment losses is approx. +45 dBm (31.6 W).

A key feature of the system was the relatively low output power (around 30 W), which could further be decreased by pulsing the power by selecting a short duty cycle. For example, 10% power, which was used in Chapter 4, was achieved by selecting a 10% duty cycle where a pulse of 100 ms “on time” was repeated for every 1 sec of system operation. This could easily be changed to obtain values of as low as 0.1% “power”. Compared to earlier experiments, such as Celandroni *et al.* (2004), where powers of up to 700 W were used, the power used in this project was much smaller. This setup had a major advantage in that the sample could be exposed to a stronger electric field, but for shorter time duration, and hence without an associated rapid increase of the sample temperature. Such a rise would be hazardous to the DNA within the sample due to sample

boiling as well as being a hazard to from the health and safety point of view (hot vapours potentially containing *C. difficile* spores). A high power without heating could also allow the investigation of the electric field effects decoupled from temperature effects which often interfere in similar experiments in published work (Novikij *et al.*, 2016).

For this part of the project, the main goal was to investigate the optimal settings on the device to maximise DNA release without increasing the temperature rise. For that, the first step was to optimise the power settings to minimise the overall heating of the sample and verify that the theoretical predicted values match the real measured effects.

The next step was to determine if the electric field, magnetic field or both affect the disruption of spores. As was discussed in Chapter 2, there are multiple effects from microwaves, including direct heating of the sample, polar molecule vibration/realignment and magnetic field effects. By limiting the overall heating of the sample, the heating effects, if any, are minimised. To investigate the origin of microwave disruption, a different microwave cavity was used, previously described by Williams *et al.* (2016). This cavity contained 3 sample holes: one for maximum electric field exposure, one for maximum magnetic field exposure, and one where both electric and magnetic fields were at approximately 50% of their maximum value. Finally, to verify if the existing power setting is optimal, the effect of field strength on the spore disruption was investigated.

5.2 Aims and objectives

The aims of this part of the project were:

- Verify the parameters of the microwave system
- Design a setup for the system to minimise sample heating to below 2 °C
- Determine the separate roles of electric and magnetic fields in spore disruption

5.3 Materials and Methods

5.3.1 Microwave system components

The components from which the microwave system (see Figure 5.1) was built were as follows. The TEG-4000-1 microwave signal generator was connected to a TES-6000-30 RF switch (both sourced from Telemakus), which in turn was connected to a ZABDC20-322H-S+ bi-directional coupler (Mini-Circuits). This was connected to a ZHL-30W-252-S+ power amplifier and to a microwave circulator to protect the circuit (NG-3548, Racal-MESL). One of the ports was connected to a ZRP-Z51 power sensors (Rhode & Schwarz), the other was connected to another ZABDC20 coupler. The output from the coupler was directly connected to the cavity, while the coupled signals were connected to two TED-8000-40 (Telemakus) power sensors, which were plugged in to a 4-way D-Link controller. The D-Link was connected to the microwave source and the RF switch to be able to operate the system.

The system was operated from a laptop (connected by USB to the controller), where a custom program (made in LabVIEW 2012) was responsible for providing the user interface for the system.

In addition to the general methods detailed in Chapter 2, the following methods were also used in this chapter.

5.3.2 Cavity Q-factor

The cavity $|S_{11}|$ was recorded with an Agilent PNA N5232A network analyser. The -3 dB bandwidth was then used with a loaded (with sample) and an unloaded (with no sample) cavity. The Q-factors were then used to determine the power going into the sample based on the formula (Clark, 2017):

$$= \frac{\text{---}}{\text{---}}$$

5.3.3 Measuring sample heating

To measure the temperature changes in the microwaved samples, the samples were set up as previously described in Section 2.4. A Luxtron fibre optic temperature sensor (LumaSense Technologies, USA) was used to measure the temperature of the sample immediately before and immediately after microwave exposure. The probe was kept away from the sample during microwaving, to avoid the probe material affecting the results. This was repeated 3 times, for each sample and the temperature rise was recorded.

5.3.4 Measuring the effect of electric field strength

The samples were set up as previously described in Section 2.4. The input power was attenuated before the power amplifier using 1, 3 and 6 dB attenuators. The new output power was verified using the built-in power meters. The effect of the reduced power was determined by using fluorescence microscopy and the ratio of fluorescent spores using propidium iodide (PI) as previously described in Chapter 4. The reduced power was converted into an electric field reduction based on the proportional relationship $P \propto E^2$.

5.4 Results

5.4.1 Verifying system properties

5.4.1.1 Verifying the power output of the system

The power recorded by Telemakus built-in power meters was 41.9 - 42.2 dBm (15.5 – 16.6 W) for the samples tested. The power recorded by the Agilent power meter connected in place of the cavity was 40.7 - 40.9 dBm (11.7 – 12.3 W), yielding an average value of 12 W.

Thus, while the power output of the system is consistent, the reading of the Telemakus power meter is related to the power reaching the cavity, minus 1.3 dB (a linear factor of 1.35), which can be attributed to the extra attenuation due to the cable connected to the cavity. The difference is statistically significant ($p < 0.0001$). The measured power level is also significantly lower than the 45 dBm (30 W) that was expected from the system, which may have been caused by the system age and power amplifier performance.

5.4.1.2 Cavity Properties

The variation was determined to be due to setup of the system in the laboratory. The relatively short cable which connects the cavity to the rest of the system was in a U-shape, putting strain on both connections, and affecting the coupling during sample exchange. When keeping the cavity setup was changed, so the cable was straight, the results were much more consistent, both in the peak depth and frequency.

The cavity Q-factor of the cavity was worked out at 4,416 for the loaded cavity, and 351 for the unloaded cavity. Based on Equation 5.1, this translated to 92% of the input power was absorbed by the sample.

Overall, this confirmed that there is no significant power reflection and that most power is absorbed by the sample, so no further optimisations were needed there.

5.4.2 Designing a minimal heating microwave setup

5.4.2.1 Initial estimations of sample heating

The predicted heating of a material is given by the following formula.

$$\Delta T = \frac{Q}{C} \quad (5.2)$$

where ΔT is the change in temperature, C is the heat capacity, and Q is the total energy added to the system. The heat capacity C of the samples in the experiment is:

$$C = cm \quad (5.3)$$

where c is the specific heat capacity of the suspension, which can be approximated to be equal to the heat capacity of water, $4.2 \text{ Jg}^{-1}\text{K}^{-1}$. m is the mass of the sample, which is 0.15 g ($150 \mu\text{l}$ of water). This gives a C value of 0.6 JK^{-1} .

Now going back to Q , its value was initially treated as being:

$$Q = Pt \quad (5.4)$$

where P is the power absorbed by the system, 11 W (92% of 12 W), while t is the total on-time. For example, at 10% duty cycle for 10 seconds, the $t = 1 \text{ sec}$, $Q = 11 \text{ J}$ and $\Delta T = 11/0.6 = 18.3 \text{ }^\circ\text{C}$. This predicted value indicated that the sample heating would be substantial, however at 1% duty cycle the sample heating would be less than $2 \text{ }^\circ\text{C}$, which would be sufficient to investigate the field effects without thermal effects. Thermal effects were the problem which prevented the Novikij *et al.* 2016 study to establish the cause of microwave-based effects, so avoiding the same problem was crucial.

5.4.2.2 Actual sample heating with initial setup

When the actual heating of the sample was measured using a temperature probe, the results were different to the expected values (see Figure 5.2). The actual heating of the sample was higher than that predicted ($p < 0.0001$), and it was apparent that another factor was affecting results. Irrespective of duty cycle setting the heating of the sample remained around $10 \text{ }^\circ\text{C}$, which indicated a power leak into the cavity.

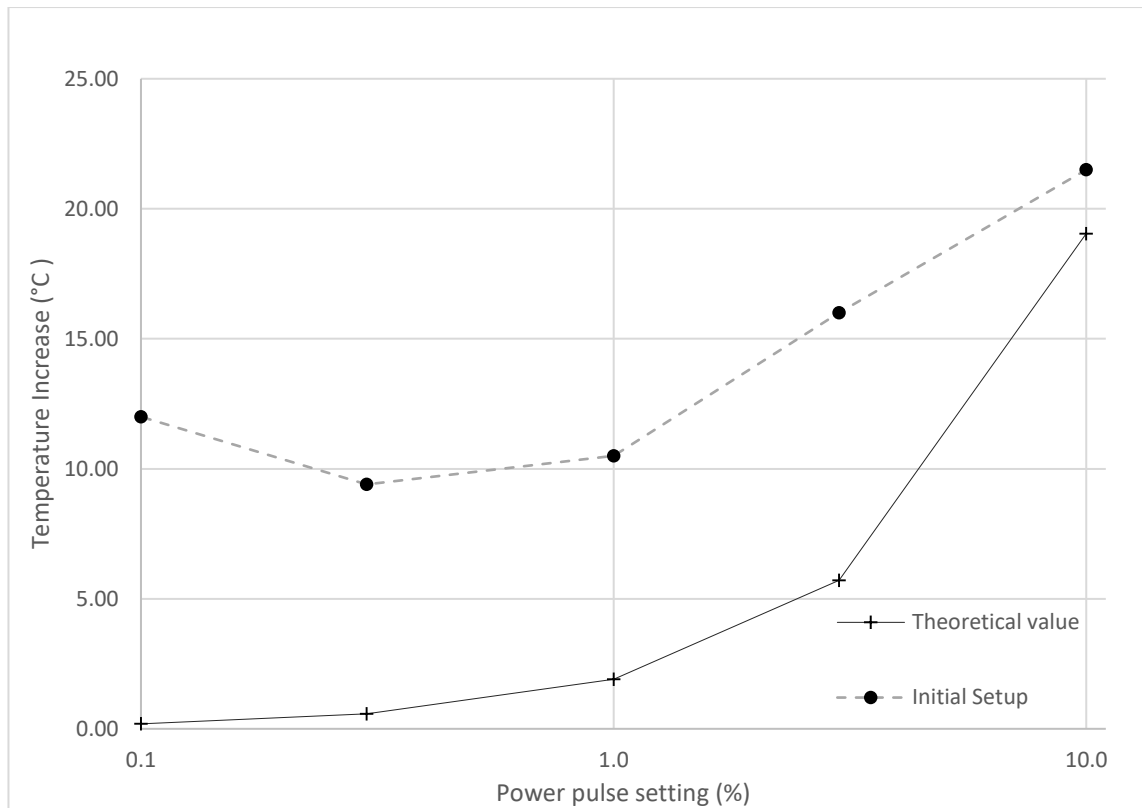


Figure 5.2. Temperature increase of a 150 μl sample following microwaving for 10 seconds at a given duty cycle. There was a difference between the heating of the sample using initial microwave setup, and the theoretical value predicted. The actual heating of the sample was significantly higher than expected remaining at around 10 $^{\circ}\text{C}$ at any low power setting.

Going back to the design and components of the microwave stem, there were two sources of the power leak identified:

- The first was the bi-directional coupler which attenuated the signal from the source into low-power. The -20 dB coupling was not providing enough attenuation for the system, letting power leak through.
- The second source was the RF switch itself, which also had insufficient isolation (-30 dB) meaning that even if the coupler was isolated, enough power would pass through the closed switch to cause sample heating.

Together, these issues combined led to a low power output of 30 dBm (0.8 W), which meant that at low pulse settings, the majority of the heat energy was provided to the sample when the power should be switched off, becoming a major systematic error in gathering data at low pulse settings. This power leak was confirmed by the internal and external power sensors and did fit the observed 10 $^{\circ}\text{C}$ heating at low power settings.

5.4.2.3 Optimising the system to eliminate power leaks

After identifying the cause of the excess heat, the circuit was changed to lower the leaked power. The RF switch was changed to one of a higher isolation (50 dB instead of 30 dB), the coupler had additional attenuators added and cables were replaced. The Labview control files were updated to operate with the modified system. The changes are summarised and illustrated on Figure 5.3.

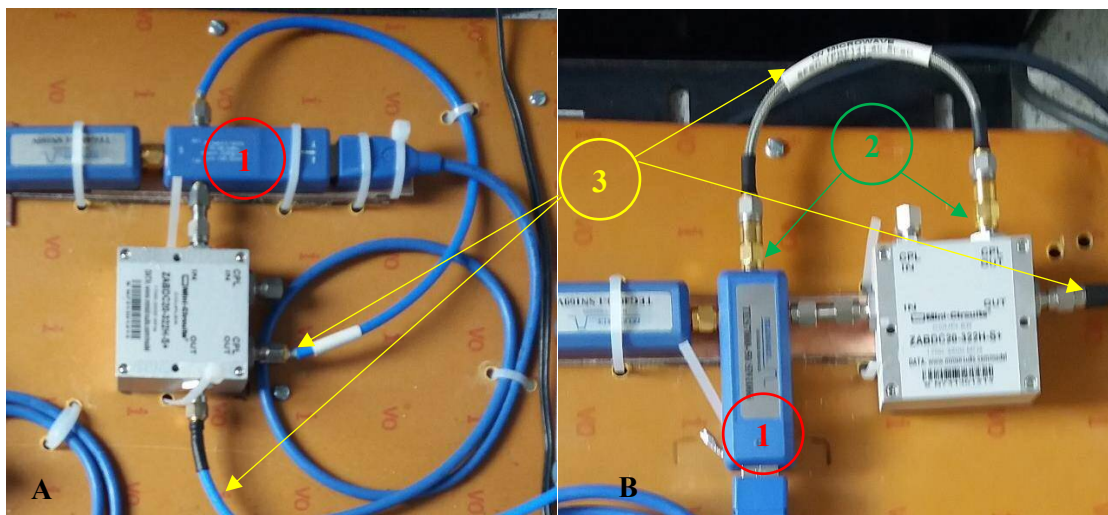


Figure 5.3. Summary of the changes to the initial microwave generator system (A) to the new setup (B) to minimise power leaks. 1: replacing the TES6000-30 RF switch with a higher isolation TES7000-50 switch. 2: adding another 24 dB isolation to the loop passing through the coupler. 3: rearranging the circuit to reduce the stress on the cable connections and replace the rope cables with more flexible metallic cables.

After these changes, the full power of the system was unchanged at around 41 dBm (12 W), but the low-power was found to have decreased to -3 dBm (500 μ W). With this power level, the observed heating of the samples aligned with those that were predicted theoretically, showing that the low-power leak was no longer an issue (Figure 5.4). The duty cycle settings of 0.3% and below resulted in sample heating of less than 2 °C and were therefore suitable for the subsequent experiments, with minimal overall sample heating.

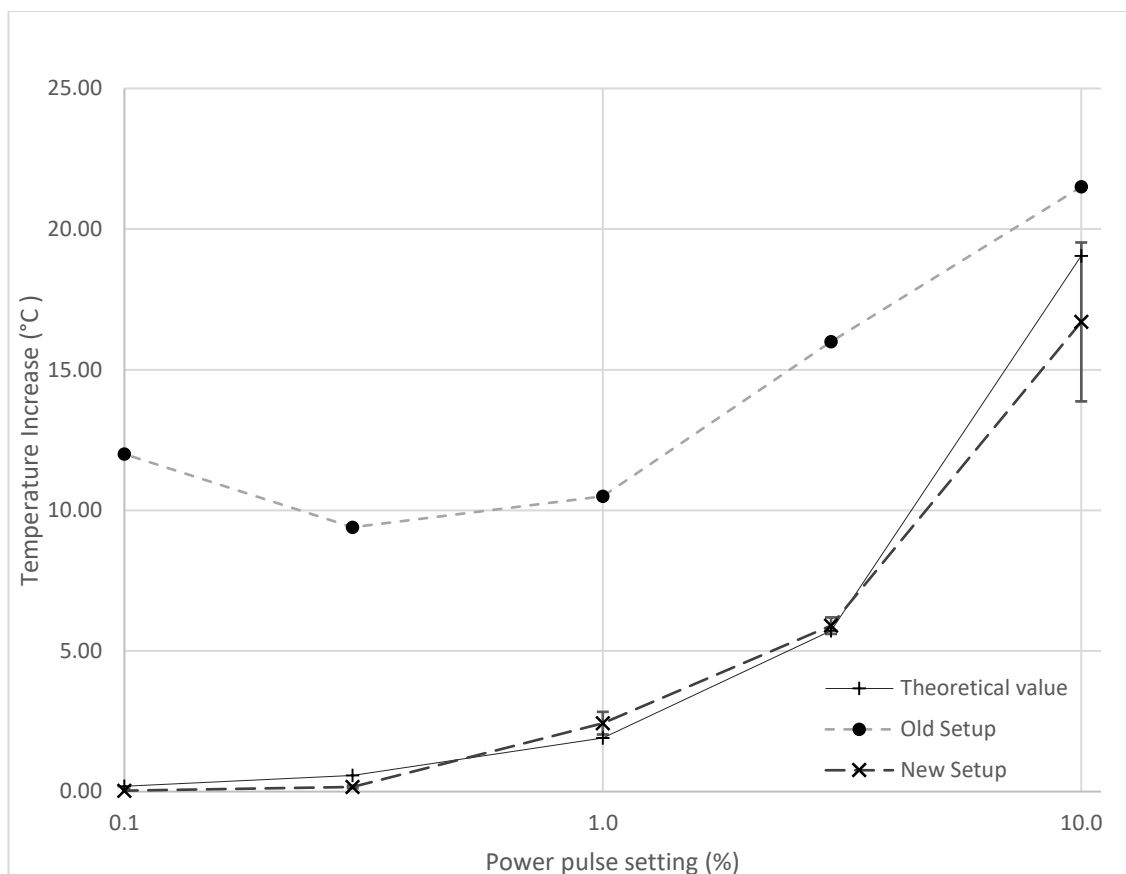


Figure 5.4. Temperature increase of a 150 μl sample following microwaving for 10 seconds at a given duty cycle. With the new setup, the values align with those predicted theoretically. Error bars (for new setup) indicate the standard deviation of results ($n=3$).

5.4.3 Differences between electric and magnetic field effects

Having updated the microwave setup to reduce sample heating, the next step was to look at the effect of the electric and magnetic fields on the sample to determine if one, or both, drive the DNA release from spores. For comparing the electric and magnetic field effects, a modified microwave cavity described previously (Williams *et al.*, 2016) was used. The difference between this cavity and the one used previously was the fact that it had 3 sample holes, instead of 1: one at the centre, just like the other (for maximum E-field), one at the radial position (for the maximum H-field) and one at the location where both E-field and M-field are at approximately 50% of the maximum field strength.

Other than the extra sample holes, the geometry and dimensions of the cavity was the same as the one used before.

5.4.3.1 Calculating field strength in the cavity

The first step was to calculate the field strengths inside the cavities. The rms power dissipated in the cavity is given by:

(5.5)

which can be rearranged to:

$$\frac{\text{---}}{\text{---}}$$

where:

- E_1 is the maximum value of the electric field
- P is the base power going into cavity, 11 W (92% of 12 W)
- f is the frequency of the system, 2.45×10^9 Hz
- V is the sample volume, 170 μl (1.7×10^{-7} m^3)
- ϵ_0 is the vacuum permittivity, 8.85×10^{-12} F/m
- ϵ_2 is the imaginary component of the relative permittivity of water, calculated at 9.2

Based on this equation, the E-field amplitude works out at **10,240 V/m** for the original (one sample) cavity.

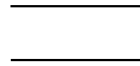
For the Williams *et al.*, cavity, the following correction needs to be made:

(5.7)

Where:

- P_1 is the power dissipated in the central sample
- P_2 is the power dissipated in the second sample, where the E-field is approx. $\frac{1}{2}$ of the strength at the first port.
- P_3 is the power dissipated at the radial port. E-field at that port is negligible by design and so is the dissipated power, so we can assume $P_3 = 0$.

The adjusted formula looks like:



Which gives adjusted E-field amplitude of **9,160 V/m** for the central sample hole.

The magnetic field formula at the cavity's perimeter is:



Since $J_1(2.405) = 0.519$, the amplitude of the azimuthal magnetic field is therefore **12.6 A/m**.

5.4.3.2 Electric and magnetic field effects

Next, the level of spore disruption was compared by loading the Williams cavity with three samples and comparing the number of spores which were observed to be fluorescent after staining with propidium iodide as previously described (see Chapter 4.4.3). The results on Figure 5.5 show that the value for magnetic field overall was not statistically different from the control ($p=0.75$), indicating that the magnetic field alone has no effect. On the other hand, the difference between control and electric field was significant ($0 < 0.0001$), as was the difference between the control and a combination of electric and magnetic field ($p < 0.05$).

In the DS1748 and DC630 strains, there appeared to be a higher proportion of spores with a combination of electric and magnetic field than with the electric field alone but using the Bonferroni post-test this was not a statistically significant difference for either of these strains.

Overall, the results indicate that the electric field drives the release of DNA from the spores, while the magnetic field has no direct effect.

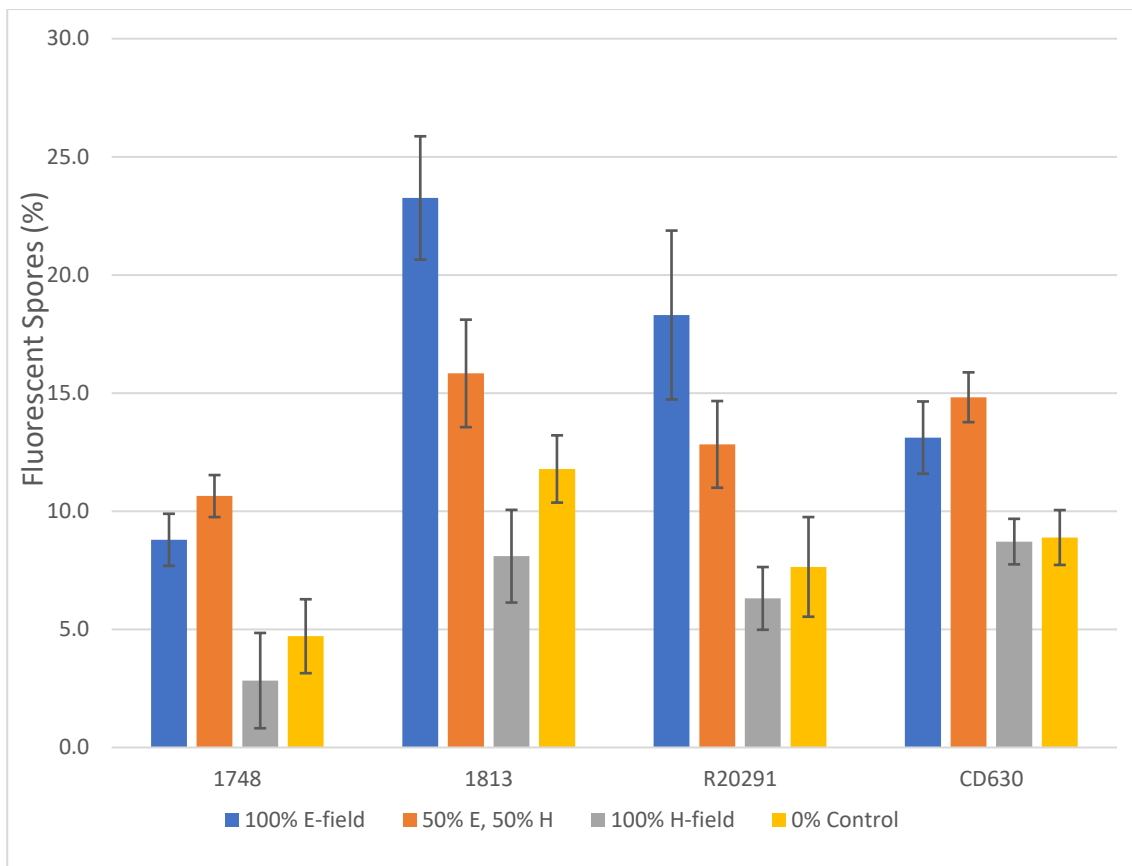


Figure 5.5. The fluorescence of *C. difficile* spores under PI exposed to electric and magnetic fields at a duty cycle of 0.3%. The highest effect was seen with the electric field alone. Error bars (for new setup) indicate the standard deviation of results (n=3).

The next step was to check if there is any effect of field strength on the spore disruption. As the electric field appears to be responsible for the spore disruption, a lower field may be as effective as higher field up to a point and so lowering the field would be a way to further reduce the power requirements of the system. Microwaves degrade DNA due to DNA also being a polar molecule, and forced realignment breaking the structure. So there may be a point where increasing power further would actually decrease the DNA release from spores due to non-optimal particle movement and increased DNA degradation.

Based on equation 5.5, the power input to the cavity is proportional to the square of the field strength ($P \propto E^2$), so by attenuating the input power, it is possible to attenuate the electric field in the cavity. The results are shown on Figure 5.6.

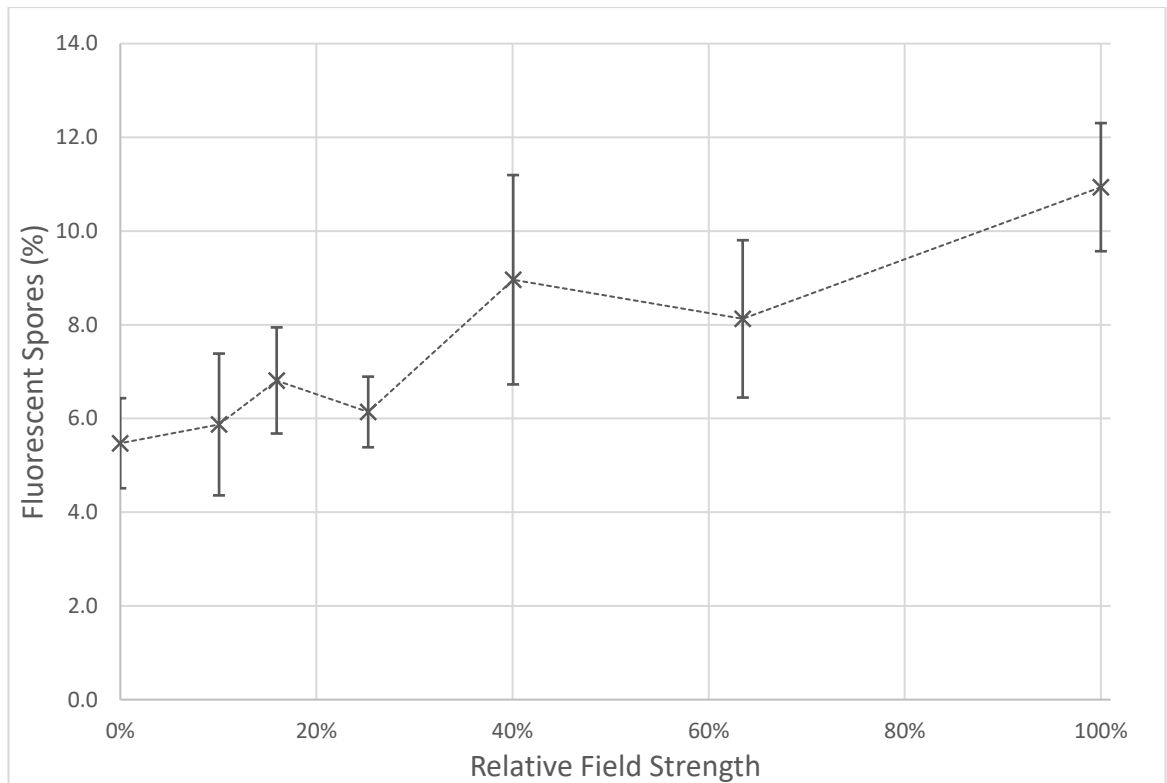


Figure 5.6. The fluorescence of DS1748 *C. difficile* spores under PI exposed to variable electric field at a duty cycle of 0.3%, with the electric field of 10.2 kV/m, attenuated down to 1 kV/m. Error bars indicate the standard deviation of results (n=3).

The results indicate that overall there is a statistically significant positive correlation ($p=0.0002$) between the electric field strength and the number of fluorescent spores, indicating that increasing the electric field strength will increase spore disruption. Based on these results, there appears to be no lower electric field optimum that could be used to lower power requirements of the system.

5.5 Discussion

This part of the work demonstrated the importance of verifying the actual parameters of any complex system/rig compared to the expected, or theoretical values. Even the basic parameters like power input to the cavity were different from those expected by more than a factor of two. There can be multiple reasons for these differences, from equipment aging, to underestimated losses in the cables, but it was important to record these values for future reference and to know what exactly is happening in the experiment.

The microwave system also had power leaking into the cavity, which increased sample heating and introduced a major systematic error at low duty cycles. This error needed to be fixed before proceeding further. The microwave system was optimised to ensure that there was no heating of the sample due to power leakage and so power leakage was reduced by 35 dB. It may have been better to redesign the system more, to completely eliminate the power leakage, but this was not possible due to time limitations. However, this idea was used in the next iteration of the microwave system in the School of Engineering, which will replace the current system in the future. In this system, there is no coupler loop, but rather an On/Off state for the microwave signal generator, meaning that in the off state, the power is zero.

The disruption of spores by the electric and magnetic fields indicate that the electric field alone results in spore disruption and the magnetic field plays no role. It was also established that stronger electric fields result in a greater spore disruption. This means that the existing setup which maximises the electric field within the sample is the optimal. It also means that focusing the electric field further, could lead to even greater spore disruption. It may also be better to use smaller sample sizes so that the power is dissipated in a smaller volume. However, that would in turn increase heating, which is undesirable.

One aspect that could not be explored in the current microwave generator setup was the frequency (which is tied to the cavity optimisation). The 2.45 GHz was originally chosen as a common microwave frequency. But the optimal spore disruption and DNA release may be at a different frequency and this could be explored in the future.

The theory and model of the electric field disrupting the spores is explored in Chapter 6.

Chapter 6

Nanoparticle and microwave spore disruption

6.1 Introduction

In the previous chapters, it was shown that the electric field generated in the microwave cavity leads to ssDNA release from spores. In Chapter 5, the microwave cavity setup was optimised to maximise spore disruption. The next step was to determine if DNA release could be further enhanced by the presence of nanoparticles.

As previously described in Chapter 1, the use of nanoparticles in bacterial disruption was explored (Aslan *et al.*, 2008, Hayden *et al.*, 2012, Chung *et al.*, 2013). Hayden *et al.*, 2012, is an example of gold spherical nanoparticles disrupting vegetative *E. coli* and *B. subtilis* and leading to cell lysis. In the context of this project, this highlights the ability of nanoparticles to disrupt membranes and release DNA. In Chung *et al.*, 2013, a 16s RNA detector was designed, using magnetic nanoparticles. The RNA would bind to both a capture bead with complimentary sequence oligonucleotides and to a 20 nm magnetic nanoparticle. This complex could then be detected using micro-NMR. In the context of this work this was a way to use nanoparticles for detection, but the inclusion of a PCR step to amplify the DNA makes this method makes this method no faster than other PCR methods.

Nanoparticles can physically break the bacterial cell wall, and that this effect is based on the shape of the nanoparticles (Acharya *et al.*, 2018). This means that different shaped nanoparticles may have different effects on the spore as well and may physically damage the spore outer surface. To investigate this, spherical nanoparticles were compared to

angled “urchin” shaped ones to test if the angled shape of nanoparticles results in damage to the spore surface.

In the work of Aslan *et al.*, 2008, silver nanoparticles were used with microwaves in the form of silver island films (SIFs), to disrupt *B. anthracis* spores. However, these were only used as substrates for fluorophores to which the DNA would bind. The hypothesis was that the DNA moves to nanoparticles by temperature gradient, with silver being colder due not being heated directly by microwaves.

More recently, 70 nm magnetite (Fe_2O_3) nanoparticles were used as an in-vitro demonstration of localised hyperthermia of biological tissue for cancer treatment (Kim *et al.*, 2016). In this experiment, the nanoparticle-treated sample reached an overall higher temperature than untreated tissue. The nanoparticles themselves do not heat significantly, but enhance the heating of tissue (Pearce *et al.*, 2016).

The work carried out in this project had a unique approach in that the goal was to use the nanoparticles to directly interact with the spores, enhancing the disruptive effect of microwaves. In this chapter, the goal was to determine to characterise the ability of nanoparticles to interact with spores, and lead to the release of DNA and to gain insight into the nature of this interaction.

To understand how the nanoparticles and spores interact, it was necessary to model these interactions. A mathematical model for nanoparticle heating steady state was built based on material properties and nanoparticle electric dipole absorption theory (Porch *et al.*, 2013), to estimate required power for heating nanoparticles in an aqueous solution. This model indicates that conductive metal nanoparticles will not heat directly when exposed to microwaves, but instead will focus the field on 2 poles. By contrast, semiconductors with conductivity in the range of 0.4 S/m will heat up directly and could be localised heat sources. To complement this model, a second model of the electric field interactions of the nanoparticles and the spores was built using COMSOL. With this model it was possible to predict how the field will be focused by the nanoparticles and which particles were likely to have the greatest effect.

With the model in place, the experiments with spores in nanoparticle suspensions were carried out and the DNA release was recorded using the Qubit detection system and compared with the DNA release of spore suspensions without nanoparticles. The data

was then analysed to determine the optimal nanoparticle types for spore disruption also involving the calculation of the statistical significance of the results.

To gain further insight into the nature of spore disruption, the spore and nanoparticle suspensions were also observed using SEM to determine if there were any changes to the spore structure which correlated to DNA release.

6.2 Aims and objectives

The aims of this chapter were:

- To develop mathematical models for the interaction of microwaves with nanoparticles and bacterial spores. And which could be used to predict the mechanisms lead to DNA release
- Through experimentation, identify the nanoparticle characteristics that enhance DNA release from spores
- To combine the model and the experimental data to understand the nature of microwave and nanoparticle interactions and potential directions to take the project further.

6.3 Methods

6.3.1 Nanoparticles used

The nanoparticles chosen and key reason behind their choice are shown on Table 6.1 below. With the exception of the germanium nanoparticles, which were sourced from US Nano, all other nanoparticle suspensions were obtained from Sigma-Aldrich. The nanoparticle suspensions from Sigma-Aldrich were supplied as a dispersion in citrate buffer at a concentration of 3.8×10^9 particles/ml. The germanium nanoparticles came with their own proprietary surfactant (formula not provided) and were mixed to a concentration 3.8×10^9 particles/ml.

Table 6.1 Nanoparticle types used

Nanoparticle	Effect being tested
100 nm gold spherical	Spherical nanoparticle field focusing
30 nm gold spherical	The effect of smaller size particles
100 nm silver spherical	The effect of field focusing combined with chemical effect from silver ions
30 nm silver spherical	The effect of smaller particles + silver ions
90 nm gold nano-urchins	Particles with a spheroid shape with many pointed protrusions
30 nm germanium	Thermal effect of the nanoparticles + field focusing

The method to test the effect of the nanoparticles is as follows. A 10 μ l aliquot of the Sorg method purified, and DNase treated spores (10^8 CFU/ml) was taken. This aliquot was mixed with 170 μ l of nanoparticle suspension (3.8×10^9 particles/ml). A 10 μ l aliquot was taken from this mixture as to serve as the non-microwaved sample. The remaining 170 μ l was loaded into the microwave cavity as previously described. The samples were exposed to microwaves using a 0.3% duty cycle for 30 seconds. The microwaved samples and the matched non-microwaved ones were then tested for ssDNA concentration using the Qubit system as previously described.

The statistical analysis of the results was carried out in Graphpad Prism 5.0. Two-way ANOVA was used to determine the overall significance of results, while Bonferroni tests were used to compare different data sets to the controls.

6.3.2 Modelling of Nanoparticles and Spores

A physical model of how the nanoparticles focus the electric field was built in Comsol 5.0. Nanoparticles were set to have the sphere diameter of 100 nm centered in a 1000 nm cube water. The relative permittivity of water was set as 80. The RF frequency was set as 2.45 GHz. The electric field was set in the z-axis, going through the whole water cube.

In a similar manner, a spore was simulated as a four-layer ellipsoid with the layer representing the exosporium, coat, membrane and core of the spore (see Chapter 1 on spore structure). The relative permittivities of the layers were set as follows: 40 for the exosporium and the core, 10 for the coat, and 2.5 for the membrane. The low permittivity of membranes is discussed in literature but varies depending on composition (Dilger et al., 1979, Tian, 2010). The exact values for spore membranes do not exist in literature, as the exact composition of the spore membrane, coat and exosporium are not fully known, so values were extrapolated from values in literature.

6.4 Results

6.4.1 Estimating nanoparticle heating

6.4.1.1 Particle heating basic model

The first step in modelling the nanoparticle interactions was to understand how the nanoparticles will heat over time when subjected to constant power dissipation per unit volume. Heating of a material (i.e. change in temperature) over time can be described by the following simple equation:

$$\frac{dT}{dt} = \frac{Q}{mC} \quad (6.1)$$

where Q is the net heating power, C is the heat capacity of the material and m is the mass of the material. We can expand Q into:

where P is the power dissipated (in our case, power absorbed by nanoparticles), h is the heat transfer coefficient, A is the total surface area of the nanoparticles, $T_p - T_w$ is the difference between the temperature of the particles and surrounding water. Thus, the original equation can be rewritten as:

$$\frac{dT}{dt} = \frac{PA}{mC}(T_w - T) \quad (6.3)$$

This is a first order, ordinary differential equation of the form:

$$\frac{dT}{dt} + kT = b \quad (6.4)$$

Where k and b are constants. This can be solved as follows:

$$T = \frac{b}{k} + C_1 e^{-kt}$$

Where T_0 is the value of the equation at time $t = 0$. The equation is solved as:

$$T = \frac{b}{k} + (T_0 - \frac{b}{k}) e^{-kt}$$

6.4.1.2 Heating model results

Using this formula, it is possible to estimate how much a suspension of nanoparticles will heat up based on the power absorbed. The resulting equation has several clear outcomes that can be seen illustrated by Figure 6.1 below. First, due to their small size, the particles reach steady-state temperature very rapidly, in less than 1ms. Secondly, particles can theoretically reach very high temperatures (in the hundreds of degrees C), even accounting for losses into the water. Finally, it must be noted, that while values of 10^{12} W/m^3 appear to be huge, it is just 0.1W of power absorbed by a 10^9 particle/ml suspension.

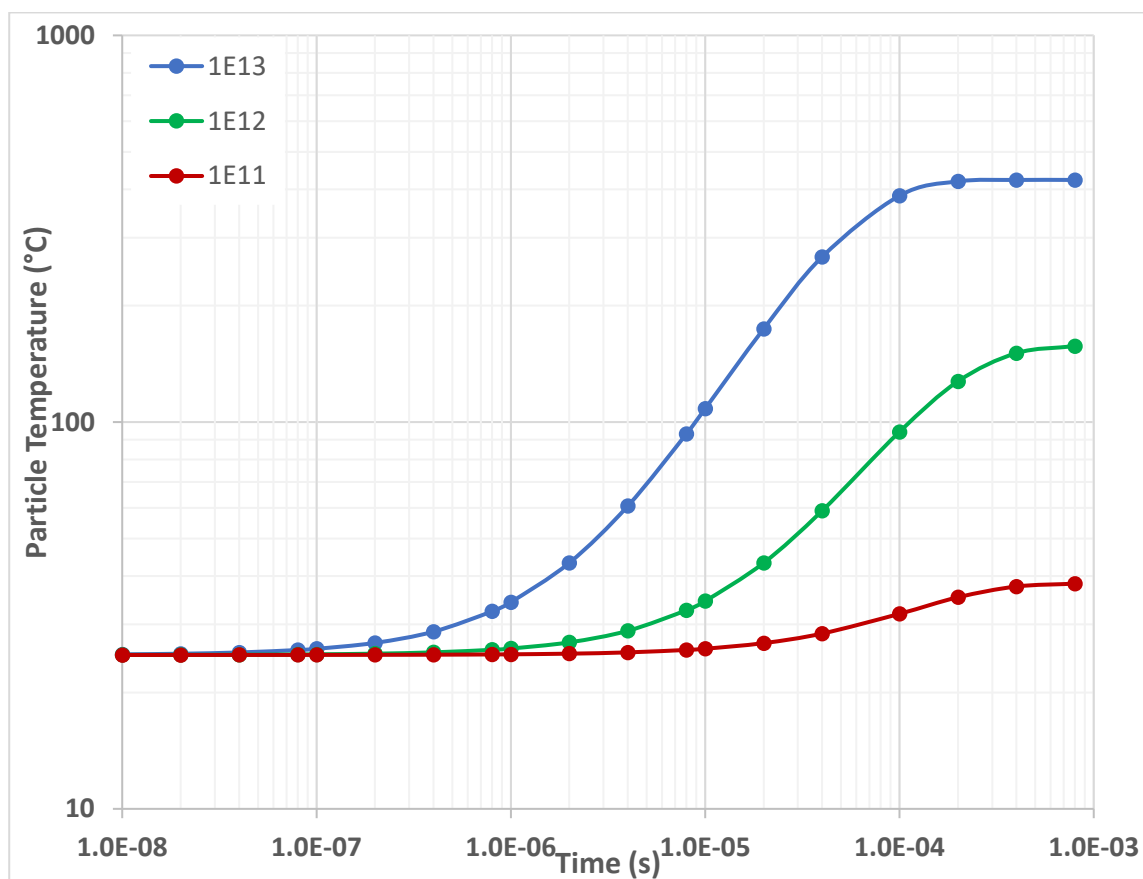


Figure 6.1. The temperature reached by 100 nm spherical nanoparticles in water, with density 5600 kg/m^3 , heat capacity $310 \text{ J kg}^{-1}\text{K}^{-1}$, depending on the power absorbed by the nanoparticle (in W/m^3 of nanoparticles), as predicted by the Equation 6.5.

The dielectric heating of nanoparticles is only significant in semiconductor particles, such as germanium. The highest possible heating value is 0.1 W/m^3 for an electric field of 1 V/m and happens at the conductivity of 0.409 S/m (Porch, 2013). The absorbance is proportional to the square of the electric field magnitude. Thus, for heating effects like shown in Fig 6.1, a field of the order of 10^6 V/m would be required. Such a field is higher

than the typical fields in the experimental cavity used in this project. With the field of 10^4 V/m as in the current system, the particles will heat up by approximately 0.01 °C over the course of the 3 ms on-time exposure. This temperature difference will be rapidly equalised by the surrounding water, so overall the heating of the particles with the current experimental conditions can be considered negligible.

This means that using the existing setup, germanium particles will not heat up directly. However, at higher field values, heating will be possible. The model also highlights the short time required to heat nanoparticles. Nanoparticles heat and reach steady-state temperature in less than 1 ms. This means with high field values, the duty cycle could be very low (1 ms on-time).

6.4.2 Electric field model using COMSOL

6.4.2.1 Nanoparticles model

The next step was to generate a model of a metallic nanoparticle using COMSOL. A metallic spherical nanoparticle was simulated in an aqueous solution. The electric field within the particle itself is approximately zero due to the screening effect of the conduction band electrons. Quantitatively, the (uniform) electric field within a spherical nanoparticle is:

where E_0 is the applied electric field the particle is subjected to and ϵ is the complex permittivity of the material (Porch *et al.*, 2013). This means that for highly conductive particles the high imaginary part of the permittivity, owing to the enormous conductivity value, will drive E down to be close to zero. Even for a semiconductor particle like germanium, the electric field within the particle will only be approximately 13% of that applied.

As for the electric field surrounding each particle, it will be focused at the poles; the focussing factor for field amplitude is 3 for a metallic sphere, varying between 1 and 3 for non-metallic particles depending on the size of the relative permittivity ϵ ; this result is predicted theoretically and has been confirmed by COMSOL simulations. By comparison, a particle with the “urchin” shape (though this applies to any shape with sharp angles), is found by simulation to have smaller hotspots focused on the spikes with a much higher focussing factor for the electric field, as large as 7.5 (Figure 6.2). Since

any action derived from the microwave electric field is expected to be proportional to the field intensity E^2 (for example, power dissipated) these focussing factors become even more significant.

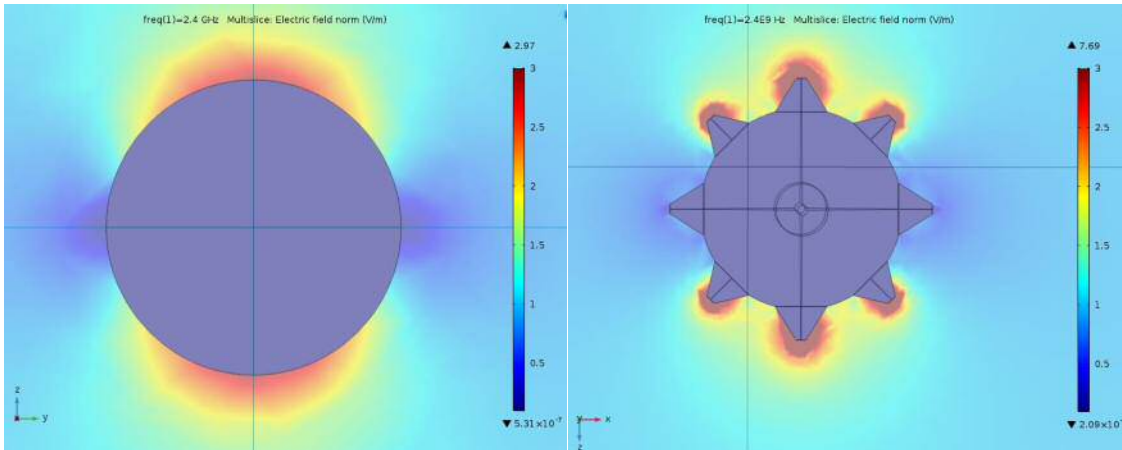


Figure 6.2. 3D model showing the focusing of an electric field by metallic nanoparticles. The urchin-shaped nanoparticles generate smaller hot-spot zones but with a more strongly focused field, up to a maximum of 7.5 greater than the applied electric field.

When nanoparticles interact with spores, the part of the spore in contact with the nanoparticle will be subjected to higher electric field. In the case of spherical nanoparticles, the enhancement is going to be limited, due to limited area of contact and low field focusing. In the case of angled nanoparticles, the field at the contact points will be higher. In addition, the angled shape will allow the focused field to penetrate deeper into the spore to improve disruption further. In conclusion, the angled nanoparticles generate hotspots with a stronger field and more suited to electric field-based spore disruption.

6.4.2.2 Spore model

The spore is a complex multi-layer structure, as described in Chapter 1, with the outer exosporium layer and the innermost core containing some water and being separated by the multiple spore coat layers and the cell membrane. The main limitation of developing a COMSOL model of a spore is the lack of information on the electric properties of these different spore layers. While values can be estimated, based on the fact that the spore layers are protein, lipid and polysaccharide, the results may not be representative of what is actually happening in the spore.

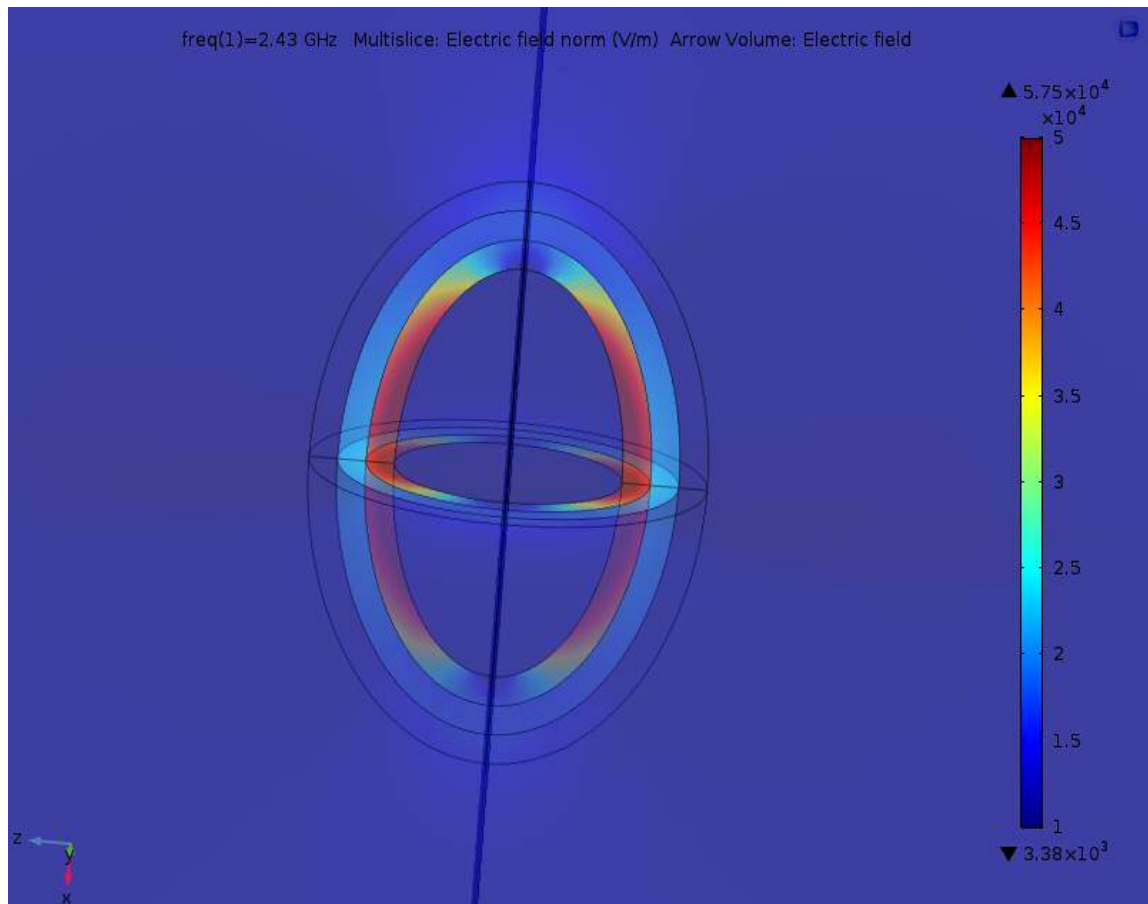


Figure 6.3 A simple 3D model of multiple spore layers under the effect of an electric field. The electric field is amplified at the simulated dielectric spore coat and membrane layers. The maximum enhancement up more than a factor of 5 in the simulated membrane layer (red), indicating that this layer will see the greatest heating and molecule realignment.

Despite the limitations of the model, a property of spores can be noted. The low permittivity layers of the spore will, by definition, absorb more energy than the areas with higher permittivity. The core is therefore partially shielded from the electric field, and the model suggests the field strength there is only 75% of the applied electric field. By contrast, the dielectric layers will have higher field values, rising to more than a factor of 5 in the sections of the membrane layer perpendicular to the applied field direction.

The low water content layers (spore coat and membrane) are dielectrics separating two conductive layers: the aqueous solution the spores are in and the spore core. This means they can function as capacitors, storing electrical energy when exposed to microwaves. Such a build up of energy could have consequences on the spore, such as structure degradation, which could lead to the DNA release.

In conclusion, the spore model provides a possible explanation about the non-destructive disruption of the spores. The spore surface is well hydrated and therefore with high relative permittivity closer to that of water. This layer will be subjected to a lower electric field and thus is unlikely to be damaged in a manner that will be visible under SEM. By contrast, the inner dehydrated layers of the coat and membrane will receive a higher level of electric field, so may be disrupted due to charged groups realignment leading to membrane damage, leading to DNA release.

6.4.3 Spore interaction with microwaves and nanoparticles

With the model predicting that nanoparticles are able to focus the microwave electric field, the next experiment was to expose spores to microwaves in the presence of different nanoparticle suspensions and to compare the observations with the model predictions.

6.4.3.1 DNA release by microwaved spores

To determine the effect of nanoparticles, if any, on DNA release the amount of microwave mediated DNA released in the absence of nanoparticles was determined first. As can be seen in Figure 6.4, the release of DNA was very small, with the highest value of 35 pg/ μ l. This level of DNA was not statistically significant ($p=0.35$ with a hypothesis of no release). This was expected, as the duty cycle used was only 0.3%, compared to a 10% duty cycle used in Chapter 4, which is a 33-fold difference and where release values of up to 200 pg/ μ l were seen.

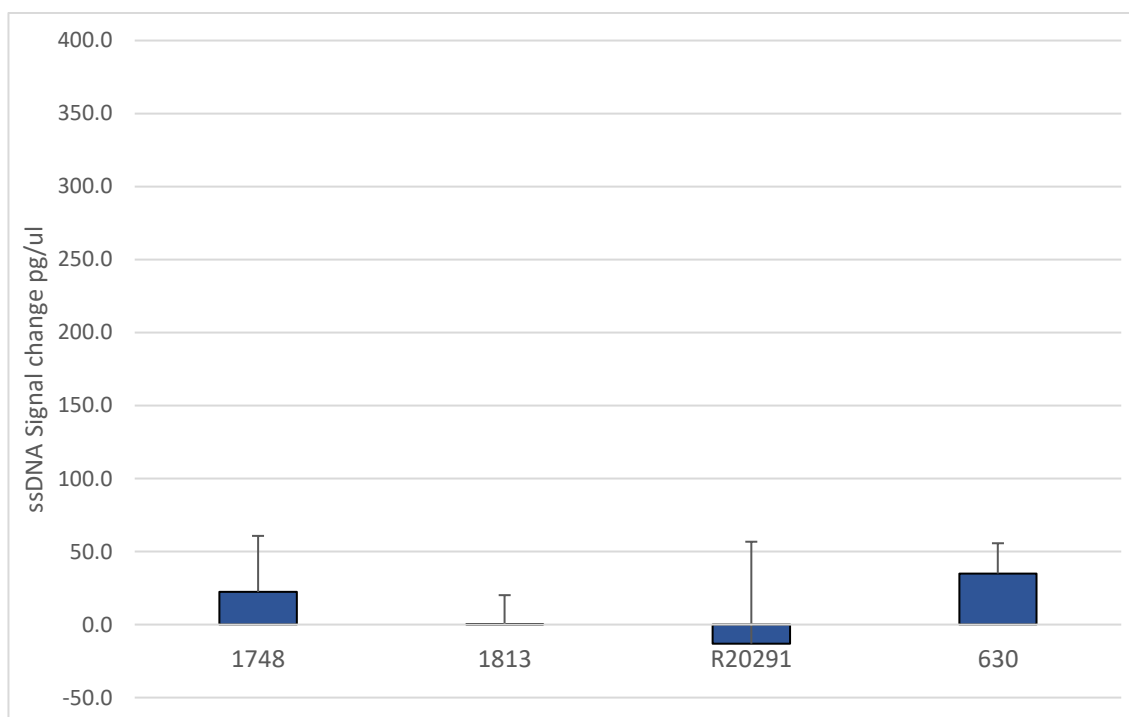


Figure 6.4. ssDNA release from *C. difficile* spores following a 0.3% duty cycle, 30 second microwave exposure ($n=3$). Overall, the change in the ssDNA signal is not statistically significant. Error bars indicate the standard deviation of results.

Next, the effect of the presence of different nanoparticles on DNA release in the presence of microwaves was determined. The results on Figure 6.5 show an increase in DNA release in the presence of nanoparticles for each test combination.

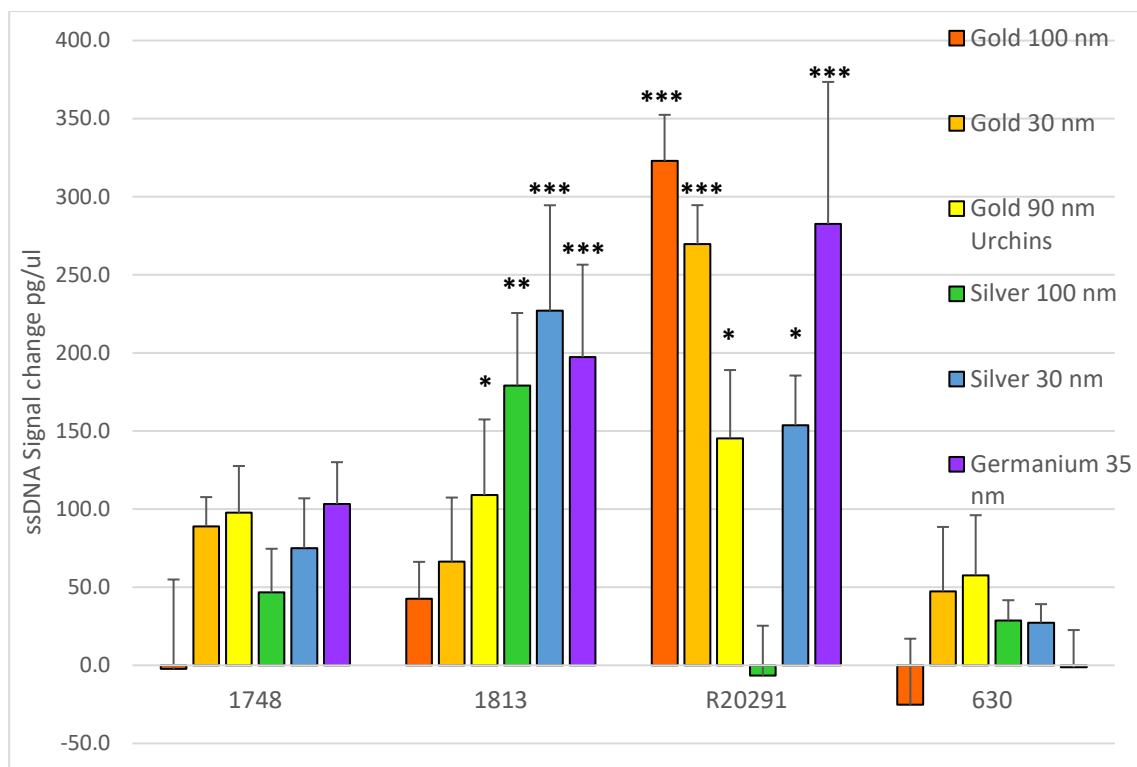


Figure 6.5. The effect of different nanoparticle suspensions on DNA release following microwave exposure. The results show the change in DNA release, compared to a control microwaved without nanoparticles (n=3). Stars indicate the degree of significance, using the Bonferroni post-test; one star for $p < 0.05$, 2 stars for $p < 0.01$, three stars for $p < 0.001$. Error bars indicate the standard deviation of results.

The degree of DNA release following microwave exposure varied depending on the clinical isolate and nanoparticle used. Overall the differences in the DNA release were statistically significant (ANOVA $p < 0.0001$), showing that nanoparticles improve spore disruption compared to the samples without nanoparticles. In the case of the R20291 strain, all nanoparticles except the 100nm silver had a statistically significant increase in DNA levels. In the case of the DS1813 strain, all nanoparticles expect 100 nm gold and 30 nm gold had a statistically significant effect. Against the CD630 strain and the DS1748, the apparent increase in the DNA release is not statistically significant.

6.4.3.2 Characterisation of spores exposed to nanoparticles

As was previously established in Chapter 4, microwaved spores released ssDNA without any visible changes to the spore surface architecture. In order to better understand the reasons of the increased DNA release in the presence of nanoparticles, the microwaved spore suspensions from the samples that were used in 6.3.3.1, were examined by using

SEM for any visual signs of spore disruption. Unfortunately, it was not possible to obtain SEM images of spores microwaved with silver particles due to SEM sample failure and lack of time.

As can be seen from Figure 6.6 and Figure 6.7, microwave exposure in the presence of 100 nm spherical gold nanoparticles had no visible effect on spore architecture. Similar results were seen in all four clinical isolates, including R20291 (Figure 6.7), where the 100 nm gold nanoparticles have been shown to have a statistically significant increase in DNA release.

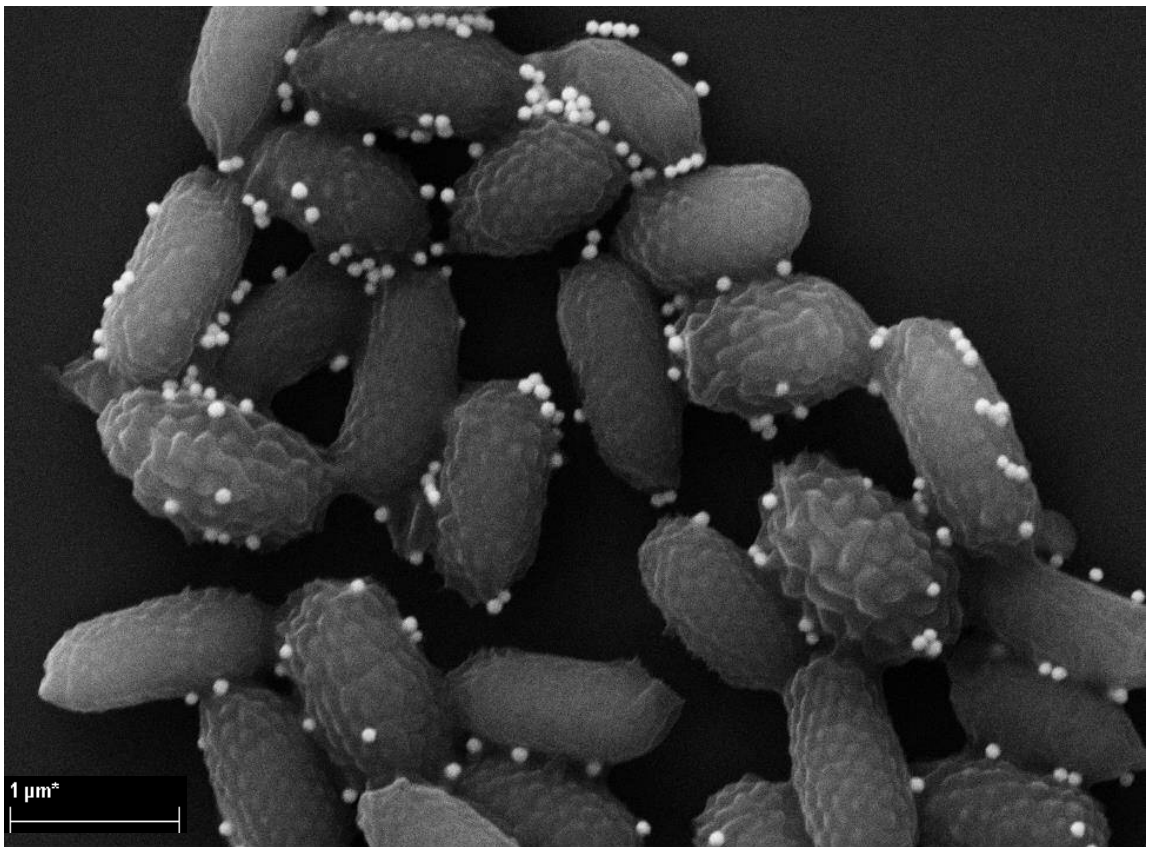


Figure 6.6. SEM of *C. difficile* spores of the DS1748 strain spores exposed to microwaves in the presence of 100 nm spherical gold nanoparticles. The magnification was x25,000. These images are representative of 10 fields of view.

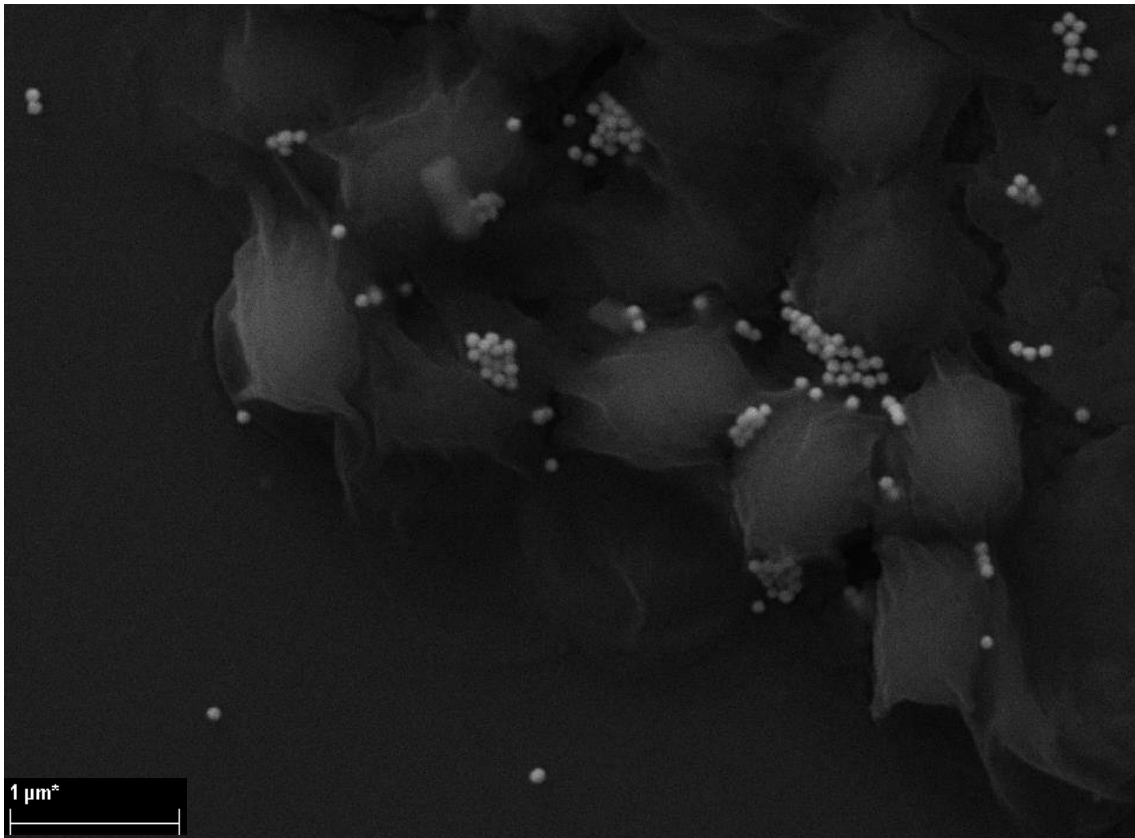


Figure 6.7. SEM of *C. difficile* spores of the R20291 strain spores exposed to microwaves in the presence of 100 nm spherical gold nanoparticles. The magnification was x25,000. These images are representative of 10 fields of view.

Neither the 30 nm spherical (Figure 6.8) or 90 nm urchin gold nanoparticles (Figure 6.9) had any visible effect on the spore surface architecture of all four clinical isolates. This is consistent with the results in Chapter 4 where the exposure of spores to microwaves led to DNA release, with to visible effect on the spore structure.

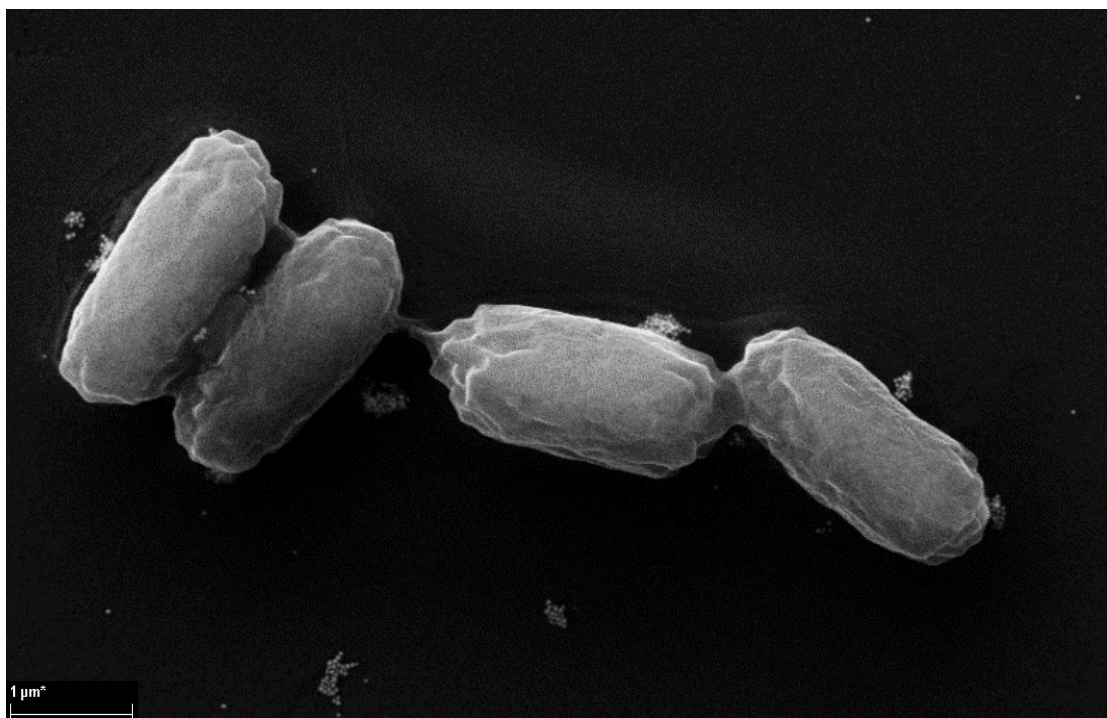


Figure 6.8. SEM of *C. difficile* spores of the DS1813 strain spores exposed to microwaves in the presence 30 nm spherical nanoparticles. The magnification was x25,000. These images are representative of 10 fields of view.

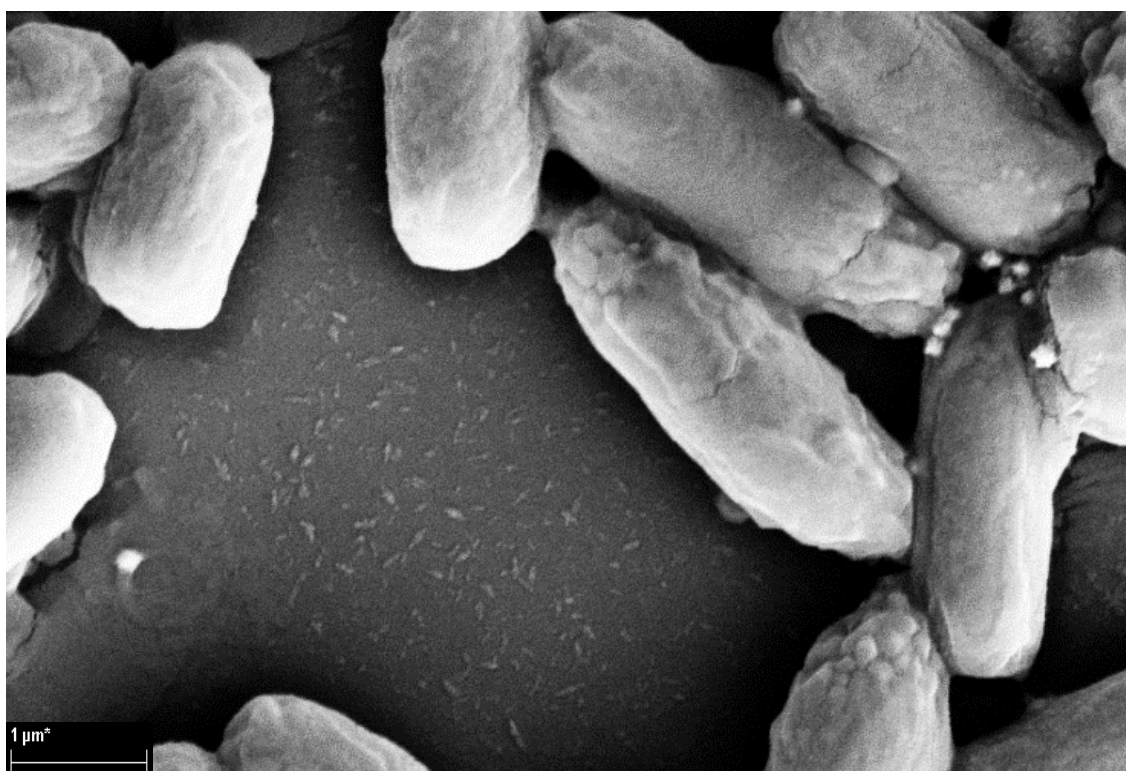


Figure 6.9. SEM of *C. difficile* spores of the DS1813 strain spores exposed to microwaves in the presence 90 nm urchin gold nanoparticles. The magnification was x25,000. These images are representative of 10 fields of view.

By contrast, spores microwaved in the presence of germanium nanoparticles were heavily disrupted, with collapsed and partially collapsed spores observed. Similar disruption was seen in all four clinical isolates, even though it did not lead to a statistically significant increase in DNA release from the DS1748 and CD630 strains.

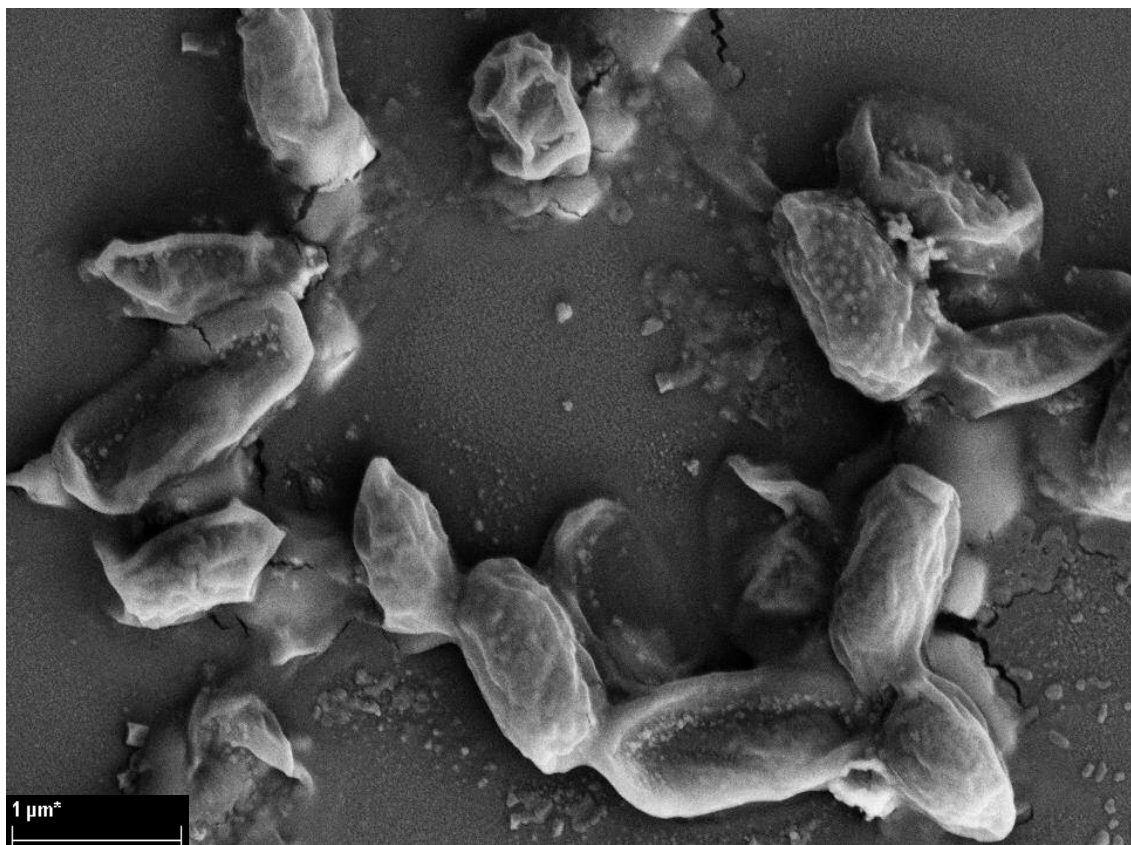


Figure 6.10. SEM of *C. difficile* spores of the DS1748 strain spores exposed to microwaves in the presence of 30 nm germanium nanoparticles. The magnification was x25,000. These images are representative of 10 fields of view.

Overall, these results show that DNA release from spores microwaved in the presence of gold spherical and urchin-shaped is not associated to with any visible spore structural damage, indicating that the disruption mechanism is similar to that of the spores in Chapter 4. Germanium nanoparticles, or their surfactant are associated with significant spore damage, suggesting a different mechanism of interaction.

6.5 Discussion

The heating simulation of the individual nanoparticles suggests that in aqueous solutions they can theoretically reach very high temperatures, providing there is sufficient electric field (of order of 10^6 V/m). However, due to the high surface area to volume ratio, this will likely be very inefficient and will only work with semiconductor materials like germanium. Under the existing setup electric field of order of 10^4 V/m, the heating will be of the order of 0.01 °C per pulse and will be completely negated by the surrounding aqueous solution.

The electric field model in COMSOL indicates that nanoparticles will focus the electric field, and angled nanoparticles, such as the urchin-shaped ones, will create small zones of very focused field, while spherical nanoparticles create larger high field areas, but with less field focusing. This means that when a nanoparticle comes in contact with the spore, only a very small area will be subjected to the higher electric fields. With angled nanoparticles, the field at the contact points will be higher and the part of the spore exposed to high fields will be higher. As was previously stated, the electric field effects scale quadratically, so a field focusing factor of 2 will be 4 times stronger effect. And with a field focusing factor of 7.5, as was predicted for the urchin model the electric field effects will be 56 times stronger. In addition, the urchin shape has multiple hotspots of focused field, allowing each particle to affect several locations on the spore. The spherical nanoparticle has only two hotspots at different poles, giving only one location where the nanoparticle will affect the spore.

The electric field model of the spore indicates that the electric field is focused in the membrane and spore coat, but not on the spore surface. This field enhancement affects most of the membrane and coat layer, except for the two polar areas of the spores which are aligned with the electric field. This presents a potential model nanoparticle-mediated DNA release improvement. Without nanoparticles, the outermost layer is intact, so DNA release is limited even if the inner coat and membrane layers are heavily disrupted. DNA is still trapped within the spore. Nanoparticles created small zones of disruption in the outer spore layers due to the electric field hotspots, giving a route for DNA to be released. Due to the size of these hotspots, they may not be visible under SEM and the spore will still appear intact.

The results from these preliminary experiments show that microwave-mediated DNA release from spores of the R20291 and DS1813 strains can be enhanced by the addition of nanoparticles, particularly the gold urchin shaped nanoparticles, 30 nm silver nanoparticles and germanium nanoparticles.

To determine the effect of shape and size on DNA release the interaction of spores of R20291 and 1813 with gold spherical (30 and 100 nm) and urchin shaped (90 nm) nanoparticles was examined. A different pattern of response for the two strains was seen with regards to DNA release which suggested that spore structure may have a major impact on how they interact with nanoparticles. Only the urchin nanoparticles caused a significant increase in DNA release from both strains, which supports the data from the electric field computer model and the prediction that the hotspots generated by the urchin-shaped nanoparticles enhance DNA release. While the urchin nanoparticles mediated DNA release from both strains, it was less effective than spherical gold nanoparticles for R20291 spores suggesting that factors other than shape may be important.

Silver nanoparticles have similar electric properties and shape to the gold nanoparticles and were also in citrate buffer but had different levels disruption. In the DS1813 strain, silver nanoparticles had a greater effect on DNA release than gold nanoparticles of the same size. By contrast, in the R20291 strain, silver nanoparticles had a smaller effect DNA release than gold nanoparticles of the same size. A possible explanation is that silver nanoparticles can release positively charged silver ions into solution, and therefore these nanoparticles will work well with strains like DS1813, where the negatively charged gold nanoparticles did poorly and vice versa. Silver ions also bind DNA bases directly and form stable homo-base pairs (Swacey *et al.*, 2015). This means that the silver ions can “glue” together some short ssDNA stable clusters potentially improving the signal from the Qubit system.

Finally, the effect of germanium nanoparticles was also analysed. Germanium nanoparticles increased spore DNA release in in the DS1813 and R20291 strains and were associated with visible destructive spore disruption. This disruption, however, did not correlate with significantly higher DNA release compared to the non-destructive disruption with gold nanoparticles. The visual signs of disruption do indicate a different mechanism may be responsible for the spore results. The modelling results rule out a heating-based effect, as the electric field in in the cavity is insufficient to cause any

heating in the test conditions used. It may however be due to a chemical effect from the surfactant. The germanium nanoparticles came from a different supplier (US-Nano) than the gold and silver nanoparticles (Sigma-Aldrich), and were supplied with a proprietary surfactant. This means the attachment of these nanoparticles to spores could be different to that of other nanoparticles dispersions. The irregular shape of the nanoparticle could also be a factor, generating hotspots similarly to the urchin-shaped nanoparticles.

The CD630 strain was the least effective at spore disruption. Only the 90 nm urchins had an average improvement of over 50 nm/ μ l of DNA release. A possible explanation is a low DNA content in the outer spore surface. This strain lacks the “pineapple” outer layer of the DS1813 and DS1748 or the large baggy outer layer of the R20291 strain. If the DNA is trapped in the spore layer as hypothesised, there may simply be less areas for the DNA to be trapped in the CD630 strain compared to others.

Considering that R20291 is the most hydrophilic strain (see Chapter 3), attachment may also play a major role in spore disruption. This attachment could potentially be enhanced by functionalisation. The nanoparticles used in the study were citrate-stabilised, and therefore had a partial negative charge on the surface (Zhao *et al.*, 2013). This could cause the particles to repel other negatively charged particles and interact poorly with hydrophobic nanoparticles such as the DS1748 and DS1813 strains. Functionalised nanoparticles could contain positive charge groups on the surface and therefore bind more easily.

One of the limitations preventing higher statistical significance of experimental results for DNA release, was the Qubit assay itself. The issues with spore clumping and nanoparticle clumping did lead to a larger variation in results, which led to higher p values.

Based on the electric field model, due to water having a very high dielectric constant for a 2.45 GHz frequency, it inevitably absorbs much of the power that goes into the sample. This means that water interferes with spore disruption and the power absorbed by the water is effectively wasted. For a more effective spore disruption it may be better to redesign the system to work with dry samples, where water is only added after microwaving, to dissolve the DNA. Such a system will need much less power, as the sample mass and total heat capacity will be much smaller. Doing this also eliminates the sources of systematic error from dispersants as well as nanoparticle and spore clumping interference in Qubit or other fluorescence assays.

In conclusion, nanoparticles were found to significantly enhance spore disruption, with gold urchin shaped and germanium irregular shaped particles showing the greatest effect. The model of nanoparticle and spore interactions indicates that the urchin and irregular shaped nanoparticles produce localised areas of concentrated field on the spore surface where spore disruption enhanced.

Chapter 7

General Discussion

This work was done in the context a Cardiff University project to develop microwave-based rapid DNA based detection system for spore forming bacteria like *B. anthracis* and *C. difficile* (Aslan *et al.*, 2008; Joshi *et al.*, 2014). This project's goal was to answer research questions about the nature of the DNA release from spores in response to microwave exposure and to identify possible ways to enhance the DNA release, including by use of nanoparticles.

The principal aim of this project was to investigate the mechanisms by which microwaves affect bacterial spores and cause the release of DNA. For that, first the spore structure of *C. difficile* was characterised to determine how different elements of the spore interact with microwaves. Then, the nature of DNA released in response to microwaving was characterised, as well as the effect of microwaving of spore structure. After that, the microwave system design was optimised, and the relative contribution of heating, electric field or magnetic field effects was determined. Finally, the effect of nanoparticles on spore DNA release was determined experimentally and supported with modelling data.

7.1 Characterisation of the spore structure of *C. difficile*

A significant variation in the spore morphology of clinical isolates of *C. difficile* was observed. Three distinct morphotypes were observed: pineapple-like, surrounded a bag-like layer and smooth spores. Differences in the spore morphology of clinical isolates of *C. difficile* have been reported by others (Pizarro-Guajardo *et al.*, 2014, 2016). When examined under transmission electron microscopy (TEM) spores of CD630 and R20291 displayed the presence of either a thin (50% and 25%) or thick (50% and 75%)

exosporium. The bag-like layer reported Chapter 3 is typical of the exosporium produced by members of the *Bacillus* species such as *B. anthracis* and *B. cereus* but was not observed by Pizarro-Guajardo and colleagues possibly due to differences in spore treatment and imaging techniques (Terry *et al.*, 2017). Pineapple-like structures on the surface of *C. difficile* spores were reported by Rabi *et al.*, 2017, where they were thought to be a common feature among *C. difficile* spores in general. The work in Chapter 3 demonstrates that the *C. difficile* appearance is varied and that the pineapple-like features were not visible at all in other strains, such as the R20291 and CD630 strains. These “pineapple” may also be related to the “bumps” observed on the surface of the spores of TL176, TL178 and R20291 using TEM, which have been linked to the “thick” exosporium morphotype, while the CD630 has been described as atypical (Pizarro-Guajardo *et al.*, 2016). However, unlike that study there were no short hair-like structures surrounding the spores in Chapter 3, possibly due to the fact that SEM machine used did not have enough resolution for them to be seen. Long hair-like features were seen projecting from R20291 spores produced using the Lawley method. Overall, this work and published research by others show that *C. difficile* spore morphology is varied between different clinical isolates and can present different phenotypes that can depend on the isolate and the methods used to culture and purify them.

On the basis of the results, the Sorg method was selected as the optimal method for spore production for this project as it lacked the sonication or proteinase steps, that were previously reported as damaging (Escobar-Cortés *et al.*, 2013). Sonication, in particular could completely remove outer spore layers, as was shown in section 3.3.2.3 including the non-baggy “pineapple” layer from spores (Figure 3.11). These results show that care must be taken in using sonication in spore purification to avoid producing spores which are not representative of their unpurified form. The adoption of a common “standard” growth and purification method for *C. difficile* spores would make it easier to compare the results obtained by different research teams.

Sonication does, however, present a potential way to further investigate spores in future work. Repeated sonication cycles could eventually begin to remove the spore coat layers, allowing the spore to be characterised layer by layer, being “peeled off” one at a time. Another way to analyse spore layers in the future could be to use nanostructuring imaging techniques. Focused ion beam (FIB) SEM or helium-ion (HI) microscopes allow

removing very small parts (<10 nm) of a sample (such as a single spore) and look at the exposed layers.

The spores also had varying hydrophobicities, which depended on the method used to grow and purify them. With the Sorg method, the “pineapple” like layer was associated with more hydrophobic spores, while the bag-like layer was associated with hydrophilic spores. Notably, these results were difficult to connect to existing literature, the hydrophobicity of the 630 wild-type strain has been reported to be in the large range from 57% to over 95%. This highlights how laboratory results may change greatly over small differences in methods, but also on how *C. difficile* adhesion to surfaces in the real world may be affected by the environment.

7.2 Characterisation of DNA release from spores

DNase-treated spore suspensions were prepared to ensure that any DNA detected in response to microwaving does in fact come from the spore, and not from vegetative debris or non-specific DNA attached to the surface. Using these “DNA-free” spores it was then confirmed that DNA is in fact released from within the spore in response to microwave exposure. The spores themselves appear undamaged under SEM, even after long exposure times at the 10% duty cycle power setting showing that the disruption is not destructive in nature.

Using fluorescence microscopy with DNA-binding dyes, it was confirmed that the DNA released was composed of ssDNA, and not dsDNA. This meant that the DNA was unlikely to be coming directly from the core of the spore as originally hypothesised, since the core contains the genome in dsDNA form. This was further evidenced by analysis of microwaved spore suspension under SEM, which revealed no visible damage to microwaved spores.

Building a spore model in Chapter 6 provided a possible explanation for these observations. The microwave electric field would be focused in the inner spore coat and the membrane. These layers will be subjected to stronger effects from the electric field, such as polar group realignment and localised heating (which would be notable in the experiments in Chapter 4, due to the higher duty cycle of 10%, compared to 0.3% in Chapter 6). In combination the selective heating and realignment of polar groups could

lead to the formation of transient pores and a temperature gradient for DNA to be released from the outer spore layers. Pore formation was previously reported for vegetative bacteria (Levine & Vernier, 2010; Ziegler & Vernier 2008), so it likely also be possible for spores. This hypothesis about the possible pore formation could be tested in the future by using dextrans and confirming their entry into deeper spore layers.

One of the limiting factors of the experiment was the Qubit fluorometer, which does not work optimally with spore suspensions (due to clumping of spores changing the fluorescence signal). As such, it was important to use AO and PI in fluorescence microscopy, to be able to tell what is really happening to the spore surface.

As future work one would need to establish if the DNA on the spore surface is indeed that of *C. difficile* and that it can be identified as such. In the context of a bacterial detector (which is the practical end goal), this is an essential question. The experiment could be run with either a fluorophore-labeled oligonucleotide or a hybridisation probe. The original location of the released DNA in the spore could be confirmed by removing outer spore layers as suggested in section 7.1. If the DNA is located in the outermost layers, then the DNA release from sonicated and DNase treated spores would be significantly lower due to the loss of the outer layer.

Another aspect that could be further explored is the single pole with high DNA concentration on one end of the spore. If indeed this is a similar structure to “apertures” reported on *C. sporogenes* their presence on *C. difficile* would be a novel insight into its structure. This concentration of DNA is also a potential target for DNA release from the spore.

7.3 Optimising the microwave generator setup

This part of the project highlighted the importance of testing parameters in custom-built systems and risk of miscommunication in multidisciplinary projects. Power going into the cavity was different by more than a factor of two compared to the expected values. Without this testing, serious systematic errors would have been made due to incorrect assumptions on the power input.

The system was optimised to reduce power leak of the system and allow it to run samples without heating. This was necessary to run further experiments with small overall sample

heating, which was impossible in the original setup. A more long-term solution is to completely replace the existing system with one which runs in an “on-off” state rather than “high-low” isolation. This would completely eliminate the problem with power leakage.

The experiments performed in this study confirmed that the electric field is responsible for the spore disruption. However, the frequency of the system was fixed approximately 2.4 GHz which may not be the optimal frequency for spore disruption. Further work in the future could be undertaken to test a range of microwave frequencies to determine if spore disruption and DNA release could be enhanced with the same input power at another frequency.

7.4 Nanoparticle and microwave spore disruption

The addition of nanoparticles was shown to significantly improve spore disruption compared to using microwaves alone, even with the overall power used being less than 0.1W (0.3% duty cycle). The usage of low power was important in the context of the practical goal of a bacterial detector. With smaller power requirements the device could be more compact and portable, without need for a large power supply.

The amount of additional DNA released in the presence of microwaves varied depending on the the nanoparticle type and the *C. difficile* strain. The gold urchin shaped, silver spherical 30 nm, and germanium irregular shaped particles showed the statistically significant effects against the DS1813 and R20291 strains. Gold spherical particles (100 nm and 30 nm) showed effects only against R20291, while the 100 nm spherical silver showed effect only against DS1813. None of the particles showed statistically significant results against the DS1748 and CD630 strains.

The models of the spore and the nanoparticles offer an explanation for the observed results. The microwaves disrupt the membrane and spore coat of the spore due to the low relative permittivity of these layers, while the nanoparticles in contact with the spore from small hotspots with high electric field and disruption on the surface, possibly the transient pore formation as suggested in section 7.2. This offers a route for DNA to be released more easily than with microwaves alone, where the surface layers are less disrupted. Since angled nanoparticles create hotspots with higher greater field focusing, these nanoparticles have the greatest effect.

There are a number of experiments which can be carried out to investigate this further as this work was only a single set of experiments and needs to be repeated in different conditions. First, the characterisation by SEM of spores microwaved with silver nanoparticles, which was not finished due to timing constraints. The different effects of silver nanoparticles compared to gold nanoparticles of the same size and shape must be caused by their chemistry, as their electric properties are very similar. The effect of silver ions on spores could be investigated. Next, more experiments could be carried with different urchin and irregular particle sizes and power settings, to see if the disruption of strains with poor DNA release such as CD630 could be improved. The apparent heavy disruption by germanium nanoparticles is worthy of further investigation, as it indicates a potential separate disruption mechanism, which could be used to improve disruption further. This may be related to the fact that germanium is a semiconductor.

The low DNA release from the DS1748 and CD630 strains also needs to be studied. This is particularly important for a bacterial detector due to the wide variation within *C. difficile*.

In terms of experimental settings, the ratio of nanoparticles to spores could be investigated as with higher levels of nanoparticle per spore, the disruption effect could be enhanced. The duty cycle could also be varied to see if disruption increases linearly with increasing power. In addition, similarly to the point raised in section 7.2, an experiment will need to be performed with either a fluorophore-labeled oligonucleotide or a hybridisation probe to confirm that the release bacterial DNA is of sufficient quality to be detected by *C. difficile* specific probes that can be used in a bacterial detector.

Finally, a new experiment could be run without water in the microwaved sample, as water is the largest power and heat sink in the sample. With no water, the power requirements in the sample will decrease by a few orders of magnitude. Dry samples could then be resuspended in aqueous solution with the probes to allow the released DNA to bind to them.

7.5 Final Conclusions

Overall, the project fulfilled the original aim of characterising the disruption of bacterial spore with microwaves and nanoparticles.

First, the structure of *C. difficile* spores was characterised, showing significant variety in morphology and hydrophobicity based on different clinical isolates and based on the method used to grow and purify them. A standardised spore production method was developed.

Second, the interaction of spores with microwaves was characterised. Microwave electric field component was shown to lead to spore disruption and DNA release in the absence of magnetic field and without bulk sample heating. The released DNA was shown to be ssDNA, and the disruption was shown to be non-destructive, meaning the DNA likely came from the outer spore layers.

Third, nanoparticles interactions with spores and microwaves were characterised and particles such as gold nano-urchins were shown to improve DNA release from spores, with modelling providing a possible mechanism for this disruption.

Fourth, a computer model of spore-nanoparticles was made which offers a plausible mechanism of action of for the nanoparticle effects.

Chapter 8

References

Acharya, D., Singha, K. M., Pandey, P., Mohanta, B., Rajkumari, J., & Singha, L. P. (2018). Shape dependent physical mutilation and lethal effects of silver nanoparticles on bacteria. *Scientific reports*, 8(1), 201.

Alyousef, A. (2013). Identification and characterisation of lysin enzymes as potential therapeutics for the treatment of *Clostridium difficile*. PhD Thesis, *Cardiff University*

Aslan, K., Previte, M. J. R., Zhang, Y., Gallagher, T., Baillie, L., & Geddes (2008). Extraction and detection of DNA from *Bacillus anthracis* spores and the vegetative cells within 1 min. *Analytical Chemistry*, 80, 4125-4132.

Aslan, K., Baillie, L. & Geddes, C. D. (2010) Ultra fast and sensitive detection of biological threat agents using microwaves, nanoparticles and luminescence. *Journal of Medical Chemical, Biological and Radiological Defense*, 8, 1-21.

Aspinall, S. T. & Hutchinson, D. N. (1992) New selective medium for *isolating Clostridium difficile* from faeces. *Journal of clinical pathology*, 45, 812.

Ball, D. A., Taylor, R., Todd, S. J., Redmond, C., Couture-Tosi, E., Sylvestre, P., Moir A. & Bullough, P. A. (2008). Structure of the exosporium and sublayers of spores of the *Bacillus cereus* family revealed by electron crystallography. *Molecular microbiology*, 68(4), 947-958.

Banik, S. B., Bandyopadhyay, S., & Ganguly, S. (2003). Bioeffects of microwave—a brief review. *Bioresource technology*, 87(2), 155-159.

Barra-Carrasco, J., Olguín-Araneda, V., Plaza-Garrido, Á., Miranda-Cárdenas, C., Cofré-Araneda, G., Pizarro-Guajardo, M., & Paredes-Sabja, D. (2013). The *Clostridium difficile* exosporium cysteine (CdeC)-rich protein is required for exosporium morphogenesis and coat assembly. *Journal of bacteriology*, 195(17), 3863-3875.

Bartlett, J. G., Chang, T. W. & Onderdonk, A. B. (1978) Will the real *Clostridium* species responsible for antibiotic associated colitis please step forward? *The Lancet*, 338.

Bartlett, J. G. (1994) *Clostridium difficile*: history of its role as an enteric pathogen and the current state of knowledge about the organism. *Clinical Infectious diseases*, 18, 265-272.

Beveridge, T. J. (2001). Use of the Gram stain in microbiology. *Biotechnic & Histochemistry*, 76(3), 111-118.

Bruggemann, H. & Gottschalk, G. (Eds.) (2009) *Clostridia: Molecular biology in the post genomic era*. Caister Academic Press.

Brunt, J., Cross, K. L., & Peck, M. W. (2015). Apertures in the *Clostridium sporogenes* spore coat and exosporium align to facilitate emergence of the vegetative cell. *Food microbiology*, 51, 45-50.

CDC *C. difficile* information http://www.cdc.gov/HAI/organisms/cdiff/Cdiff_infect.html accessed 01/05/2015

Celandroni, F., Longo, I., Tosoratti, N., Giannesi, F., Ghelardi, E., Salvetti, S., Baggiani, A., Senesi, S. (2004) Effect of microwave radiation on *Bacillus subtilis* spores. *Journal of Applied Microbiology* 97 (6) 1220–1227

Chen P-K., Rosana M.R., Dudley G.B., Stiegman A. (2014). Parameters affecting the microwave specific acceleration of a chemical reaction. *J Org Chem* 79(16):7425–7436

Chung, H. J., Castro, C. M., Im, H., Lee, H., & Weissleder, R. (2013). A magneto-DNA nanoparticle system for target specific bacterial identification. *Nature Nanotechnology*, 8(5), 369–375.

Clark, N. (2017). *Microwave Methods for Additive Layer Manufacturing*. PhD Thesis, Cardiff University

[CRDN \(Public Health England\) Clostridium difficile Ribotyping Network \(CDRN\) for England and Northern Ireland 2011 – 13 Report.](#)

Collins J.M., Leadbeater N.E. (2007). Microwave energy: a versatile tool for the biosciences. *Org Biomol Chem* 5(8):1141–1150. doi:10.1039/b617084f

Cosa, G., Focsaneanu, K. S., McLean, J. R. N., McNamee, J. P., & Scaiano, J. C. (2001). Photophysical properties of fluorescent DNA-dyes bound to single-and double-stranded DNA in aqueous buffered solution. *Photochemistry and Photobiology*, 73(6), 585-599.

Đapa, T., Leuzzi, R., Ng, Y. K., Baban, S. T., Adamo, R., Kuehne, S. A., Unnikrishnan, M. (2013). Multiple Factors Modulate Biofilm Formation by the Anaerobic Pathogen *Clostridium difficile*. *Journal of Bacteriology*, 195(3), 545–555.

Delmee, M., Van Broeck, J., Simon, A., Janssens, M. & Avesani, V. (2005) Laboratory diagnosis of *Clostridium difficile*-associated diarrhoea: a plea for culture. *Journal of Medical Microbiology*, 54, 187-191.

Díaz-González, F., Milano, M., Olguin-Araneda, V., Pizarro-Cerda, J., Castro-Córdova, P., Tzeng, S. C., ... & Paredes-Sabja, D. (2015). Protein composition of the outermost exosporium-like layer of *Clostridium difficile* 630 spores. *Journal of proteomics*, 123, 1-13.

Dilger, J. P., McLaughlin, S. G., McIntosh, T. J., & Simon, S. A. (1979). The dielectric constant of phospholipid bilayers and the permeability of membranes to ions. *Science*, 206(4423), 1196-1198.

Escobar-Cortés K, Barra-Carrasco J, Paredes-Sabja D. (2013). Proteases and sonication specifically remove the exosporium layer of spores of *Clostridium difficile* strain 630. *J Microbiol Methods* 93:25-31.

Fawley, W. N., Underwood, S., Freeman, J., Baines, S. D., Saxton, K., Stephenson, K., Jr., R. C. O. & Wilcox, M. H. (2007) Efficacy of hospital cleaning agents and germicides against epidemic *Clostridium difficile* strains. *Infection Control and Hospital Epidemiology*, 28, 920-925.

Fordtran, J. S. (2006). Colitis due to *Clostridium difficile* toxins: underdiagnosed, highly virulent, and nosocomial. In *Baylor University Medical Center. Proceedings* (Vol. 19, No. 1, p. 3). Baylor University Medical Center.

Freeman, J., Vernon, J., Morris, K., Nicholson, S., Todhunter, S., Longshaw, C., & Wilcox, M. H. (2015). Pan-European longitudinal surveillance of antibiotic resistance among prevalent *Clostridium difficile* ribotypes. *Clinical Microbiology and Infection*, 21(3), 248-e9.

Gerding, D. N., Johnson, S., Rupnik, M., & Aktories, K. (2014). *Clostridium difficile* binary toxin CDT: Mechanism, epidemiology, and potential clinical importance. *Gut Microbes*, 5(1), 15–27.

Geric, B., Carman, R. J., Rupnik, M., Genheimer, C. W., Sambol, S. P., Lyerly, D. M., Gerding, D. N. & Johnson, S. (2006) Binary toxin-producing, large clostridial toxin-negative *Clostridium difficile* strains are enterotoxic but do not cause disease in hamsters. *The Journal of infectious diseases*, 193, 1143-1150.

Gerigk, F. (2011). Cavity types. *arXiv preprint arXiv:1111.4897*.

Giel, J. L., Sorg, J. A., Sonenshein, A. L., & Zhu, J. (2010). Metabolism of Bile Salts in Mice Influences Spore Germination in *Clostridium difficile*. *PLoS ONE*, 5(1), e8740.

Goldenberg, S. D. & French, G. L. (2011) Diagnostic testing for *Clostridium difficile*: a comprehensive survey of laboratories in England. *Journal of Hospital Infection*.

Goorhuis, A., Bakker, D., Corver, J., Debast., S. B, Harmanus., C., Notermans., D. W., Bergwerff., A., Dekker., F. W. & Kuijper, E. J. (2008) Emergence of *Clostridium difficile* Infection Due to a New Hypervirulent Strain, Polymerase Chain Reaction Ribotype 078. *Clinical Infectious Diseases* 47 (9), 1162-1170.

Gupta, S., Maclean, M., Anderson, J. G., MacGregor, S. J., Meek, R. M. D., & Grant, M. H. (2015). Inactivation of micro-organisms isolated from infected lower limb arthroplasties using high-intensity narrow-spectrum (HINS) light. *Bone & Joint Journal*, 97(2), 283-288.

Gunalan, S., Sivaraja, S., Rajendranb V. (2012) Green synthesized ZnO nanoparticles against bacterial and fungal pathogens *Progress in Natural Science: Materials International* 22 (6), 693–700

Gurunathan, S., Han, J. W., Dayem, A. A., Eppakayala, V., & Kim, J. H. (2012). Oxidative stress-mediated antibacterial activity of graphene oxide and reduced graphene oxide in *Pseudomonas aeruginosa*. *International journal of nanomedicine*, 7, 5901.

Halstead, F. D., Thwaite, J. E., Burt, R., Laws, T. R., Raguse, M., Moeller, R., ... & Oppenheim, B. A. (2016). The antibacterial activity of blue light against nosocomial wound pathogens growing planktonically and as mature biofilms. *Applied and Environmental Microbiology*, AEM-00756.

Hayden, S.C., Zhao, G., Saha, K., Phillips, R.L., Li, X., Miranda, O.R., Rotello, V.M., El-Sayed, M.A., Schmidt-Krey, I., Bunz, U.H.F. (2012) Aggregation and interaction of cationic nanoparticles on bacterial surfaces *Journal of American Chemical Society* 134 (16), 6920–6923

Heeg, D., Burns, D. A., Cartman, S. T., & Minton, N. P. (2012). Spores of *Clostridium difficile* Clinical Isolates Display a Diverse Germination Response to Bile Salts. *PLoS ONE*, 7(2), e32381.

Herman, L. M., De Block, J. H., & Waes, G. M. (1995). A direct PCR detection method for *Clostridium tyrobutyricum* spores in up to 100 milliliters of raw milk. *Applied and environmental microbiology*, 61(12), 4141-4146.

Higgins, D., & Dworkin, J. (2012). Recent progress in *Bacillus subtilis* sporulation. *FEMS microbiology reviews*, 36(1), 131-148.

Hinkson, P. L., Dinardo, C., Deceiro, D., Klinger, J. D. & JR., R. H. B. (2008) Tolevamer, an anionic polymer, neutralizes toxins produced by the BI/027 strains of *Clostridium difficile*. *Antimicrobial Agents and Chemotherapy*, 52, 2190–2195.

Jiang, S., Wan, Q., Krajcikova, D., Tang, J., Tzokov, S. B., Barak, I., & Bullough, P. A. (2015). Diverse supramolecular structures formed by self-assembling proteins of the *Bacillus subtilis* spore coat. *Molecular microbiology*, 97(2), 347-359.

- Jank, T., & Aktories, K. (2008).** Structure and mode of action of clostridial glucosylating toxins: the ABCD model. *Trends in microbiology*, 16(5), 222-229.
- Joshi, L. T., Phillips, D. S., Williams, C. F., Alyousef, A., & Baillie, L. (2012)** Contribution of Spores to the Ability of *Clostridium difficile* To Adhere to Surfaces. *Applied and Environmental Microbiology*, 78(21), 7671–7679.
- Kelly C.P., Lamont J.T. (1998)** *Clostridium difficile* infection. *Annual Review of Medicine*, 49m 375-390.
- Kim, K. H., Fekety, R., Batts, D. H., Brown, D., Cudmore, M., Silva, J., & Waters, D. (1981).** Isolation of *Clostridium difficile* from the environment and contacts of patients with antibiotic-associated colitis. *Journal of infectious diseases*, 143(1), 42-50.
- Kim, S.Y., Shin S.J., Song, C.H., Jo, E.K., Kim, H.J., Park, J.K. (2009)** Destruction of *Bacillus licheniformis* spores by microwave irradiation *Journal of Applied Microbiology*, 106 (3) 877–885
- Kim, K., Seo, T., Sim, K., & Kwon, Y. (2016).** Magnetic nanoparticle-assisted microwave hyperthermia using an active integrated heat applicator. *IEEE Transactions on Microwave Theory and Techniques*, 64(7), 2184-2197.
- Kuehne, S. A., Cartman, S. T., Heap, J. T., Kelly, M. L., Cockayne, A. & Minton, N. P. (2010).** The role of toxin A and toxin B in *Clostridium difficile* infection. *Nature*, 467, 711-713.
- Kuipers, E. J., & Surawicz, C. M. (2008).** *Clostridium difficile* infection. *The Lancet*, 371(9623), 1486-1488.
- Lawley, T. D., Croucher, N. J., Yu, L., Clare, S., Sebahia, M., Goulding, D., Dougan, G. (2009).** Proteomic and Genomic Characterization of Highly Infectious *Clostridium difficile* 630 Spores *Journal of Bacteriology*, 191(17), 5377–5386.
- Levine, Z. A., & Vernier, P. T. (2010).** Life cycle of an electropore: field-dependent and field-independent steps in pore creation and annihilation. *The Journal of membrane biology*, 236(1), 27-36.

- Leung, Y. H., Ng, A. M., Xu, X., Shen, Z., Gethings, L. A., Wong, M. T., ... & Lee, P. K. (2014).** Mechanisms of antibacterial activity of MgO: non-ROS mediated toxicity of MgO nanoparticles towards *Escherichia coli*. *Small*, *10*(6), 1171-1183.
- Lyerly, D. M., Krivan, H. C. & Wilkins, T. D. (1988)** *Clostridium difficile*: Its disease and toxins. *Clinical Microbiology Reviews*, *1*, 1-18.
- Lyras, D., O'Connor, J. R., Howarth, P. M., Sambol, S. P., Carter, G. P., Phumoonna, T., Rood, J. I. (2009).** Toxin B is essential for virulence of *Clostridium difficile*. *Nature*, *458*(7242), 1176–1179.
- Maclean, M., McKenzie, K., Moorhead, S., Tomb, R. M., Coia, J. E., MacGregor, S. J., & Anderson, J. G. (2015).** Decontamination of the Hospital Environment: New Technologies for Infection Control. *Current Treatment Options in Infectious Diseases*, *7*(1), 39-51.
- McDonald L.C., Killgore G.E., Thompson A., Owens R.C. Jr., Kazakova S.V., Sambol S.P., Johnson S., Gerding D.N. (2005)** An epidemic, toxin gene-variant strain of *Clostridium difficile*. *New England Journal of Medicine* *353*, 2442-2449
- McKenney, P. T., Driks, A., & Eichenberger, P. (2013).** The *Bacillus subtilis* endospore: assembly and functions of the multilayered coat. *Nature Reviews Microbiology*, *11*(1), 33-44.
- McNulty C., Logan M., Donald I. P., Ennis D., Taylor D., Baldwin R. N., Bannerjee M., & K A Cartwright (1997)** Successful control of *Clostridium difficile* infection in an elderly care unit through use of a restrictive antibiotic policy. *Journal of Antimicrobial Chemotherapy* *40* (5), 707-711.
- Office of National Statistics (UK)** Deaths Involving *Clostridium difficile*, England and Wales, 2012 http://www.ons.gov.uk/ons/dcp171778_323989.pdf accessed 01/06/2018
- Owens, R. C. (2006).** *Clostridium difficile*–associated disease: an emerging threat to patient safety: insights from the Society of Infectious Diseases Pharmacists. *Pharmacotherapy: The Journal of Human Pharmacology and Drug Therapy*, *26*(3), 299-311.

Paredes-Sabja, D., Shen, A. & Sorg J. (2014) Clostridium difficile spore biology: sporulation, germination, and spore structural proteins 22 (7), 406–416.

Pearce, J. A., Cook, J. R., & Emelianov, S. Y. (2010). Ferrimagnetic nanoparticles enhance microwave heating for tumor hyperthermia therapy. In *Engineering in Medicine and Biology Society (EMBC), 2010 Annual International Conference of the IEEE* (pp. 2751-2754). IEEE.

Pellerin, C. (1994). Alternatives to Incineration: There's More Than One Way to Remediate. *Environmental Health Perspectives*, 102(10), 840–845.

Pereira, F. C., Saujet, L., Tomé, A. R., Serrano, M., Monot, M., Couture-Tosi, E., ... & Henriques, A. O. (2013). The spore differentiation pathway in the enteric pathogen Clostridium difficile. *PLoS genetics*, 9(10), e1003782.

Permpoonpattana, P., Tolls, E. H., Nadem, R., Tan, S., Brisson, A., & Cutting, S. M. (2011). Surface layers of Clostridium difficile endospores. *Journal of bacteriology*, 193(23), 6461-6470.

Permpoonpattana, P., Phetcharaburanin, J., Mikelson, A., Dembek, M., Tan, S., Brisson, M.-C., Cutting, S. M. (2013). Functional Characterization of Clostridium difficile Spore Coat Proteins. *Journal of Bacteriology*, 195(7), 1492–1503.

Phetcharaburanin J., Hong H.A., Colenutt C., Bianconi I., Sempere L., Permpoonpattana P., Smith K., Dembek M., Tan S., Brisson M.C., Brisson A.R., Fairweather N.F., Cutting S.M. (2014) The spore-associated protein BclA1 affects the susceptibility of animals to colonization and infection by Clostridium difficile. *Molecular Microbiology*, 92 (5) 1025–1038.

Piyasena, P., Dussault C., Koutchma, T., Ramaswamy H.S., Awuah, G.B. (2003) Radio frequency heating of foods: principles, applications and related properties--a review. *Critical Reviews in Food Science and Nutrition*, 43 (6) 587-606.

Pizarro-Guajardo, M., Olguín-Araneda, V., Barra-Carrascom J., Brito-Silvam C., Sarker, M.R., Paredes-Sabjam D. (2014) Characterization of the collagen-like exosporium protein, BclA1, of Clostridium difficile spores. *Anaerobe*, 25, 18-30

Planche, T. & Wilcox, M. (2011) Reference assays for *Clostridium difficile* infection: one or two gold standards? *Journal of clinical pathology*, 64, 1-5.

Porch, A., Slocombe, D., Edwards, P.P. (2013) Microwave absorption in powders of small conducting particles for heating applications. *Physical Chemistry Chemical Physics* 15(8):2757-63

Pothoulakis C., Lamont, J.T. (2001) Microbes and microbial toxins: paradigms for microbial-mucosal interactions II. The integrated response of the intestine to *Clostridium difficile* toxins. *American Journal of Physiology - Gastrointestinal and Liver Physiology*, 280 (2), 178–83.

Poutanen, S. M. & Simor, A. E. (2004) *Clostridium difficile*-associated diarrhea in adults. *Canadian Medical Association Journal*, 171, 51-58.

Poxton, I. R., McCoubrey, J. & Blair, G. (2001) The pathogenicity of *Clostridium difficile*. *Clinical Microbiology & Infection*, 7, 421-427.

Public Health England (2013) *Clostridium difficile* infection: guidance on management and treatment (first published 1 June 2013).

Public Health England *C. difficile* annual data
<https://www.gov.uk/government/statistics/clostridium-difficile-infection-annual-data>
accessed 01/05/2015.

Public Health Wales monthly *C. difficile* bacteraemia update
<http://www.wales.nhs.uk/sites3/page.cfm?orgid=379&pid=67899> accessed 01/05/2015.

Rabi, R., Turnbull, L., Whitchurch, C. B., Awad, M., & Lyras, D. (2017). Structural Characterization of *Clostridium sordellii* Spores of Diverse Human, Animal, and Environmental Origin and Comparison to *Clostridium difficile* Spores. *mSphere*, 2(5), e00343-17.

Rigler R. (1966) Chapter 3: The Binding of Acridine Orange to Nucleic Acids Influence of the nucleic acids' secondary structure. *Acta Physiol Scand.* 1966;67(s267):32–51. doi:10.1111/j.1748-1716.1966.tb03357.x

- Rosenberg, M. (1984)** Bacterial adherence to hydrocarbon: a useful technique for studying cell surface hydrophobicity. *FEMS Microbiology Letters*, 22, 289–295.
- Ramalingam, B., Parandhaman, T., & Das, S. K. (2016).** Antibacterial effects of biosynthesized silver nanoparticles on surface ultrastructure and nanomechanical properties of gram-negative bacteria viz. *Escherichia coli* and *Pseudomonas aeruginosa*. *ACS applied materials & interfaces*, 8(7), 4963-4976.
- Rupnik, M. (2008)** Heterogeneity of large clostridial toxins: importance of *Clostridium difficile* toxinotypes. *FEMS Microbiology Reviews*, 32, 541–555.
- Salyers, A. A. & Whitt, D. D. (2002)** Bacterial Pathogenesis: A Molecular Approach. 2nd Edition ed., ASM Press.
- Sebahia, M., Wren, B. W., Mullany, P., Fairweather, N. F., Minton, N., Stabler, R., Thomson, N. R., Roberts, A. P., Cerdeno-Tarraga, A. M. & Wang, H. (2006)** The multidrug-resistant human pathogen *Clostridium difficile* has a highly mobile, mosaic genome. *Nature Genetics*, 38, 779-786.
- Semenyuk, E. G., Laning, M. L., Foley, J., Johnston, P. F., Knight, K. L., Gerding, D. N., & Driks, A. (2014).** Spore formation and toxin production in *Clostridium difficile* biofilms. *PloS one*, 9(1), e87757.
- Setlow, P. (2007)** I will survive: DNA protection in bacterial spores. *Trends in Microbiology* 15(4), 172–180
- Sharp, S. E., Ruden, L. O., Pohl, J. C., Hatcher, P. A., Jayne, L. M., & Ivie, W. M. (2010).** Evaluation of the C.Diff Quik Chek Complete Assay, a New Glutamate Dehydrogenase and A/B Toxin Combination Lateral Flow Assay for Use in Rapid, Simple Diagnosis of *Clostridium difficile* Disease. *Journal of Clinical Microbiology*, 48(6), 2082–2086.
- Schichnes, D., Nemson, J. A., & Ruzin, S. E. (2006).** Fluorescent staining method for bacterial endospores. *MICROSCOPE-LONDON THEN CHICAGO-*, 54(2), 91.
- Smits, W. K., Lyras, D., Lacy, D. B., Wilcox, M. H., & Kuijper, E. J. (2016).** *Clostridium difficile* infection. *Nature Reviews Disease Primers*, 2, 16020.

- Snell, H., Ramos, M., Longo, S., John, M., & Hussain, Z. (2004).** Performance of the TechLab *C. DIFF* CHEK-60 Enzyme Immunoassay (EIA) in Combination with the *C. difficile* Tox A/B II EIA Kit, the Triage *C. difficile* Panel Immunoassay, and a Cytotoxin Assay for Diagnosis of *Clostridium difficile*-Associated Diarrhea. *Journal of Clinical Microbiology*, 42(10), 4863–4865.
- Sorg, J. A. & Sonenshein, A. L. (2008)** Bile salts and glycine as cogerminants for *Clostridium difficile* spores? *Journal of Bacteriology*, 190, 2505-2512.
- Sorg, J. A., & Sonenshein, A. L. (2010).** Inhibiting the Initiation of *Clostridium difficile* Spore Germination using Analogs of Chenodeoxycholic Acid, a Bile Acid. *Journal of Bacteriology*, 192(19), 4983–4990.
- Sorrentino, R. & Bianchi, Giovanni (2010)** Microwave and RF Engineering, (Vol. 1, Chapter 4). John Wiley & Sons.
- Spigaglia, P. & Mastrantonio, P. (2002)** Molecular analysis of the pathogenicity locus and polymorphism in the putative negative regulator of toxin production (TcdC) among *Clostridium difficile* clinical isolates. *Journal of Clinical Microbiology*, 40(9), 3470–3475.
- Sylvestre, P., Couture-Tosi, E., & Mock, M. (2003).** Polymorphism in the Collagen-Like Region of the *Bacillus anthracis* BclA Protein Leads to Variation in Exosporium Filament Length. *Journal of Bacteriology*, 185(5), 1555–1563.
- Stubbs, S. L. J., Brazier, J. S., O'Neill, G. L. & Duerden, B. I. (1999)** PCR targeted to the 16S-23S rRNA gene intergenic spacer region of *Clostridium difficile* and construction of a library consisting of 116 different PCR ribotypes. *Journal of Clinical Microbiology*, 37, 461.
- Tan, M. W. (2002)** Cross-species infections and their analysis. *Annual Reviews in Microbiology*, 56, 539-565.
- Tedesco, F. J., Barton, R. W. & Alpers, D. H. (1974)** Clindamycin-associated colitis. A prospective study. *Annals of internal medicine*, 81, 429.

Tenover, F. C., Novak-Weekley, S., Woods, C. W., Peterson, L. R., Davis, T., Schreckenberger, P., Fang, F. C., Dascal, A., Gerding, D. N. & Nomura, J. H. (2010) Impact of strain type on detection of toxigenic *Clostridium difficile*: comparison of molecular diagnostic and enzyme immunoassay approaches. *Journal of Clinical Microbiology*, 48, 3719-3724.

Tenover, F. C., Baron, E. J., Peterson, L. R. & Persing, D. H. (2011) Laboratory diagnosis of *Clostridium difficile* infection: Can molecular amplification methods move us out of uncertainty? *The Journal of Molecular Diagnostics*.

Terry, C., Jiang, S., Radford, D. S., Wan, Q., Tzokov, S., Moir, A., & Bullough, P. A. (2017). Molecular tiling on the surface of a bacterial spore—the exosporium of the *Bacillus anthracis/cereus/thuringiensis* group. *Molecular microbiology*, 104(4), 539-552.

Tian, P. (2010). Computational protein design, from single domain soluble proteins to membrane proteins. *Chemical Society Reviews*, 39(6), 2071-2082.

UniProt protein sequence database <http://www.uniprot.org> accessed 25/06/2018

Vaid, A. and Bishop, A. H. (1998). The destruction by microwave radiation of bacterial endospores and amplification of the released DNA. *Journal of Applied Microbiology*, 85, 115–122

Voth, D. E. & Ballard, J. D. (2005) *Clostridium difficile* Toxins: Mechanism of action and role in disease. *Clinical Microbiology Reviews*, 18, 247-263.

Wang, L., Hu, C., & Shao, L. (2017). The antimicrobial activity of nanoparticles: present situation and prospects for the future. *International journal of nanomedicine*, 12, 1227.

Wiegand, P.N., Nathwani, D., Wilcox, M.H., Stephens J., Shelbaya A, Haider S. (2012) Clinical and economic burden of *Clostridium difficile* infection in Europe: a systematic review of healthcare-facility-acquired infection. *Journal of Hospital Infection* 81(1), 1–14

Wilson, K. H. (1983). Efficiency of various bile salt preparations for stimulation of *Clostridium difficile* spore germination. *Journal of Clinical Microbiology*, 18(4), 1017–1019.

Ziegler, M. J., & Vernier, P. T. (2008). Interface water dynamics and porating electric fields for phospholipid bilayers. *The Journal of Physical Chemistry B*, 112(43), 13588–13599.

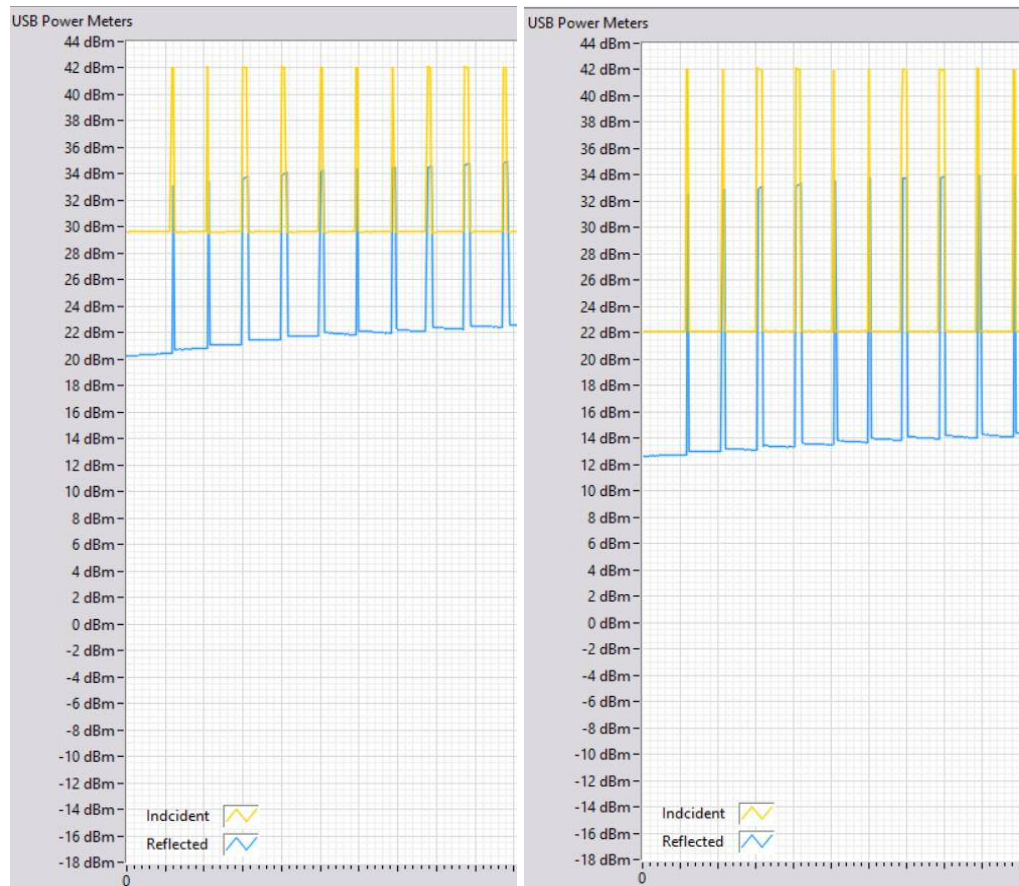
Appendix

Appendix A



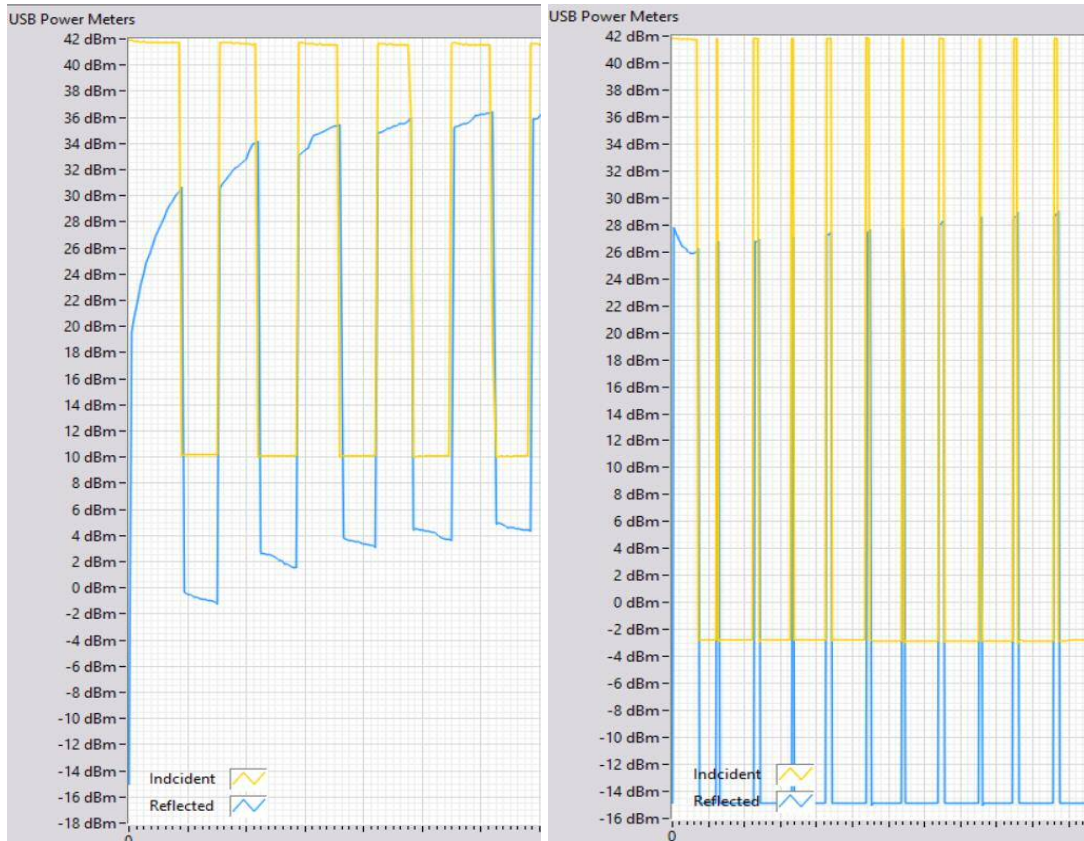
The microwave system used in this project. A: signal generator. B: RF switch. C: bi-directional couplers. D: Power amplifier. E: Circulator. F: power sensors. G: Controller. H: connection to the microwave cavity.

Appendix B



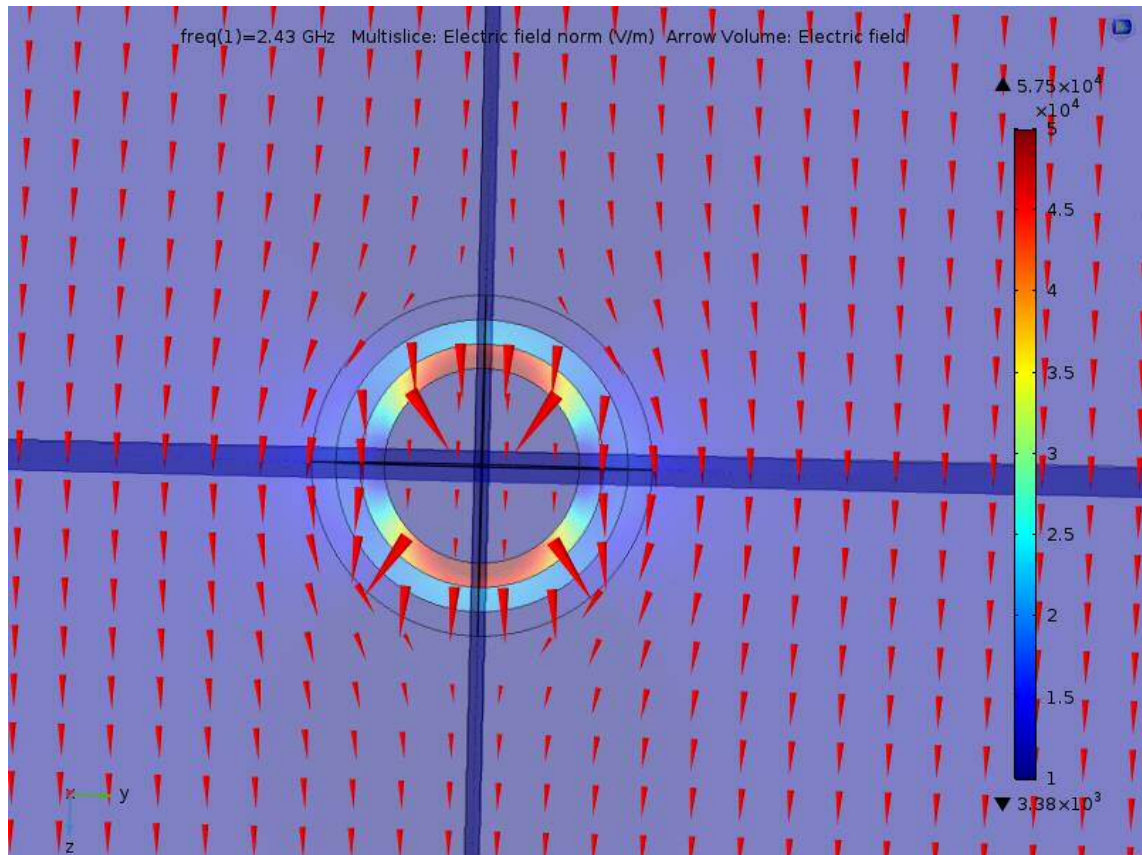
Incident and reflected microwave power detected by the built-in power meters in the microwave system. Peak are the “on” power, while the baseline is the “off” power. Left: initial system configuration. Right: first iteration of changes to the system with extra attenuation.

Appendix C



Incident and reflected microwave power detected by the built-in power meters in the microwave system. Peak are the “on” power, while the baseline is the “off” power. Left: system after the initial changes and replacement of the RF switch. Right: final version of the system.

Appendix D



Arrow volume of the electric fields inside a spore, based on the COMSOL model, showing the high concentration and direction changes of the field in the inner coat and membrane layers, and the low field concentration in the core.